MICROSTRUCTURE STUDIES OF POLYCRYSTALLINE REFRACTORY OXIDES

SUMMARY REPORT

AVSSD-0211-67-RR

25 March 1966 to 24 April 1967

Prepared by

A.H. Heuer
W.H. Rhodes
D.J. Sellers
T. Vasilos

Prepared under U.S. Naval Air Systems Command
Contract NOw-66-0506-(d)

April 24, 1967

AVCO CORPORATION
Avco Space Systems Division
Lowell, Massachusetts

Distribution of this document is unlimited.

MICROSTRUCTURE STUDIES OF POLYCRYSTALLINE REFRACTORY OXIDES

SUMMARY REPORT

AVSSD-0211-67-RR

25 March 1966 to 24 April 1967

Prepared by

A.H. Heuer
W.H. Rhodes
D.J. Sellers
T. Vasilos

Prepared under U.S. Naval Air Systems Command
Contract NOw-66-0506-(d)

April 24, 1967

AVCO CORPORATION
Avco Space Systems Division
Lowell, Massachusetts

Distribution of this document is unlimited.

FOREWORD

This report was prepared by the Space Systems Division of Avco Corporation under U.S. Navy Contract NOw-65-0506-(d) entitled "Research on the Microstructure of Polycrystalline Refractory Oxides."

The work was administered under the direction of the U.S. Department of the Navy, Air Systems Command, with Mr. Charles F. Bersch, Code AIR-52032A, acting as project engineer.

This report covers work conducted from 25 March 1966 to 24 April 1967.

The writers are pleased to acknowledge the contributions of the following individuals to this program; R. Gardner for ceramographic preparation, W.R. Mitchell, J. Centorino and P. Daniels for materials preparation, P. Burnett and P. Houck for electron microscopy, R.M. Haag and P. Berneburg for X-ray studies, and R.M. Haag and A.S. Bufferd for useful discussions.

ABSTRACT

A program to fabricate dense, polycrystalline high-purity alumina and magnesia has begun. Fine-particle size powders of suitable purity have been obtained and characterized. Techniques for analysis and handling of these high-purity powders were established and initial fabrication experiments had a limited success.

Hot working polycrystalline alumina, utilizing a press forging technique, was extensively investigated. Primary recrystallization followed the working and resulted in either single crystals (strain-anneal technique) or relatively fine-grained structures. The basal texture present after recrystallization was identical to the deformation texture; this and the equiaxed recrystallized structures suggested that oriented nucleation was important. At larger grain sizes, an elongated grain structure was observed and was attributed to oriented growth. The marked basal texture suggested that basal slip was the predominant deformation mode; the probability of other deformation mechanisms was also discussed.

Addition of 1/4% MgO retarded recrystallization and a number of such samples, possessing a pronounced basal deformation texture, were used for mechanical properties determination. The working led to no less of structural integrity, and the strength was surprisingly constant with grain size, at least in the range 3.5-10.5 microns. The larger-grained worked samples were stronger than hot-pressed samples of equivalent porosity and grain size.

The high ductility, up to 75% height reduction being achieved without much difficulty, suggested that hot working could be used to produce shaped bodies.

TABLE OF CONTENTS

TABLE OF CONTENTS (concl'd)

LIST OF FIGURES (cont'd)

LIST OF FIGURES (concl'd)

LIST OF TABLES

I. INTRODUCTION

This program is concerned with a general study of the effects of microstructure and chemistry on the physico-mechanical properties of oxide ceramics.

Work has started on the fabrication of high density polycrystalline alumina and magnesia of substantially higher purity than presently available. Particular attention was devoted to the procurement and characterization of the necessary high purity powders and initial fabrication experiments were started.

A major effort of the program was devoted to the processes and mechanisms involved in hot working alumina. Primary recrystallization following the hot working was observed, and the resulting microstructures varied with the amount of working. Deformation produced a pronounced basal texture, which was maintained upon recrystallization. Additions of 1/4% MgO was found to markedly retard recrystallization and a number of such deformed (but not recrystallized) samples were subjected to mechanical tests. The hot working did not cause any loss of structural integrity and the strength of the samples was relatively insensitive to grain size, at least in the range 3 to 10 u. The high ductility exhibited during working was attributed, at least in part, to the onset of rhombohedral slip.

Flame-polishing in polycrystalline alumina and grain growth in ultra high pressure sintered magnesia were also studied.

II. SYNTHESIS OF DENSE, HIGH PURITY CERAMICS

2.1 Introduction

Many of the physical properties which have been determined for ceramic materials are believed to be extrinsic (i.e., impurity controlled). This is particularly true for such point-defect-sensitive properties as electrical conductivity and diffusion. The mechanical properties of both single and polycrystalline metals and ceramic single crystals are known to be defect-sensitive. It is probable that the same is true for polycrystalline ceramics, and the present work was the initial step in testing this thesis. Considerable efforts have been expended in the past in characterizing the strength dependence on microstructure for materials which had as a basis, Linde A Al_2O_3 (99.98%) and Fisher Electronic Grade MgO (99.4%). Recently, Leipold(1) showed that MgO of this purity developed visible grain boundary precipitates upon heat treatment, and that as-hot-pressed material certainly had grain boundary impurity segregation if not a second phase. It is most probable that the mechanical properties of polycrystalline MgO are controlled by these impurities, and similar effects are almost certainly important in Al_2O_3. The objective of the present program was to obtain dense materials significantly purer than the above mentioned Al_2O_3 and MgO.

Initial attempts were made to fabricate high-purity powders into dense, pure, polycrystalline bodies; the ultimate objective will be to critically test the mechanical properties of such samples.

2.2 High Purity Al_2O_3 and MgO Sources

Six 0.5-1.0 gram quantities of raw material samples were received from various suppliers during the course of the year and were characterized in terms of particle size and shape. Only sub-micron powders were considered for further experimentation; previous experience had indicated great difficulties in consolidating larger size powders to full density (densification rates are proportional to particle size^{-3}). They were also rated according to the vendors stated purity, and the powders shown in Table 2.1 were selected for further characterization and fabrication experiments.

In the case of Al_2O_3, several sources satisfied the initial purity and particle size criteria, and also represented powders obtained by different processing methods. The Linde powder was made by triple recrystallization of an alum solution which was subsequently calcined. The other two powders are both thought to be produced by the oxidation of zone-refined aluminum.

While several initial samples of MgO looked very good from the standpoint of the purity, none of these had particle sizes under 1 micron. One grade of MgO (United Mineral-Johnson Matthey) had a reported impurity concentration (determined by emission spectroscopy) of 7 ppm. Spark source mass spectroscopy (Dr. Fred Leipziger, Sperry Rand Corp.) detected 84 ppm impurities in this same powder. This difference can be largely attributed to anion impurities, which are readily detected by mass spectroscopy, but not by emission spectroscopy. Thus, a higher impurity concentration was expected although a total of 84 ppm impurities was considered to indicate a very high purity material. However, this powder could not be densified by pressure sintering at 1175°C at 20,000 psi to a density above 60% of theoretical. In view of this result, it was decided to purchase Johnson Matthey, and Co., $Mg(OH)2$, which was supposed to be of similar purity as their MgO, and then to conduct the calcination of this material in our laboratories. From the work of Gordon(2), it is known that $Mg(OH)_2$ fragments to ultrafine particles during its decomposition to MgO. Therefore, it was thought that the proper calcination treatment could be obtained to yield high purity MgO, which then could be easily densified. Very recently a small test sample of Johnson-Matthey MgO was submitted for consideration. This sample appears much more satisfactory than the earlier MgO samples in that the particle size was found to be only 0.2 microns, and the impurity level (emission spectroscopy) is still reported to be 8 ppm. This latest MgO powder has not yet been purchased in bulk.

TABLE 2.1

POWDER SOURCES FOR HIGH PURITY STUDY

Material	Supplier	Lot No. or Grade	Suppliers' Reported Purity
Al_2O_3	Linde Division, Union Carbide Co., Indianapolis, Indiana	Laser Grade	99.9975
Al_2O_3	United Mineral (distributor for Johnson Matthey) New York 13, New York	S.1	99.9995
Al_2O_3	Cominco American Co., Spokane, Washington	HPM 240	99.9999
$Mg(OH)_2$	United Mineral (distributor for Johnson Matthey) New York 13, New York	GH 182	99.9955
$Mg(OH)_2$	United Mineral (distributor for Johnson Matthey) New York 13, New York	GH 194	99.9980

2.3 Powder Characterization and Analysis

The most effective means of characterizing the shape and size of sub-micron powders is by electron microscopy techniques. A thin film of carbon is evaporated onto a copper grid, and the powder which has previously been dispersed in a liquid carrier, is placed on the grid for direct viewing in the microscope. Consequently, the powder itself is exposed to the electron beam, and if the particles are thin enough (~ 1000 A°) they transmit electrons, allowing particle thickness to be estimated and electron diffraction patterns to be obtained.

Four to six electron micrographs were taken of typical particle clusters for each powder, and one such micrograph for the powders listed in Table 2.1 is shown in Figures 2.1-2.4. Also a micrograph (Figure 2.5) of United Mineral's fine particle size MgO powder is included as it will probably be incorporated into the program.

From each series of micrographs a particle size analysis was made. Approximately 100 particles were measured, and the results are given in Table 2.2.

The United Mineral Al_2O_3 (Figure 2.2) powder appears quite irregular in shape, thus suggesting a roughly spherical symmetry. This powder exhibited good green packing characteristics as was expected.

The Cominco Al_2O_3 powder (Figure 2.3) exhibited hexagonal morphology. The particles were thought to be platelets. The electron transparency results from the fine particle size; however, the rectangular particles in these micrographs have a lower electron transmission, and it is suggested that these are platelets standing on edge (i.e., parallel to the viewing direction). Furthermore, it is known that the C direction is often a slow growth direction in flux-growth of sapphire, and this results in crystals with a platy habit. Thus, a similar morphology in these very fine powders is not surprising.

Examination of $Mg(OH)_2$ (Figure 2.4) was not entirely satisfactory as the brucite decomposed in the electron beam. Electron diffraction patterns on this powder correlated well with known lattice spacings for MgO, and no diffraction evidence for $Mg(OH)_2$ was obtained. Therefore, it is thought that the small particles shown were probably MgO and the larger particles which were encountered (not illustrated in this report) were $Mg(OH)_2$. Previous studies by Gordon and Kingery[2] gave similar results, in that the heat generated by the electron beam of a microscope decomposed $Mg(OH)_2$, and that the MgO product had a fine particle size with a relic type relation to the $Mg(OH)_2$ crystallites.

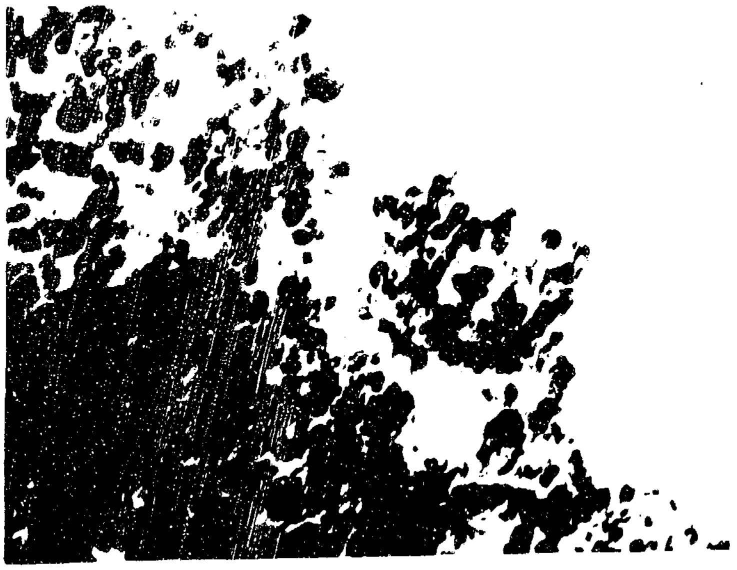

66692 240,000X

Figure 2.1 Al_2O_3 (Linde Laser Grade) Showing a Particle Size average of 120A°

67041 180,000X

Figure 2.2 Al_2O_3 (United Mineral) Showing Particles of Small and Average Size (Average - 300A°)

#67054 30,000 X

Figure 2.5 MgO (United Mineral) Exhibiting Extremes in Particle Size, 430-3500A°, and Cubic Habit.

TABLE 2.2

PARTICLE SIZE OF ALUMINA AND MAGNESIA POWDERS

Composition	Source	Average Particle Size, A°	Range, A°
Al_2O_3	Linde	133	94-320
Al_2O_3	Cominco	500	220-1900
Al_2O_3	United Mineral	300	110-3900
MgO	United Mineral	2000	430-3500
$Mg(OH)_2$	Johnson Matthey	--	300-2000

The MgO powder (Figure 2.5) was quite interesting in that the morphology of almost every particle is cubic. Also there are two populations of sizes; approximately 450 A° and 3000 A° with very few particles falling in between. Particles having 2000 A° sides are on the boderline of being electron transparent. Therefore, these MgO particles are most likely nearly perfect cubes and would probably give high green packing densities.

The Al_2O_3 and $Mg(OH)_2$ powders were examined by X-ray diffraction Debye-Scherrer techniques for major phase and the possible presence of unreacted starting materials. The results are summarized in Table 2.3.

TABLE 2.3

X-RAY DIFFRACTION IDENTIFICATION OF HIGH PURITY POWDERS

Material Source	Major Phase	Minor Phase
United Mineral	$\alpha\,Al_2O_3$	none
Cominco	$\gamma\,Al_2O_3$	K and $\alpha\,Al_2O_3$
Linde	$\gamma\,Al_2O_3$	η and $\delta\,Al_2O_3$
United Mineral	$Mg(OH)_2$	MgO

No unreacted material was found. The K, γ, η, and δ structures are low temperature phases of Al_2O_3 encountered during low temperature decomposition of aluminum salts. They should in no way interfere with subsequent fabrication as they convert to αAl_2O_3 at 1100°C.

Two principle analytical techniques have been utilized in this phase of the program; namely, emission spectroscopy and plasma source mass spectroscopy. Emission spectroscopy is a well known analytical technique for determining cation impurity concentrations with a typical detection limit of from 1-10 ppm. Plasma source mass spectroscopy is less common, but if offers great sensitivity, flexibility, and mass coverage (ion mass from 1-1000). A beam of high energy inert gas ions (argon or xenon) bombards the sample surface, and material is sputtered away by either a focused or defocused ion beam. The elements within the sample are ionized and carried into a double-focusing mass analysis system. The focused plasma beam can sputter away layers of the sample microns thick, thus allowing the analysis of interior sample regions. Also, the specimen can be fractured just prior to entering the vacuum chamber, thus reducing the chance for extraneous contamination.

Spark source mass spectroscopy was utilized for one analysis on this program. This technique is often compared with the plasma source technique, but there are major differences, as follows:

1. The potential is about 50KV for spark source as compared with with 5-10KV for the plasma source. Consequently, the ionizing potential of each element governs the ion intensity for that element in the plasma source analysis, and corrections for the variation of ionization potential must be applied. As this factor may be matrix sensitive, it is very difficult to determine experimentally, and lends some uncertainty to the analysis. In the spark source analysis, the high potential leads to a multiplicity of peaks for any one ion (up to Mg+), which also leads to some errors. There exists a striking difference of opinion between analysts using each method as to which technique offers the highest accuracy based on these considerations.

2. It is presently necessary to incorporate the sample into an electrically conducting matrix (usually C, Au, or Ag) for the spark analysis, and this is an obvious point of potential contamination, especially for a solid sample, which would require grinding prior to analysis. (Of course, blank runs for the matrix metal are conducted.) For the plasma mass analysis, a solid sample is fractured; however, a powder sample must be compacted to a form having some degree of strength (cold compaction is sufficient).

A glove box was reserved for use with this program and was outfitted with a 0.3 micron filter to remove solid particles from the incoming and outgoing tank argon gas used throughout the sample transfer operation. Cold pressed compacts were consolidated in an Al_2O_3 die fabricated from Linde A alumina. The die loading operation took place within the glove box while both the consolidation and the extraction were conducted under ambient laboratory conditions. The compact was fractured to expose a fresh surface prior to insertion into the plasma source chamber.

The powder analyses for the Linde Laser Grade Al_2O_3 is reported in Table 2.4 where three areas were examined by mass spectroscopy and two separate laboratories conducted emission spectroscopy determinations. It will be noted that large descrepancies exist among the analyses for the three regions by the plasma technique and especially large descrepancies exist between the two techniques. Four separate analyses were conducted in the area adjacent to region 3; that is, sample material was sputtered away for three consecutive analyses prior to recording the analysis listed in Table 2.4. Figure 2.6 shows the variation in impurity ion concentration as a function of distance from the sample surface.

The analyses indicate a nonhomogeneous distribution of impurity within the powder compacts. It is not known if this is an intrinsic powder property or is a result of contamination during specimen preparation. Similar plots for the other grade of Al_2O_3 were made, and although these showed different levels of the impurity concentration (Table 2.5), the nonhomogeneity was equivalent. The analyst contends that this is not due to a lack of precision within the instrument, as similar analyses on semi-conductor grade Si show excellent homogeneity within the specimen.

TABLE 2.4

EMISSION AND PLASMA SOURCE SPECTROSCOPIC
ANALYSES OF LINDE LASER GRADE Al_2O_3 POWDER

Species	Region 1*	Region 2*	Region 3*	Avco ≠	Linde ≠
H+	1000	80	3		
Li+	1	ND	ND		
B+	30	10	30	25	
C+	ND	10	ND		
F+	ND	10	ND		
Na+	100	4	0.03		
Mg+	20	1	ND	6	2
Si+	20	1	40	12	12
P+	20	ND	ND		

TABLE 2.4 (concl'd)

EMISSION AND PLASMA SOURCE SPECTROSCOPIC ANALYSES OF LINDE LASER GRADE Al_2O_3 POWDER

Species	Region 1*	Region 2*	Region 3*	Avco ø	Linde ø
Ce+	40	40	30		
K+	120	4	0.1		
Ca+	124	6	0	1	2
Ti+	100	50	1		
Cr+	150	25	0	1	2
Fe+	ND	50	2	0.6	5
Ba+	100	10	ND		
Mn+	50	10	ND		
P+					
Cu+	40	10	ND	1	
Zn+	50	10	ND		
Ga+	50	ND	ND		
As+	40	ND	ND		
V+	40	ND	ND		

* Plasma Source Mass Spectroscopy - by Dr. Frank Satkiewicz
G.C.A. Corporation, Bedford, Massachusetts

ø Emission Spectroscopy

ND Not detected

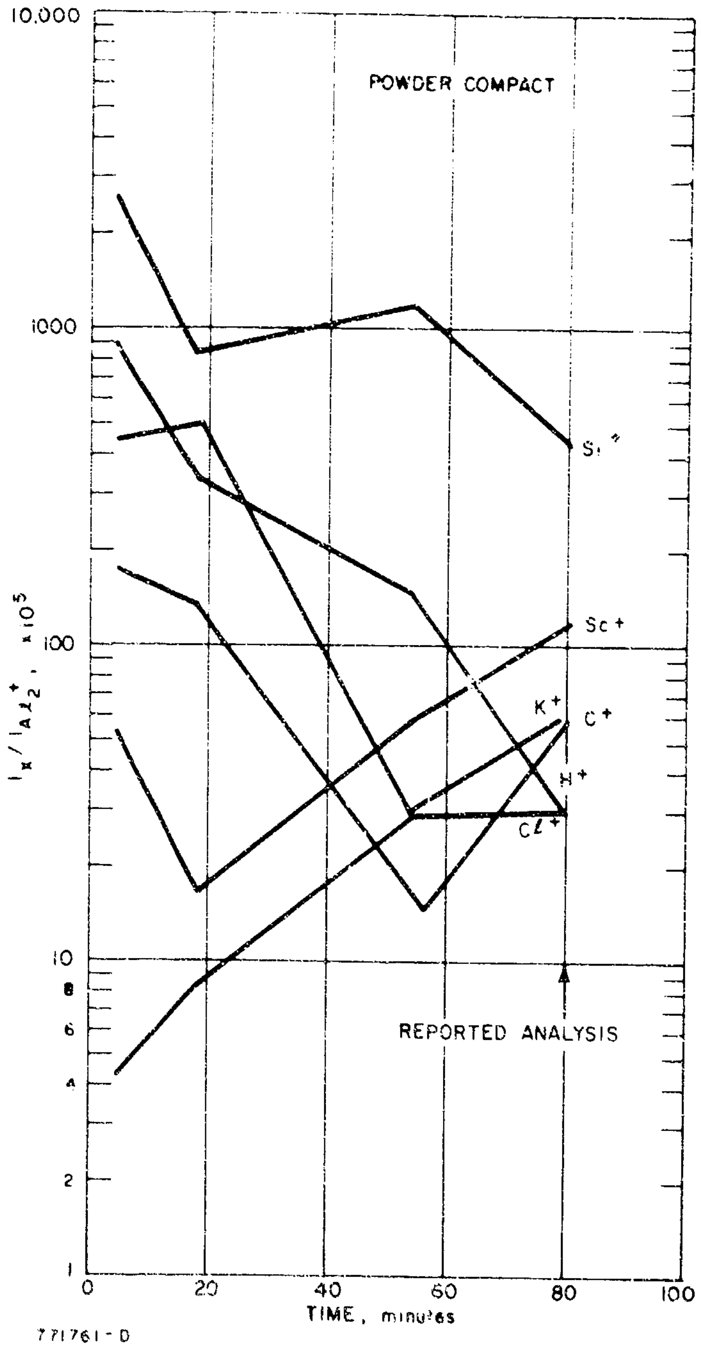

Figure 2.6. IMPURITY PROFILE FOR LINDE LASER GRADE Al_2O_3 COLD PRESSED COMPACT (PLASMA SOURCE MASS SPECTROSCOPY)

TABLE 2.5

PLASMA SOURCE MASS SPECTROSCOPY FOR Al_2O_3 POWDER

Species	Impurity Concentration in ppm United Mineral	Cominco
H+	67	15
Li+	0.07	ND
B+	ND	ND
C+	100	40
F+	67	ND
Na+	0.2	0.04
Mg+	1	0.05
Si+	100	1
Cl+	100	150
K+	0.2	0.03
Ca+	ND	ND
Ti+	ND	ND
Cr+	ND	ND
Fe+	7	1
Y+	100	ND

2.4 Consolidation of High Purity Powders

Several of the high purity Al_2O_3 powders were vacuum hot-pressed with two main objectives; to work out techniques for retaining purity levels, and to compare the hot pressing kinetics with Al_2O_3 powders of a lower purity (~ 99.98%) which had been extensively studied previously.

The filtered glove box discussed earlier was utilized for all powder transfer operations. The hot pressings were conducted in a high-density SiC die which was utilized solely for these high purity Al_2O_3 hot pressings. Between pressings, the die cavity and punch faces were honed with diamond compound. Following this, the entire assembly was cleaned with soap and water and finally rinsed with alcohol. After placing the die assembly in the glove box, the argon purging operation commenced.

The die was loaded and pistons inserted prior to exposing the die to air. The hot pressings conducted on these powders are listed in Table 2.6 One attempt (1177) was made to hot press the high purity powder so that it was not in contact with the SiC die. This specimen was fabricated as follows: the high purity powder was cold pressed in an alumina die confined to a glove box; the green specimen was then loaded into a larger graphite die in which the high purity specimen was surrounded with a shield of Linde A alumina powder. After hot pressing, the high purity specimen could in theory be extracted from the center of the composite. Sample 1177 resulted in a crack free specimen, although the density was quite low (88% theoretical). A metallographic examination disclosed a high density (~ 95%) outer Linde A skin and a porous interior. In sintering, the specimen with the highest green density usually has the highest final density after sintering. Exactly the opposite result occurred for this experiment, and this is not as yet understood.

Of course, the puritities of the materials were different, but a subsequent experiment (1178) demonstrated that Linde Laser Grade material could be densified to near theoretical density. No other explanation for the observed microstructure is obvious.

Figure 2.7 compares the densification kinetics for two high purity alumina powders (α and γ) and two lower purity powders having similar particle sizes and crystal structures. These latter were: Linde A α - 0.3 micron - 99.98% Al_2O_3, Baymal γ - 0.03 micron - 99.90% Al_2O_3.

The data shows that the high purity Linde Laser Grade γ Al_2O_3 densified initially at an increased rate compared with the less pure Baymal Al_2O_3. However, as the process proceeds, the rates become equivalent at approximately 88% density. This would be considered the intermediate stage of densification where diffusional processes become important. At 97% density, the densification rate for the Linde material slows down considerably whereas the Baymal is densifying at a constant rate (assuming as has been done for many other densification studies that the process is best represented

TABLE 2.6

FABRICATION CONDITIONS FOR HIGH PURITY Al_2O_3

Sample No.	Material	Temperature °C	Pressure Kpsi	Time min.	Density gm/cc	Vacuum mm Hg
1177*	Linde	1330	15	60	3.50	2×10^{-4}
1178	Linde	1330	15	16	3.94	1×10^{-3}
1188	U. Mineral	1350	15	3	3.88	1.8×10^{-4}
1189	U. Mineral	1350	15	8		6×10^{-3}
		1200	15	82		9×10^{-3}
		1350	15	14	3.88	9×10^{-3}
1190	U. Mineral	1350	15	4	3.90	5×10^{-4}
1195	U. Mineral	1350	15	30	3.83	4×10^{-4}
1196	Cominco	1320	15	30	3.74	6×10^{-6}

* Sandwich with Linde A

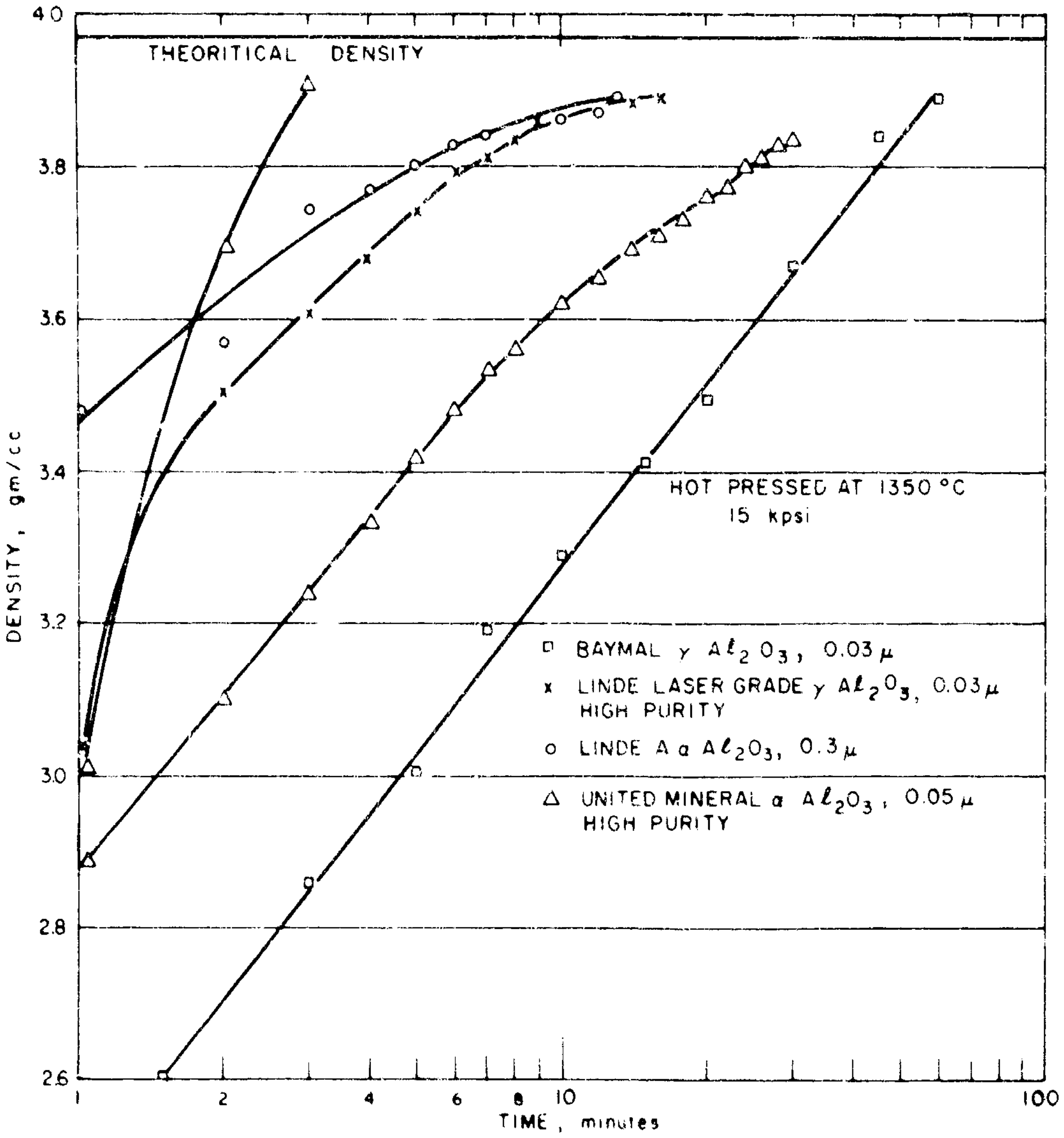

771762-D

Figure 2.7 PRESSURE-SINTERING DENSIFICATION KINETICS FOR HIGH AND LOW PURITY ALUMINA POWDERS by density vs. logarithm time). The decreased rate is probably due to pore entrapment within grains. Increased grain growth rates have been noted for other high purity materials, and this kinetic data may be a result of the same effect.

Two kinetic runs of high purity α Al_2O_3 gave quite different results, and the reason for this is at this time unknown. However, the densification rates for both of these were equivalent to or greater than Linde A. The high purity material has not yet been hot pressed to full density, so pore entrapment could still be a limiting factor, but these initial results look quite encouraging.

An electron fractograph (Figure 2.8) of sample 1178 demonstrated that a fine equiaxed structure was readily produced which had an average grain intercept of 0.45 microns. It is considered feasible to fabricate this powder into a truly unique material; submicron grain size, fully dense, and with very high purity. Such materials have heretofore not been prepared let alone evaluated.

2.5 Chemical Analysis of Fabricated Samples

One hot pressed specimen (1188) was analyzed by the plasma source mass spectrographic technique. A fresh surface (previously unexposed to the atmosphere) was bombarded by the plasma for analysis. Some 14 analyses were conducted on this sample. Nonhomogeneous impurity distribution similar to that shown in Figure 2.6 was also found for this 98% dense sample. This analysis is graphically presented in Figure 2.9, and the semi-quantitative estimation of impurity concentrations is listed in Table 2.7.

The tabulated analysis is an approximate average of the impurity concentration observed (see Figure 2.9). There was not a systematic variation of concentration with increased ion bombardment - this suggests that surface contamination is insignificant. A comparison of the graphically plotted impurity concentration shows that B+, C+ and Ca+ definitely increased during the consolidation step. In addition, Cr+, Ba+, Sm+, and Pb+ showed some evidence of having increased, but their concentration is near the limit of detection, so that a definite conclusion is not possible. Other ions such as H+, Na+ and Mg+ appear to have increased concentrations in the hot-pressed sample, but a plot similar to Figure 2.9 for the powder showed variations within the limits apparent in Table 2.7. It is possible that the concentration of some ions may be decreased with a suitable heat treatment, but clearly improved techniques for maintaining purity during fabrication are required.

#66805 30,000 X

Figure 2.8 Microstructure of Hot Pressed Al_2O_3 Fabricated from Linde Laser Grade Powder. Average Linear Intercept is 0.45 micron. Marker is 1 micron.

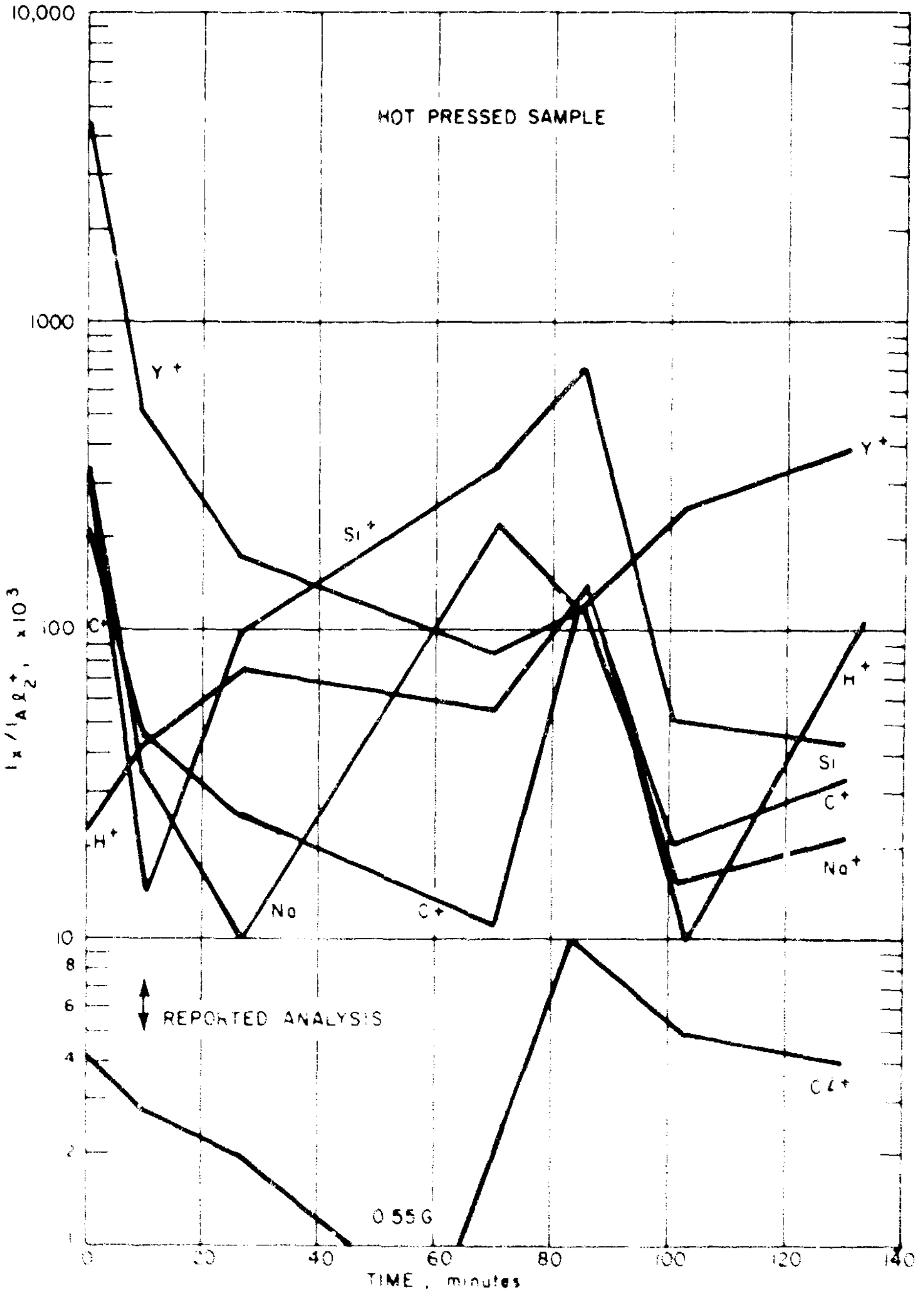

Figure 2.9. IMPURITY PROFILE FOR HOT-PRESSED ALUMINA SPECIMEN FABRICATED FROM UNITED MINERAL Al_2O_3 (PLASMA SOURCE MASS SPECTROSCOPY)

TABLE 2.7

COMPARISON OF IMPURITY CONCENTRATIONS FOR ALUMINA HOT PRESSED SAMPLE 1188 AND BASE POWDER (U. MINERAL)

	Atomic ppm	
Species	**Hot Pressed**	**Powder**
H+	150	67
Li+	0.07	0.07
B+	25	-
C+	1600	100
F+	12	67
Na+	2	0.2
Mg+	5	1
Si+	50	100
Cl+	100	100
K+	1	0.2
Ca+	20	
Ti+	0.1	.05
Cr+	0.6	
Fe+	9	7
Y+	200	100
Ba+	0.2	
Sm+	0.8	
Pb+	1	

2.6 Summary

Progress was made in several areas in the program to fabricate fine-grained high purity polycrystalline Al_2O_3 and MgO. Several good sources of fine particle size aluminas with purity levels significantly higher than Linde A α Al_2O_3 were established in addition to one source of high purity $Mg(OH)_2$. It also appears that this same supplier can under certain conditions produce submicron pure MgO.

Emission spectroscopy calibration curves were generated for Al_2O_3, and experience was gained in using and interpreting the results from spark source mass spectroscopy and plasma source mass spectroscopy.

Initial fabrication studies were conducted which showed that some contamination occurred during hot pressing, but densification kinetics for two high purity alumina were equivalent to or greater than the lower purity (99.9+) pure material. It appears that the diffusional portion of pressure sintering does not have a strong (or measureable) extrinsic function.

III. PRIMARY RECRYSTALLIZATION AND HOT WORKING IN POLYCRYSTALLINE ALUMINA

3.1 Introduction

The discovery(3) that alumina single crystals could be grown in the solid-state by a strain-anneal method was a convincing demonstration that primary recrystallization occurred during or just subsequent to hot working. A major emphasis of work to be reported has been to clarify some of the details of this process, although several important questions are still to be resolved. Previously reported work(3) will be included in this discussion where it bears on the elucidation of the mechanisms of deformation and recrystallization.

There was also evidence in the previous work(3) that mechanical properties of hot-worked alumina was superior to that of hot-pressed alumina of equivalent porosity and grain size. This has now been studied in detail.

Primary recrystallization can be defined as the growth of strain-free nuclei into a deformed matrix, the reduction in strain energy providing the driving force.(4) The problem of nucleation was not considered extensively; such information is particularly difficult to obtain in the case of alumina because deformation, recovery, and recrystallization are all occurring simultaneously. In metals, this area is still unresolved, and research is active (see Reference (5) for a recent review). However, as in deformed metals, it may be assumed that there are copious strain-free nucleation sites present in deformed alumina, particularly at grain boundaries, pores, deformation bands, and free surfaces, and that nucleation will not be the rate limiting step in primary recrystallization. Further, the number of nuclei increases with increasing strain, and this accounts for the relationship shown in Figure 3.1 - increasing deformation leads to a progressively finer-grained structure after recrystallization.

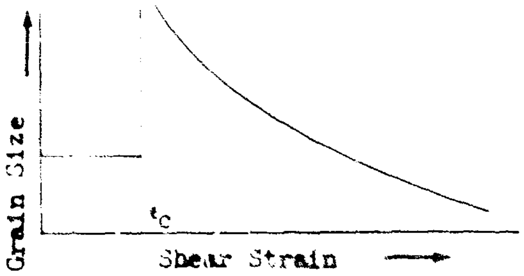

Figure 3.1 Variation of recrystallized grain size with deformation. Note that no recrystallization will occur below a critical strain.

Microstructural evidence that this relationship is observed in alumina is shown in Figure 3.2. This structure can be interpreted as follows:

The coarse grained area on the left corresponds to an area strained less than ϵ_c ; the single crystal was subjected to a strain equal to or just greater than the critical amount, and the fine grained area on the right was recrystallized from a more heavily worked matrix. The fine grain size of this region is truly remarkable, considering the long times this sample was subjected to high temperature and pressures (5 hours at 1870°C and 6000 psi).

It can thus be seen that hot working offers considerable scope for microstructural control and for the production of unique microstructures, as well as a new approach for the synthesis of ceramic single crystals. Heretofore, its application to ceramics has been almost negligible*, although deformation/recrystallization processes are utilized in the production of the majority of polycrystalline metals and for the single crystal growth of some metals.

Press forging was utilized for all the hot working experiments, and the process is described in the first section. Particular emphasis will be given to the problems of maintaining structural and geometrical integrity during hot working, in addition to the other important experimental details.

The remaining discussion is devoted to the following considerations of the hot working and recrystallization processes:

1. Orientation and properties of single crystals produced by primary recrystallization,
2. Production of fine-grained deformed and recrystallized structures,
3. Microstructural and crystallographic texture, both after deformation and after recrystallization,
4. Deformation mechanisms during hot working,
5. Effect of MgO additions on recrystallization,
6. Effect of annealing on the microstructure of deformed and recrystallized materials,

---

* It is important to mention that recrystallization has been observed by Stokes and co-workers(6) after tensile deformation of MgO, and that Rice and Hunt(7) have been examining hot extrusion in polycrystalline magnesia and alumina.

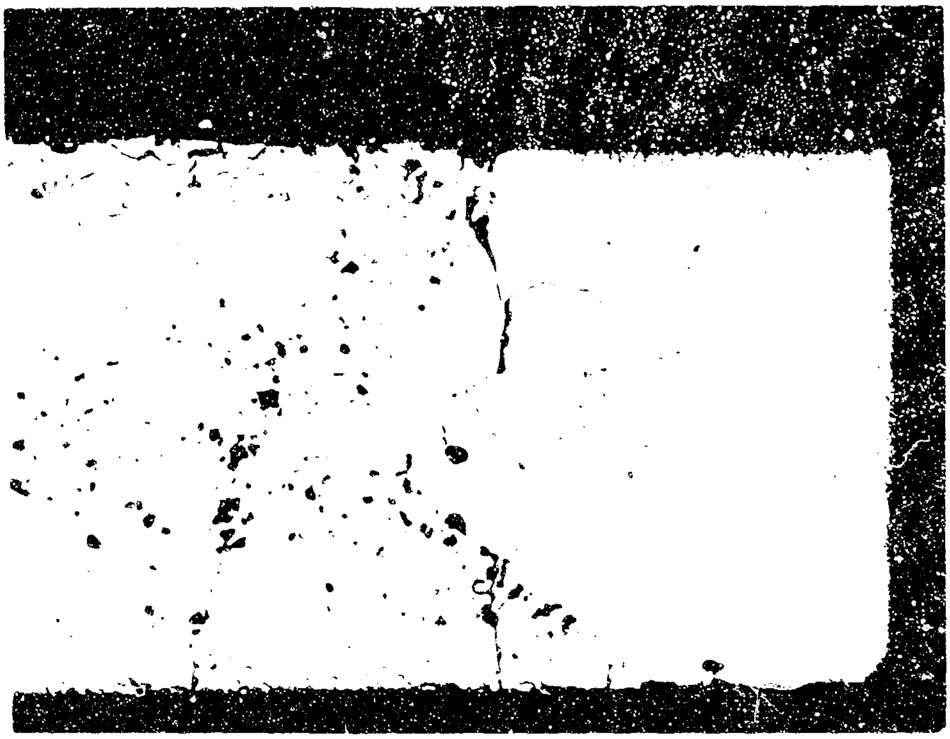

4448

15 X

Figure 3.2 Area of Hot-worked Billet Showing Transition From Coarse-grained Unrecrystallized Structure to a Single Crystal Region to a Dense Fine-grained Recrystallized Structure

7. Removal of porosity during hot pressing, deformation, and recrystallization. This is particularly important in the working of porous composites, and

8. The mechanical properties of worked materials, deformed under conditions where no single crystal growth occurred.

3.2 Hot-Working of Alumina

All the hot-working experiments to be described utilized a press-forging arrangement in a standard pressure-sintering apparatus (Figure 3.3). The important difference to be noted is that there was no die wall-sample contact; the sample was able to expand laterally in the die wall cavity upon the application of pressure.

Two types of forging were employed; forging from a powder which was allowed to sinter to a fairly porous compact prior to the application of pressure, and forging of a relatively dense, previously hot-pressed or sintered billet. In both cases, molybdenum spacers were used to prevent reaction with the graphite punches. Pyrolytic graphite spacers and a BN wash was also tried, but were not as satisfactory as the molybdenum spacers in preventing reaction.

Table 3.1a lists the pure Al_2O_3 "powder" forgings examined during this study* (this table does not include data previously reported$^{(3)}$) while Table 3.1b lists the powder forgings of the composition Al_2O_3 + 1/4% MgO. In almost all cases, the pure alumina billets were uncracked after the forging and fully dense if maintained at temperature and pressure for more than 2 hours. The Al_2O_3 + 1/4% MgO composition, on the other hand, could not be used successfully for powder forgings, because reaction with the die body and punches occurred, which caused severe cracking in the billet. It is not known exactly why the molybdenum spacers are unsuccessful as a diffusion barrier for this composition.

The forgings from dense billets are listed in Table 3.2a for pure Al_2O_3 and 3.2b for Al_2O_3 + 1/4% MgO. (The hot pressing conditions for the starting billets are given in Table 3.3.) In the case of the latter composition, reaction with the punches and subsequent cracking was avoided by rapid forging; cracking was a problem when billets were kept at pressure and temperatures for any length of time (FA-143-146).

Doming was a problem encountered in many of the forgings, and is indicated in Table 3.1 by the maximum height differential and in 3.2 by the spread in percentage height reduction. This doming is caused mainly by hydrostatic (as opposed to shear) stresses present during compression, as well as the relative softness of the graphite punches at the forging temperature. The following factors were found to significantly reduce or eliminate doming:

---

* Some of these billets were fabricated under Contract No. N178-8986, U.S. Naval Weapons Laboratory, but characterized in the present study.

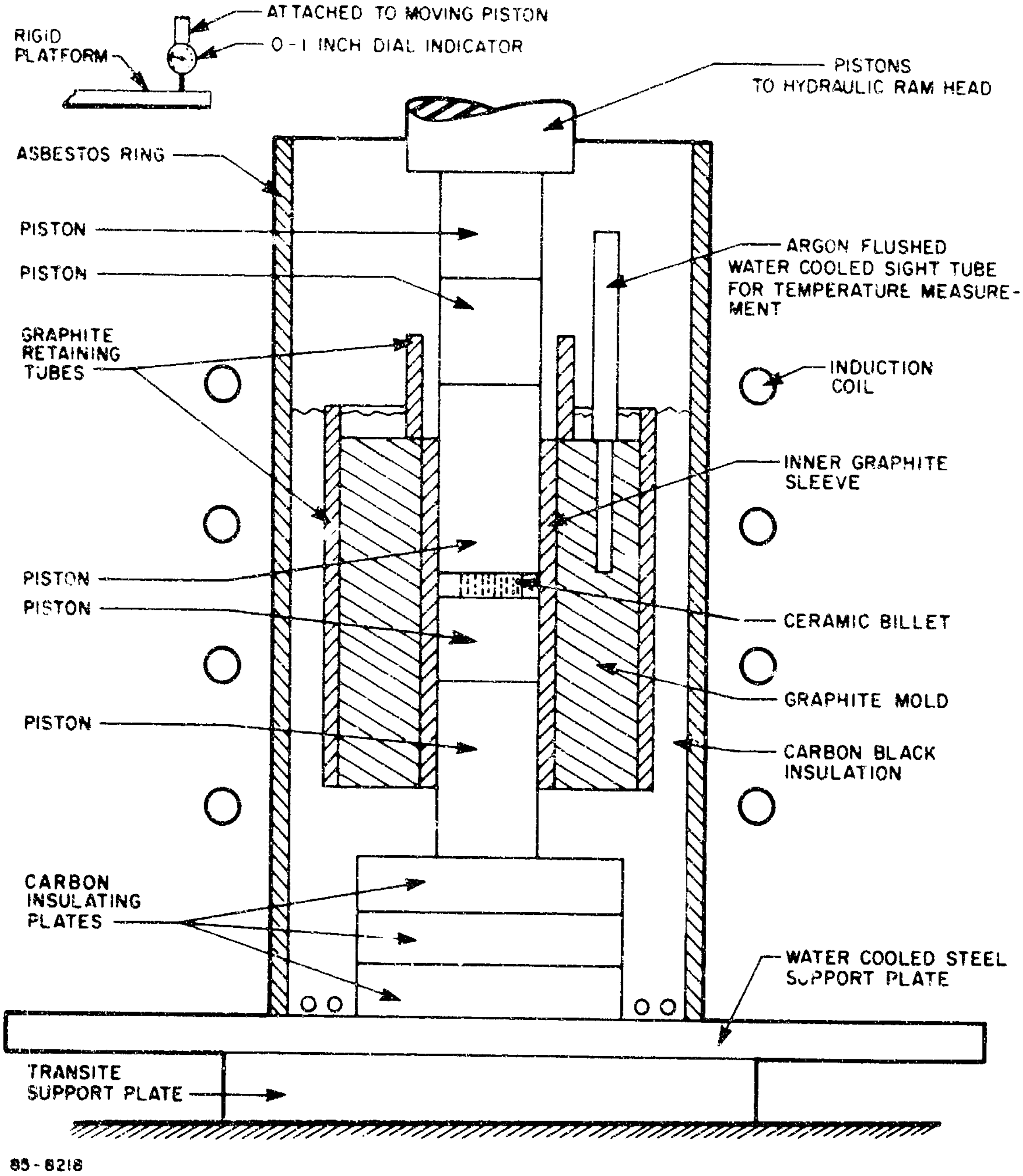

Figure 3.3. PRESSURE SINTERING APPARATUS USED FOR PRESS-FORGING EXPERIMENTS. NOTE THAT PRIOR TO FORGING, THERE IS NO CONTACT BETWEEN THE SPECIMEN AND THE DIE BODY.

TABLE 3.1

a. CONDITIONS FOR FORGINGS FROM Al_2O_3 POWDER

Forging No.	Forging Temp °C	Forging Pressure (psi)	Time to Max. Pressure (min)	Time at Max. Pressure (min)	Maximum Height Differential (%)
FA-44	1840-1860	4000	55	120	25
FA-45	1810-1830	4000	45	215	5
FA-46	1820-1860	5400	46	300	5
FA-47	1850-1880	5400	35	335	5
FA-96	1840-1870	5650	18	360	5
FA-97*	1170-1840	5400	45	360	5
FA-98*	1250-1840	5100	55	135	5
FA-100	1860	5100	20	5	20
FA-101	1860-1870	5100-5400	25-35	320	30
FA-102	1840	5200	7-30	180	19
FA-103	1860	5400	15	1800	--
FA-104	1860	6000	20	180	5
06	1870	6000	25	133	47
FA-108	1860	--	--	5	--
FA-109	1860-1880	6800	30	250	5
FA-110	1860-1880	6800	20	230	5
FA-128	1840-1870	8700	15	240	5
FA-137	1860	5650	15-17	380	5
FA-140	1860	5400	24	71	15
FA-142	1860	5670	20	30	26

* See next page

TABLE 3.1

b. CONDITIONS FOR FORGINGS FROM Al_2O_3 + 1/4% Mg POWDER

Forging No.	Forging Temp °C	Forging Pressure (psi)	Time to Max. Pressure (min)	Time at Max. Pressure (min)	Maximum Height Differential (%)
FA-136	1860	6000	22	143	5
FA-141	1860	5670	20	30	26

* These are essentially high temperature hot-pressings, as the load was applied before sintering commenced.

TABLE 3.2

a. CONDITIONS FOR FORGING DENSE Al2O3 BILLETS

Forging No.	Original Billet	Original Height	Forging Temp. °C	Time to Max. Pressure (min)	Maximum Pressure psi	Height Reduction (%)
FA-119	FA-118		1860-1880	35 + 215	7,000	none
FA-125	FA-123 (70% T.D.)		1860-1880	30+	25,000	75
FA-133	FA-119		1850	10 -15 + 180	13,400	0-42
FA-135	FA-12	0.5 x 0.23" dia.	1880-	5 - 10 + 125	20,000	73.5 - 80.6
JC-4	FLU-2C		1350	34	35,000	4.0
JC-7	FLU-2C		1350	7	35,000	1.5
JC-8	V-21		1350	205	35,000	45
JC-9	V-21		1425	112	35,000	50

TABLE 3.2

b. CONDITIONS FOR FORGING DENSE Al_2O_3 + 1/4% MgO BILLETS

Forging No.	Original Billet	Original Height	Forging Temp.	Time to Max. Pressure (min)	Maximum Pressure (psi)	Section Reduction in Height (%)	Grain Size (u)
FA-49	FA-48	0.271	1880-1910	8	5500	44.6 - 48.0	4 x 8
FA-52	FA-51	0.241	1860	14	8500	47 - 58.5	4 x 6.2
FA-53	FA-50	0.270	1725-1750	17	8600	17.4, 14.8, 24.4, 19.6	6.5
FA-55	FA-54	0.331	1820	18	5650	33 - 35	7 x 11
FA-80	FA-68	0.275	1850	16	4100	39.3, 40.4, 40.7, 41.5	8.2 x 6.4
FA-81	FA-62	0.275	1850	3	2800	5.4 - 3.6	5.3
FA-84	FA-71	0.277	1850	7	4800	15.5 - 16.2	5.5
FA-86	FA-70	0.281	1850	23	4800	35.6 - 40.6	8.6 x 6.4
FA-87	FA-79	0.498	1850	43	4800	46.0, 42.6, 41.2, 38.5	10.4
FA-88	FA-75A	0.100	1850	35	4800	0 - 39	5.5(0%) 6.2(20%)
FA-89	FA-75B	0.100	1850	23	5940	0 - 30	3.9(0%) 6.2(20-35%)
FA-90	FA-78	0.279	1900	20	5100	25.0, 22.9, 21.1	9.4 x 8.2
FA-91	FA-77	0.281	1900	33	6200	48.0, 43.5, 42.0, 40.6	7.2
FA-92	FA-76	0.281	1900-1925	19	6000	40.3, 40.6, 42.8, 95.1	6.2
FA-93	FA-73	0.277	1750	13-15	6200	28.0, 22.0, 16.8, 21.6	

TABLE 3.2 (concl'd)

b. CONDITIONS FOR FORGING DENSE Al_2O_3 + 1/4% MgO BILLETS

Forging No.	Original Billet	Original Height	Forging Temp.	Time to Max. Pressure (min)	Maximum Pressure (psi)	Section Reduction in Height (%)	Grain Size (u)
FA-94	FA-69	0.282	1750	15-17	6800	38.0, 35.6, 35.6, 34.4	5.2 x 3.8
FA-120	FA-58	0.267	1900-1920	6	17,000	64.5 - 70%	---
FA-124	FA-57	0.267	1730-1750	16	19,000	34. + 47.0%	---
FA-126	FA-105	0.270	1850	15-20	21,000	63.7 - 72.9	---
FA-132	Lucalox	0.250	1850	30-45+180	15,000-17,000	5.4	
FA-143	FA-111	0.5	1860	10+230	5650	5	
FA-144	Lucalox	0.250	1860-1880	15+115	18,000	16 - 55	
FA-145	Lucalox	0.250	1860	8 + 125	18,000	10 - 53	
FA-146	Lucalox	0.250	1870-1880	32 + 180	18,000	35 - 50	

TABLE 3.3

PROCESS CONDITIONS FOR FABRICATION OF Al_2O_3 + 1/4% MgO BILLETS

Billet No.	Thickness (inches)	Temperature (°C)	Time at Maximum Pressure (min.)	Maximum Pressure (psi)	Density-% of Theoretical
FA-48	0.3	1575	10	6000	98.5-99.0
FA-50	0.3	1475	135	5100	98.5
FA-51	0.3	1560	85	5650	98.5
FA-54	0.3	1580	90	5100	99.0+
FA-56	0.3	1575	73	5100	99.5+
FA-57	0.3	1570	110	5100	-
FA-58	0.3	1580	90	5100	-
FA-59	0.3	1605	120	5600	-
FA-60	0.3	1600	96	2900	-
FA-61	0.3	1600	60	5100	-
FA-62	0.3	1580	60	5400	99.5+
FA-63	0.3	1580	90	5400	99.5+
FA-65	0.3	1580	70	5400	99.5+
FA-66	0.3	1580	75	5400	-
FA-67	0.3	1580	105	5400	-
FA-68	0.3	1580	55	5400	-
FA-69	0.3	1580	75	5400	99.5+
FA-70	0.3	1580	72	5400	99.5+
FA-71	0.3	1580	70	5500	-
FA-72	0.3	1580	80	5600	99.5+

TABLE 3.3 (concl'd)

PROCESS CONDITIONS FOR FABRICATION OF Al_2O_3 + 1/4% MgO BILLETS

Billet No.	Thickness (inches)	Temperature (°C)	Time at Maximum Pressure (min.)	Maximum Pressure (psi)	Density % of Theoretical
FA-73	0.3	1590	69	5300	99.5+
FA-74 A&B	0.1	1580	85	5600	99.5+
FA-75 A&B	0.1	1570	67	5500	99.5+
FA-76	0.3	1580	75	5400	99.5+
FA-77	0.3	1580	75	5600	99.5+
FA-78	0.3	1580	60	5400	99.5+
FA-79	0.5	1580	110	5500	99.5+
FA-105	0.3	1580	70	6000	99.5+
FA-111	0.5	1590	65	5650	99.5+
FA-113	0.5	1585	113	5400	99.5+
FA-114	0.5	1580	120	5400	99.5+
FA-115	0.5	1580	120	5400	99.5+
FA-116	0.5	1580	130	5400	99.5+
FA-123*		1310	40	2000	70
V-21*+	0.25	1400-1420	200	6400	99.5+
FLU-20*+	0.25	1400	180	6000	99.5+

* pure alumina
\+ vacuum hot pressed

1. Large aspect (height:diameter) ratios. This is the single most important parameter, as the amount of hydrostatic forces increases with decreasing aspect ratios. However, at very high aspect ratios, the opposite to this, viz., "barreling", could occur; this, however, has not yet been observed during forging of alumina.

2. Slow application of pressure, the use of surface lubricants such as a BN wash, or pyrolytic graphite paper, and temperatures in excess of 1870°C all helped reduce the incidence of doming.

As the data in Table 3.2 show, alumina is remarkably ductile. In the case of the solid forgings, it was possible to calculate true strains (as opposed to engineering strains) and strain rates and these data are shown in Table 3.4. A measure of the "ease of forging" can be obtained from the ratio of stress: strain rate (low values are indicative of a relatively "easy" forging), and these ratios are plotted as a function of aspect ratio in Figure 3.4. The difficulty of forging at low aspect ratios is a real effect and due to the large hydrostatic forces referred to above, the center areas of specimens with a low aspect ratio of 0.033, where the hydrostatic forces were at a maximum, could not be forged at all (FA-88 and 89). It is not known if there is a maximum ease of forging at an aspect ratio of ~0.1; there is too much scatter at the larger aspect ratios to draw firm conclusions. However, it is reasonable to expect that forgings should continue to become easy as the aspect ratio increases, perhaps until barrelling becomes evident.

Run FA-108 was terminated before appreciable forging had commenced. The powder had shrunk away from the 3" diameter die body to a disc 2 [illegible]" diameter which had a density of 60% of theoretical. It may be assumed that all the powder forgings behaved similarly, and the low pressures needed for forging (compared to the solid pure alumina forgings) indicate that this large amount of porosity greatly facilitated the working. A further comparison of FA-125 and FA-133 substantiates this conclusion. In addition, the solid hot pressed Al_2O_3 + 1/4% MgO billets all forged fairly readily; this is attributed to the fine grain size of these billets (the ability of MgO to retard grain growth in discussed in Section 3.7) and comparison with forging of larger-grained lucalox (FA-132, 144-146) supports this contention. Considerably greater pressures were needed to effect forging in the latter specimens.

In summary, a total of 22 powder forgings, 28 forgings from solid billets, and 34 hot pressings were conducted on this phase of the program. The remainder of this section is devoted to a discussion of the microstructures and properties of these worked samples and to the important processes occurring during working.

TABLE 3.4

FORGING STRAIN RATE DATA

Forging No.	Starting Height (inches)	Finishing Height (inches)	Maximum True* Strain $\left(-\ln\frac{hi}{hf}\right)$	Forging Time (min)	Average Strain Rate ε/min	Aspect Ratio	Overall Reduction (%)
FA-49	0.271	0.146	.621	8	.0776	0.12	
FA-52	0.241	.095-0.128	.9325	14	.0666	0.11	47 - 60.5
FA-53	0.270	.204-.230	.278	17	.01635	0.12	14.8 - 27
FA-55	0.331	0.215-0.220	.432	18	.0240	0.10	33 - 35
FA-80	0.275	0.164-0.173	.580	16	.0362	0.083	33.2 - 41.8
FA-81	0.275	.260-.270	.0564	3	.0188	0.094	2 - 6.40
FA-84	0.277	.288-.236	.195	7	.0278	0.105	14.8 - 18.2
FA-86	0.281	0.157-0.185	.5825	23	.0253	0.094	34.1 - 44.2
FA-87	0.498	0.260-0.310	.649	43	.0151	0.166	38 - 48
FA-88	0.100	0.061-0.100	.495	35	.0141	0.032	0 - 39
FA-89	0.100	0.070-0.100	[illegible]	[illegible]	[illegible]	0.033	0 - 30
FA-90	0.279	0.201-0.220	.3315	20	.01656	0.093	21.5 - 27.9
FA-91	0.281	0.135-.166	.733	33	.0222	0.094	37.7 - 52.0
FA-92	0.281	0.145-0.174	.663	19	.0347	0.094	39.0 - 48.5
FA-93	0.277	0.181 - 0.232	.444	13-15	.9317	0.093	16.8 - 34.6

* See next page

TABLE 3.4 (concl'd)

FORGING STRAIN RATE DATA

Forging No.	Starting Height (Inches)	Finishing Height (inches)	Maximum True* Strain $\left(\ln \frac{hi}{hf}\right)$	Forging Time (min)	Average Strain Rate ϵ/min	Aspect Ratio	Overall Reduction %
FA-44	0.282	0.[illegible]5 - .[illegible]34	.5[illegible]	15-17	.0336	0.094	34.8 - 41.5
FA-120	0.267	.080 - .095	1.205	6	.201	0.178	64.5 - 70.0
FA-124	0.267	.141 - .176	.638	16	.0391	0.1[illegible]9	34.1 - 47.0
FA-126	0.270	0.077 - 0.095	1.255	15-20	.0717	0.180	63.7 - 72.9

*ln = natural logarith,
hi = initial height,
hf = final height

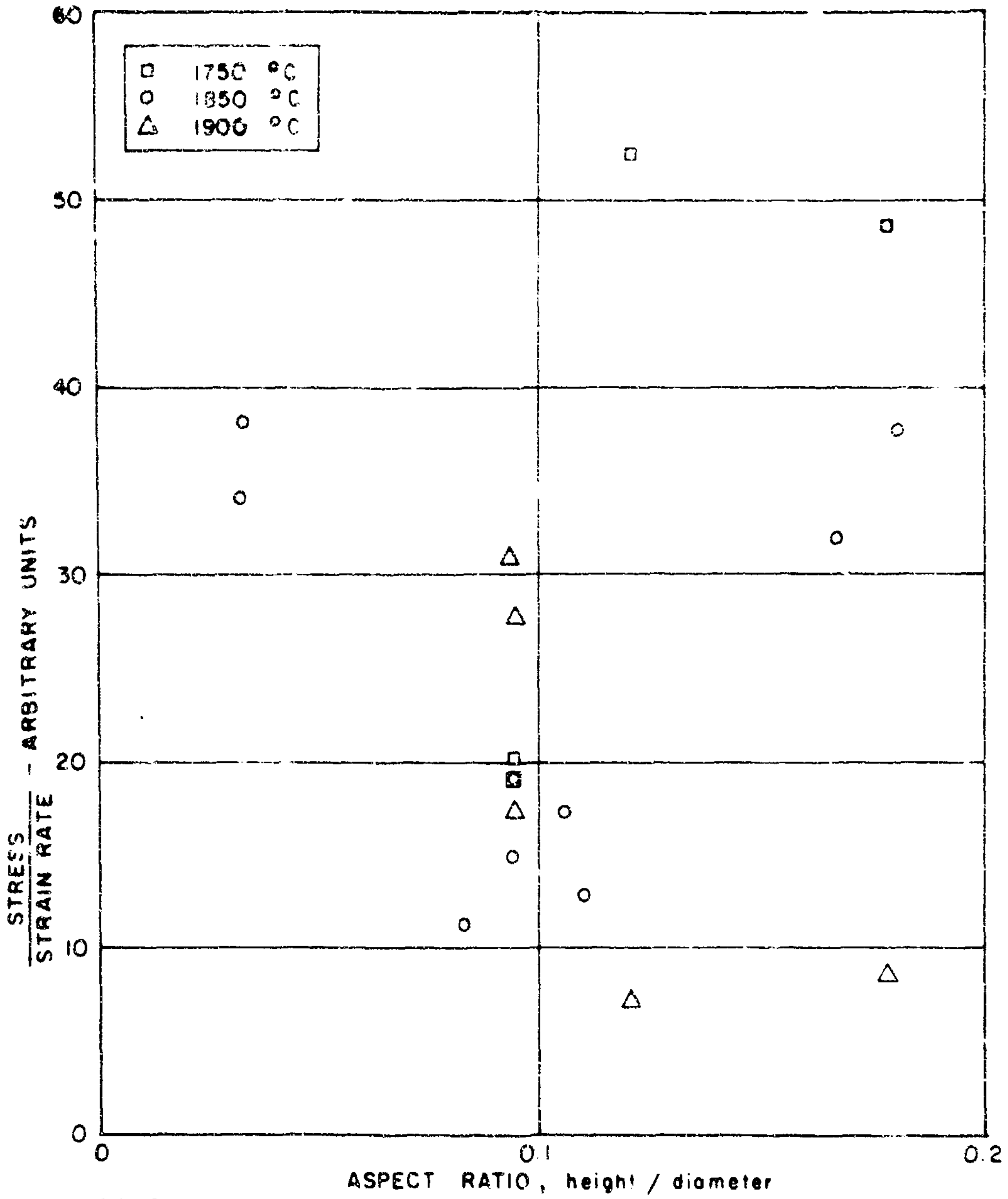

771763-D

Figure 3.4 PLOT OF STRESS STRAIN RATE AS A FUNCTION OF ASPECT RATIO. LOW VALUES OF THIS PARAMETER INDICATE A RELATIVELY EASY FORGING

3.3 Orientation and Properties of Single Crystals Grown by Strain Anneal

3.3.1 Orientation and Location of Single Crystals

Standard Laue X-ray back-reflection photographs were used to determine the orientation of a number of single crystals, varying in volume from .001 to 7 cm^3. A typical Laue photograph is shown in Figure 3.5 and indicates that a high degree of crystalline perfection had been achieved. These results are plotted on a standard (0001) projection, (Figure 3.6) which shows the pressing direction relative to the "c" and "a" axis for each of the crystals. It is apparent that the choice of orientation of the favorably situated nuclei is essentially random, even though the matrix may possess a pronounced basal deformation texture (see Section 3.5). Such behavior is also observed in the strain-anneal growth of metal crystals, where special precautions must be taken to obtain crystals of specified orientation.(8) This random orientation of the growing crystals is also evidence that "texture-inhibited" secondary recrystallization(8), i.e., the growth of a secondary grain of preferred orientation into a matrix with a strong primary texture, different from that of the secondary grain, is not operative in the present experiments.

The location of the single crystal areas in a number of billets is shown in Figure 3.7, reproduced from an earlier report. The single crystals most commonly occurred in a toroidal-shaped area, roughly half-way between the center and the circumference of the press forged billets (Specimens FA-21, 24, 28, 32 and 33) and Figure 3.8 (a higher magnification of Figure 3.2) shows such a single crystal. It has already been mentioned that the shear deformation must increase radially outward from the center of the billet during press forging. The porous large-grained area to the left of the single crystal was near the center of the billet, and had not been strained sufficiently to undergo recrystallization. The single crystal almost certainly nucleated in a region of strain at/or just in excess of the critical amount, where the small strain prevented excessive nucleation. For single crystal growth to be possible, growth of the first nucleus must proceed at such a rate that possible nucleation sites in adjacent areas are consumed. The area to the left of the single crystal had been deformed more extensively; hence, the nucleation rate was higher and recrystallization to a fine-grain matrix occurred before the deformed matrix was incorporated into the growing single crystal. When recrystallization to a fine-grained matrix was complete, the driving force promoting the fast growth of the single crystal was eliminated.

It was usual for these areas of single crystal growth to contain a small number of randomly oriented single crystals (there being no circumferential driving force for crystal growth due to the radial symmetry inherent in press forging) and Figure 3.6 shows two examples (180° apart) of differently oriented crystals in a single billet.

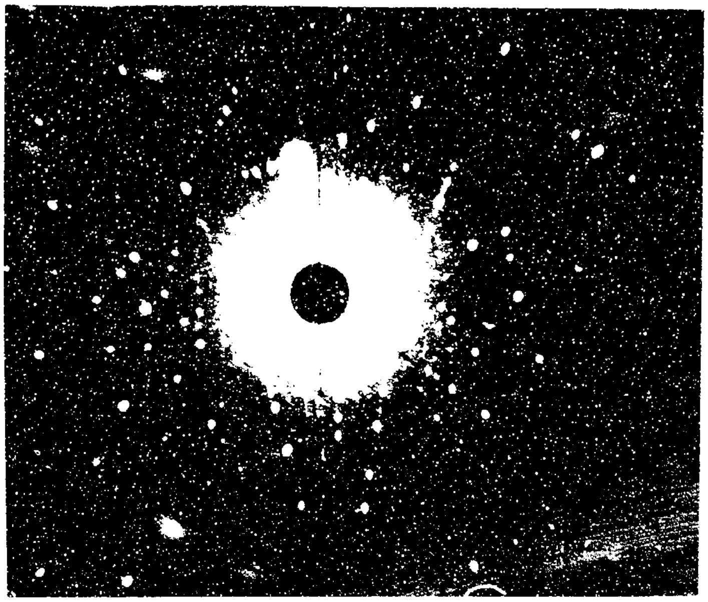

Figure 3.5 Laue X-ray Back Reflection Photograph of Strain-Anneal Single Crystal in Billet FA-14

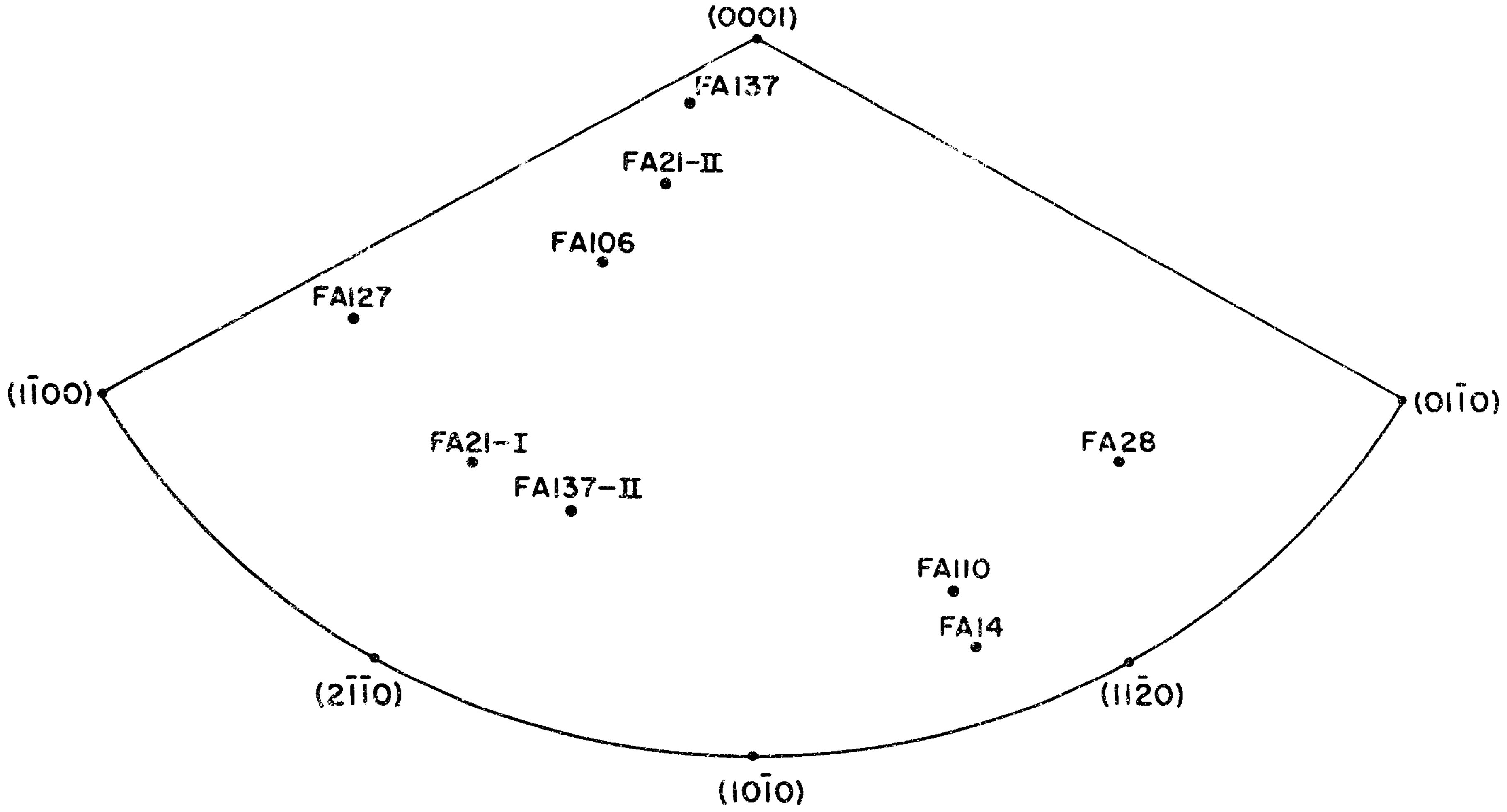

Figure 3.6. STEREOGRAPHIC ORINETATION OF VARIOUS SINGLE CRYSTALS GROWN BY STRAIN ANNEAL. THE PRESS-FORGING DIRECTION OF EACH CRYSTAL IS PLOTTED ON A STANDARD BASAL PLANE PROJECTION

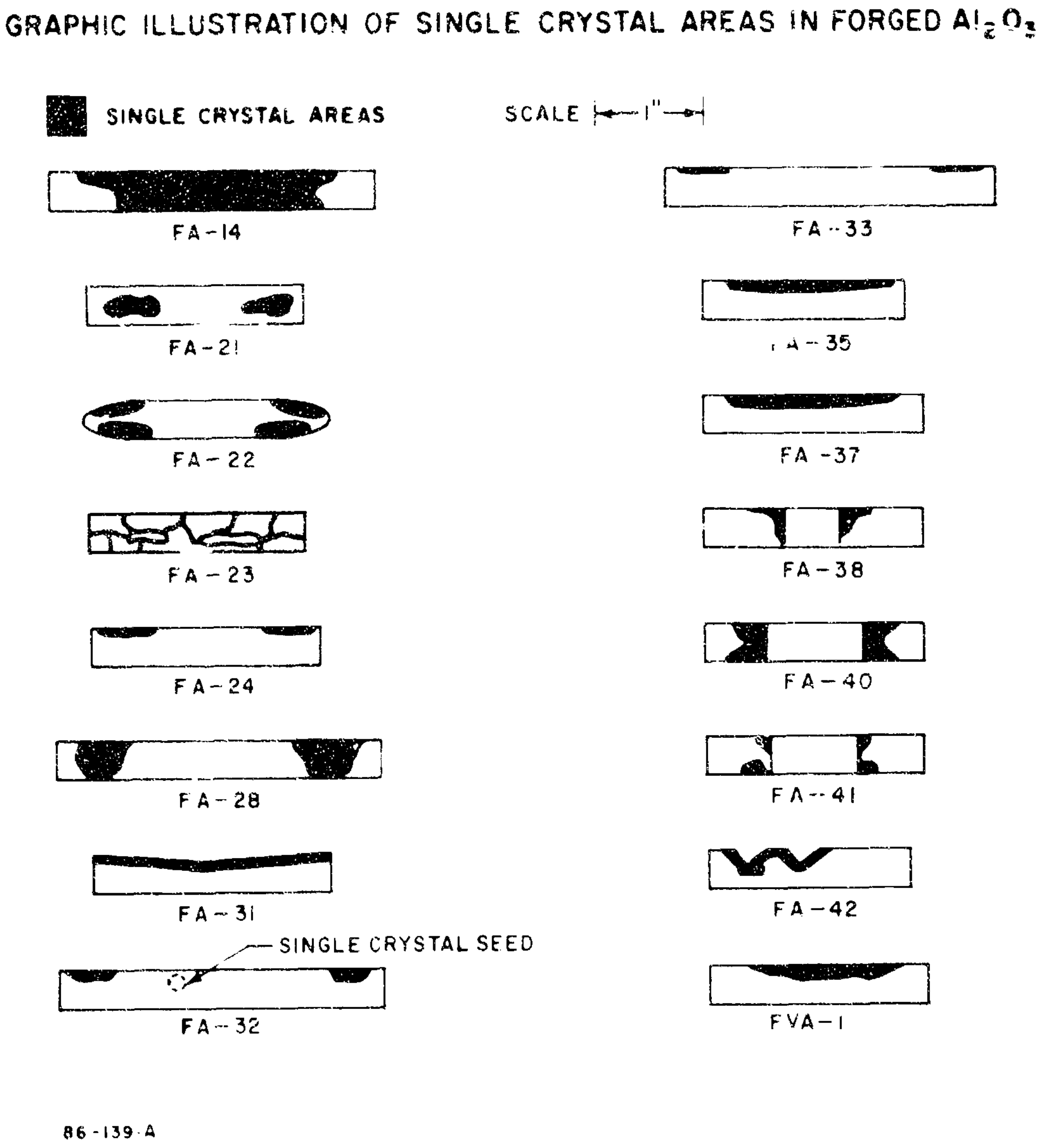

Figure 3.7. LOCATION OF SINGLE CRYSTAL AREAS IN A NUMBER OF PRESS-FORGED BILLETS

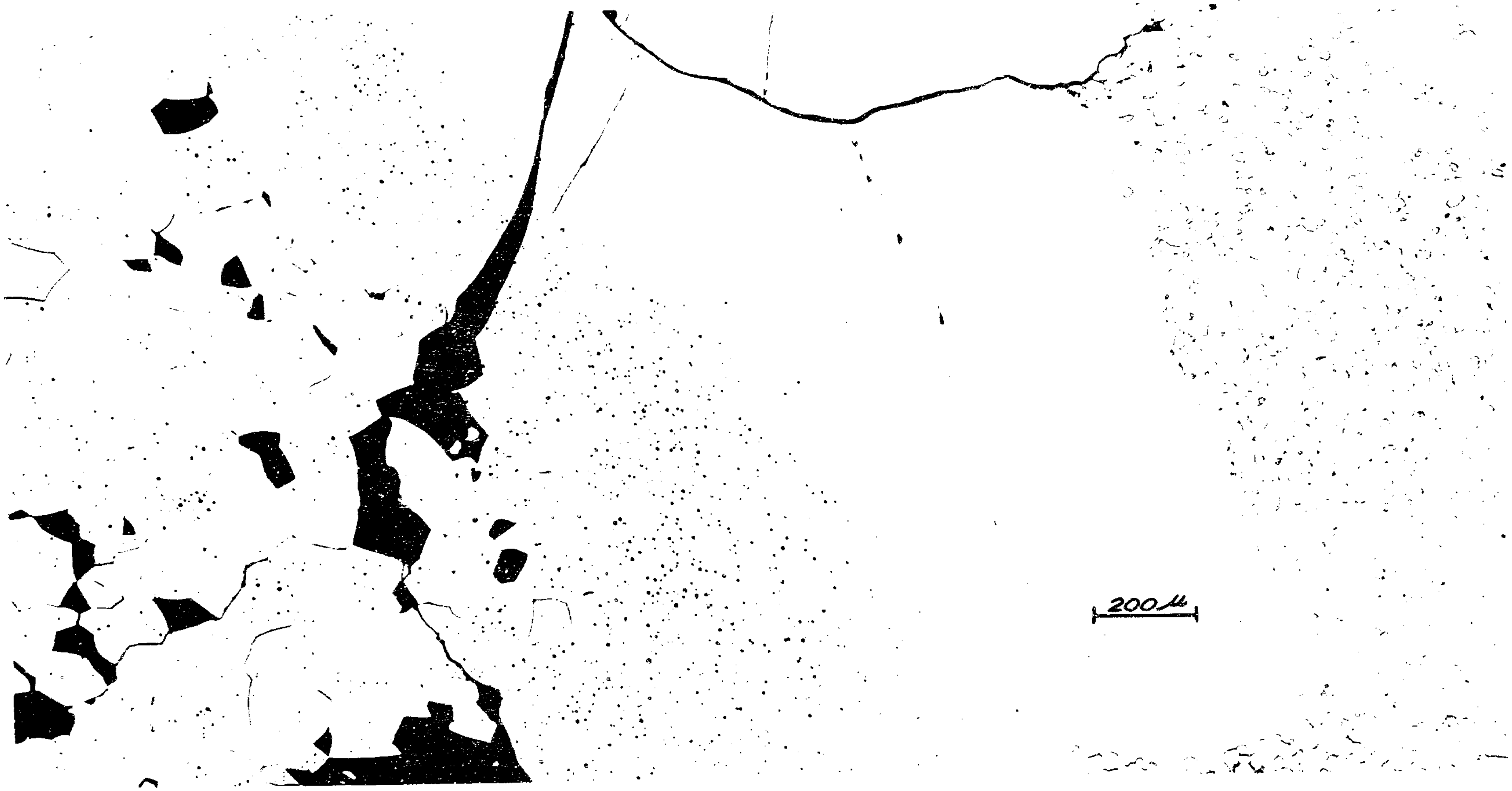

Figure 3.8 Composite micrograph encompassing coarse unrecrystallized area at the left, a single crystal in the center, and a fine-grained recrystallized structure at the right. The porosity gradient is discussed in Section 3.9.

In addition, it can be seen in Figure 3.7 that in a number of cases, nucleation of single crystals appeared to proceed from a surface in contact with a graphite punch, and this could be emphasized using 2° or 3° domed punches (FA-31, 35, and 37) or punches with small right angle cones extending from the surface (FA-42). This is partly because the shear strain is a maximum at the surface, and also because friction between the billet and punches may produce very heavy local deformation at the surface, which favored nucleation. Most of the single crystals so produced were relatively small, which is further support for this hypothesis.

Several dense toroids were also formed (FA-38, 40, and 4[illegible]) and single crystal growth occurred at the free interior surface of the toroid, but was otherwise similar to the billets mentioned above. This again resulted from the high shear strains at free surfaces; in addition, a similar effect is noted in metals, where a high dislocation density is found in surface layers 30-50 u thick, even in the absence of an oxide layer, and this results in preferred nucleation of new grains at such surfaces upon annealing deformed single crystals.(9)

3.3.2 Etching of a Large Alumina Single Crystal Produced by Strain Anneal

FA-14 contained the largest single crystal achieved to date--7 cm^3 in volume. A portion of the billet containing the polycrystalline matrix and polished basal and $\{11\bar{2}0\}$ prism planes was chemically etched in $K_2S_2O_7$ for 30 seconds at 700°C.(10) Etch pits were produced on both faces, but they were unusual in several respects. Firstly, the triangular etch pits on basal planes were flat-bottomed and sometimes terminated in pores (Figure 3.9). Although flat-bottomed pits have been reported in a number of ceramic single crystals, they have not previously been reported in sapphire. They are usually attributed to the movement of dislocations during etching or between two etchings, in contrast to pointed etch pits at a stationary dislocation. (It is possible that the critical experiments needed to detect such pits have not been conducted with sapphire.) However, the etch pits were larger than would have been expected from the short time of etching. For these reasons, the etch pits are not believed to be the termini of emergent dislocations, but may have been caused by impurities or other point defects. Although low dislocation densities are not characteristic of metal crystals grown by strain-anneal, it might be expected that ceramic crystals grown by this technique would be appreciably better than those grown from the melt; the energy needed to form a dislocation in alumina is appreciably higher than in metals, and low dislocation contents might thus be an added benefit of this solid-state crystal growing technique. The area immediately adjacent to the polycrystalline matrix in Figure 3.9 appeared to be essentially pit-free. This is not completely understood, as the crystal was thought to be growing into the polycrystalline matrix in this region. One possibility is that the impurities (or other point defects) responsible for the etch-pits were in solution during the strain-anneal crystal growth but precipitated at some time after growth had ceased; those impurities near the single crystal boundary might then have been able to diffuse to the boundary. Figure 3.10 shows one of the grains of the matrix completely surrounded, but not annihilated by

4183E

1000 X

Figure 3.9 Basal Plane of Strain-anneal Single Crystal after Etching in $K_2S_2O_7$ at 700°C for 30 seconds. The white singularities are subsurface porosity.

41830 10 μ

Figure 3.10 Basal Plane of Strain-anneal Alumina Single Crystal after Etching in $K_2S_2O_7$ at 700°C for 30 Seconds.

the strain-anneal crystal. Such entrapped grains have also been observed in strain-anneal metal crystals,(11) and are probably due to only a small orientation difference between the growing crystal and the entrapped grain.

On $\{11\bar{2}0\}$ prism planes (Figure 3.11) the rhombic etch pits were also flat-bottomed and were similar in size to the triangular etch pits on basal planes; they probably had a similar origin. In addition to these, smaller rhombic etch pits (arrowed in Figure 3.11) were arranged in parallel rows. It is suggested that these small pits represent emergent dislocations, perhaps produced by basal slip after the single crystal growth had ceased. Further evidence for this can be seen in Figure 3.12, an area in the polycrystalline matrix. In those grains properly oriented for etching, two types of etch pits were found. The shape of the larger pits suggested that the etched surfaces were also $\{11\bar{2}0\}$. This surface of the polycrystalline matrix was parallel with the pressing direction. It will be shown (Section 3.5) that the polycrystalline aggregate probably had a pronounced basal texture, with the c-axis of the individual grains parallel to the pressing direction; thus, $\{11\bar{2}0\}$ faces should be observed in preference to (0001) which is consistent with the morphology of the larger pits.

3.4 Dense, Fine-Grained Elongated and Equiaxed Microstructures

3.4.1 Elongated Structures after Hot-Working

It has been possible to produce dense, fine-grained elongated structures by hot working, and such a structure, taken from a previous report, is shown in Figure 3.13. In the case of pure alumina, the exact conditions leading to this structure are not known with certainty. However, it will be suggested in a later section that this fine-grained elongated structure is in fact evidence of a deformation (rather than a recrystallization) texture. Thus, it may be that fast strain rates, followed by an effective quench, would prevent recrystallization and thereby promote the retention of elongated microstructures.

Elongated microstructures are most easily produced by heavily forging hot-pressed billets of the composition $Al_2O_3 + 1/4\%$ MgO. An additional benefit is the retention of finer grain sizes, and a typical structure is shown in Figure 3.14. This effect of MgO is discussed fully in Section 3.7.

3.4.2 Equiaxed Structures after Hot-Working

The area to the right of the single crystal in the composite of Figure 3.8 is dense and equiaxed, and differs in grain size from the area to the left of the single crystal by a factor of ~6 (14 u compared with 90 u). The coarser microstructure is similar to microstructures of samples hot-pressed (but not worked) at this temperature (Figure 3.15). Furthermore, the fine grained equiaxed structure possesses a crystallographic texture (see Section 3.5) which, because of the absence of grain elongation, must be a

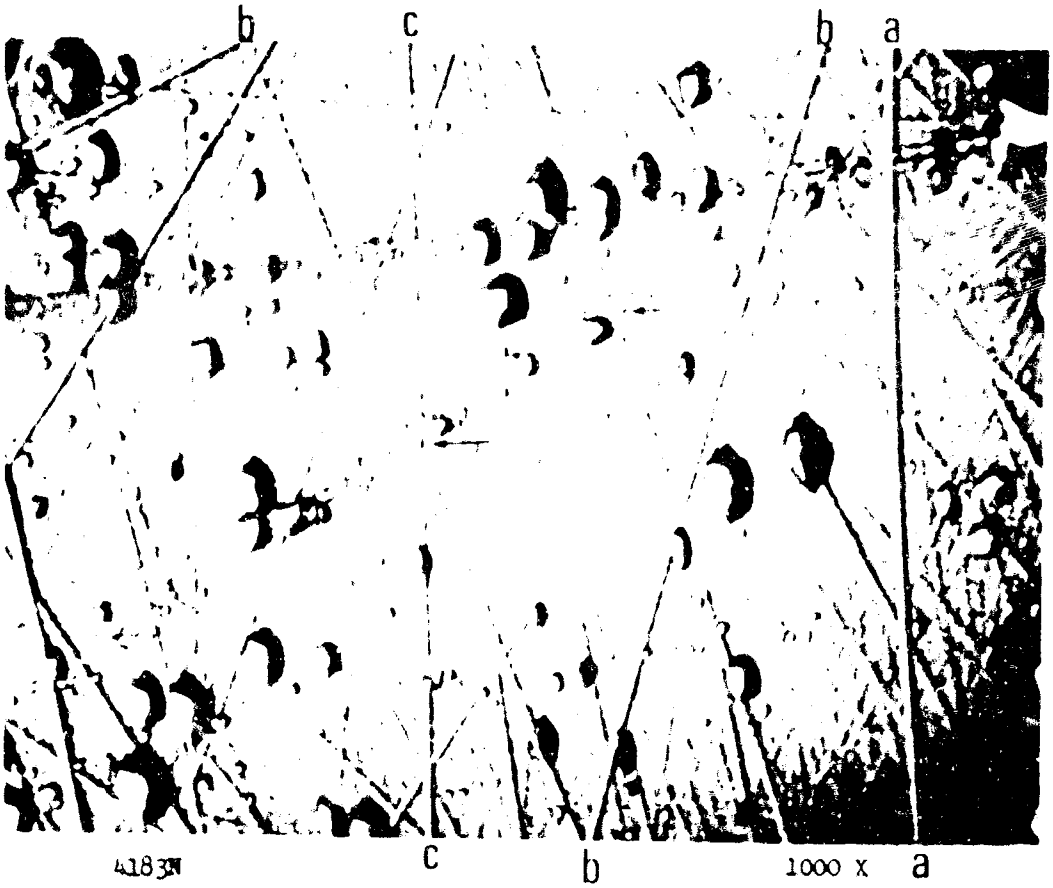

Figure 3.11 $\{11\bar{2}0\}$ prism plane of strain-anneal alumina single crystal after etching in $K_2S_2O_7$ at 700°C for 30 seconds. The smaller pits (arrowed) all lie in parallel rows. The etch furrows (A, B, C) are due to polishing scratches.

41836

1000 X

Figure 3.12 Polycrystalline matrix of billet FA-14 near strain-anneal single crystal after etching in $K_2S_2O_7$ at 700°C for 30 seconds.

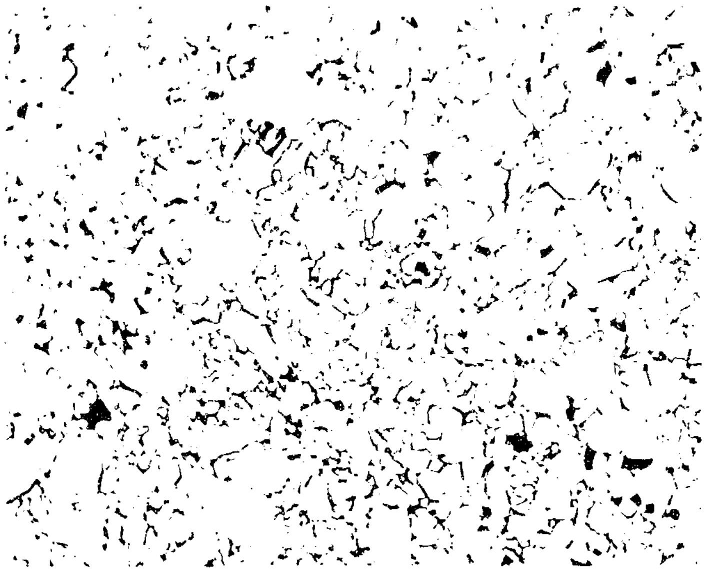

4032 (etched) 250 X

(a)

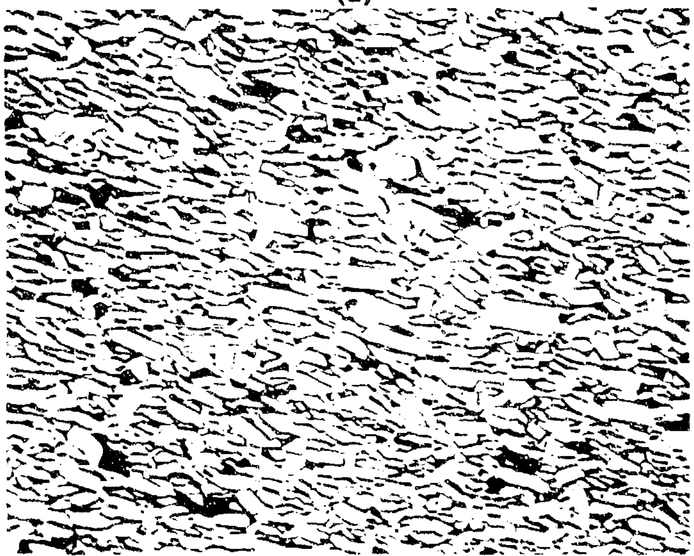

3970A (etched) 250 X

(b)

Figure 3.13 Microstructure of FA-34 (pure Al_2O_3) looking Parallel (a) and Perpendicular (b) to Press-forging Direction.

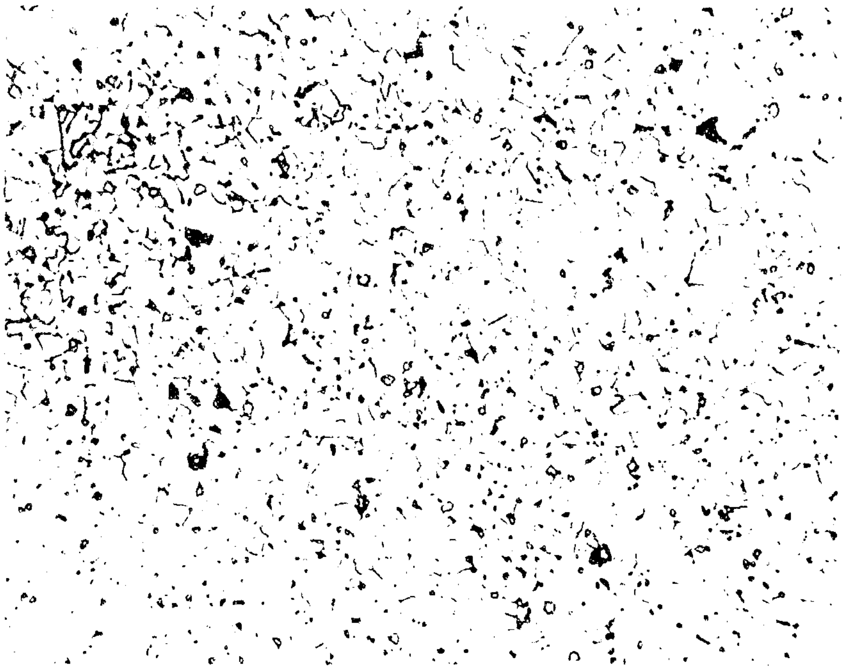

4159A a 500X

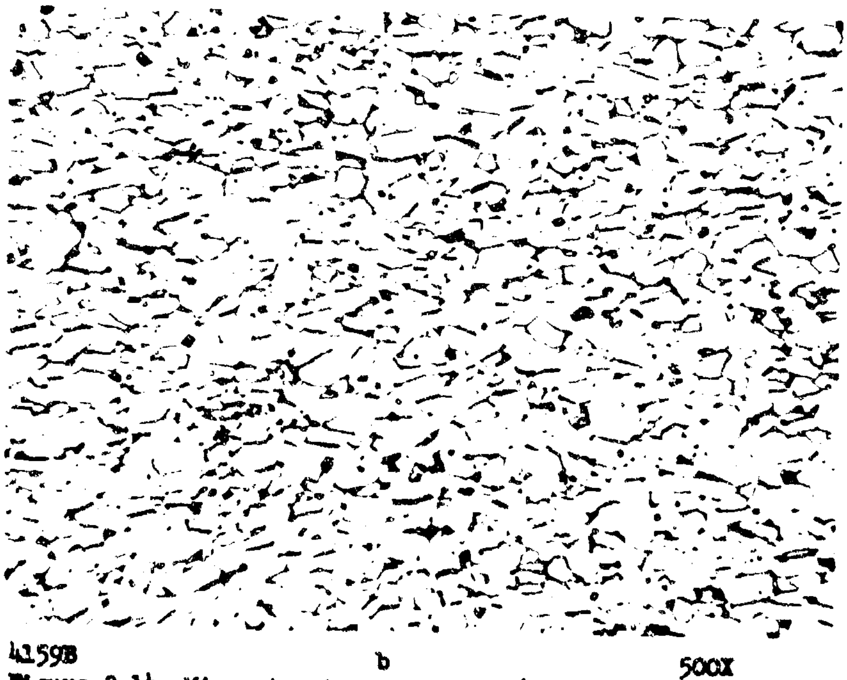

4159B b 500X

Figure 3.14 Microstructure of FA-52 (Al_2O_3+ 1/4% MgO) looking parallel (a) and perpendicular (b) to press-forging direction.

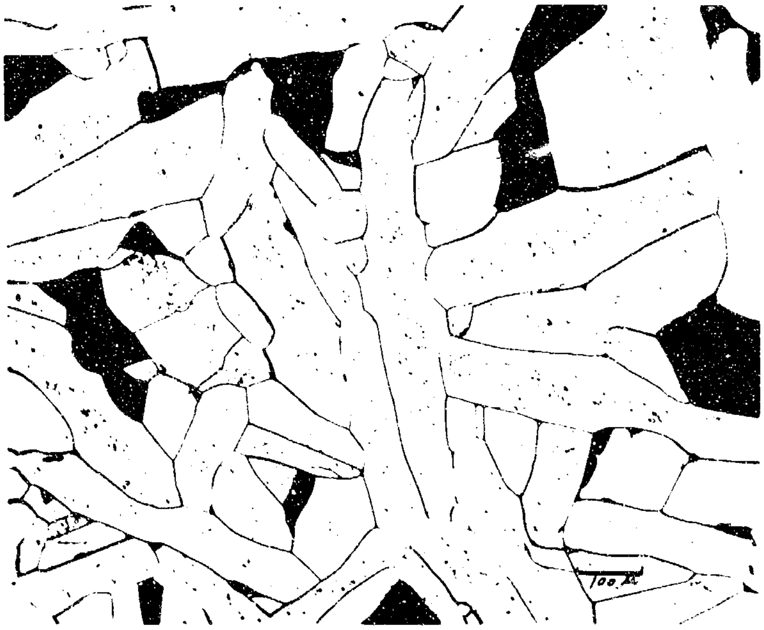

4357D 100 X

Figure 3.15 Microstructure of FA-97 after High Temperature Hot-pressing (1840°C) recrystallization, rather than a deformation texture. It has been possible to produce such microstructures throughout large portions of a billet, and Figures 3.16 and 3.17 are examples of billets where single crystal formation was suppressed, and large portions of the billet had a fine-grained equiaxed microstructure. This microstructure has been achieved most successfully in forging of powder billets, although it has been very difficult to ascertain the exact forging conditions needed to reproduce such structures. However, as these billets possess a marked recrystallization texture, it may be that a slow uniform strain rate is needed to obtain this structure.

3.5 Crystallographic Textures after Deformation and Recrystallization

Pronounced crystallographic textures are a further very interesting effect of hot working. These textures were observed in materials with both equiaxed and elongated microstructures. The preferred crystallographic orientation in equiaxed structures is almost certainly associated with a recrystallization texture; crystallographic texture in recrystallized metals is commonly found in equiaxed materials. In those materials containing both a microstructural and crystallographic texture, this texture could also be due to recrystallization and an example of such a large-grained elongated structure will be shown in Section 3.8. However, it is believed that relatively fine-grained elongated structures possess a deformation texture and evidence in support of this will be given in the next section.

In both these cases, the actual texture is the same, with the "c" axis of the individual grains aligned parallel to pressing direction of the forging. This basal texture was described in the previous work(3), but has now been examined in more detail.

Figure 3.18 shows a pole figure of billet FA-126 (deformed to a 63% height reduction in 15 minutes at 1850°C). The plane of the stereographic projection corresponds to the top of the disc-shaped billet, and the pressing direction is at the center. The contour lines refer to the intensity of a basal reflection above background, and the peak intensity near the center of the projection shows clearly the strong basal texture. The pole figure has not been extended past 30° because the basal reflection then falls off to the same level as background. It is also interesting that this texture exhibited an almost perfect circular symmetry, which is consistent with the radial symmetry present during press forging. Portions of this billet were examined by transmission electron microscopy and showed considerable evidence for dislocation networks and dipoles (Section 3.6); thus, this pole figure probably represents a deformation texture. Although no pole figures have been determined on samples with a recrystallization texture, other X-ray work (below) suggests that an identical pole figure would be obtained.

The determination of X-ray pole figures are particularly tedious, and for most determinations of crystallographic texture, it was convenient

Figure 3.16 Microstructure of FA-107, Forged for 2 Hours at 1870°C and 6000 psi. Note the equiaxed recrystallized structure.

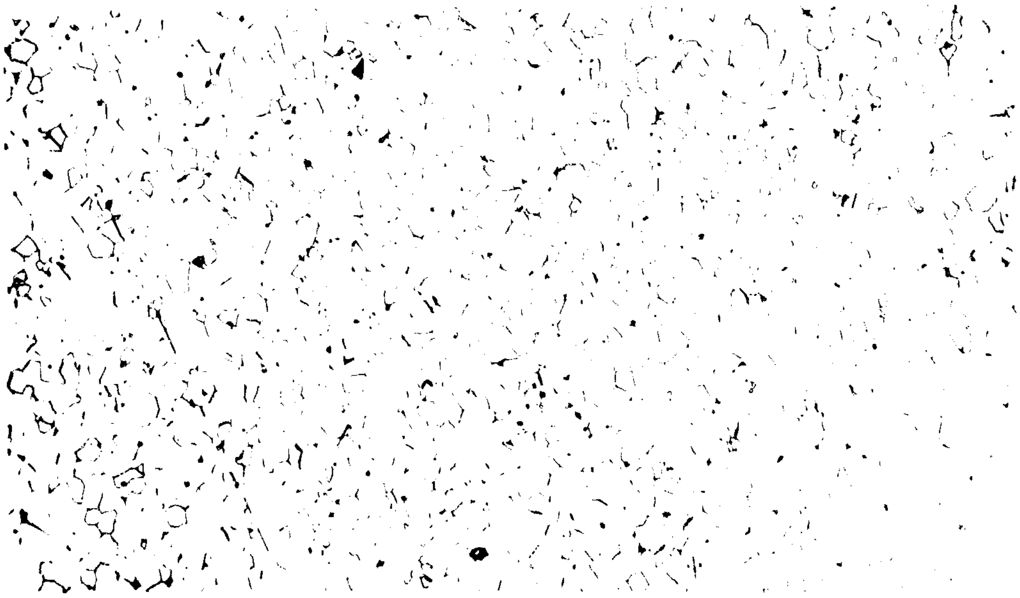

Figure 3.17 Microstructure of FA-109, Forged for 4 Hours at 1860-1880°C and 6800 psi. Note the equiaxed recrystallized structure.

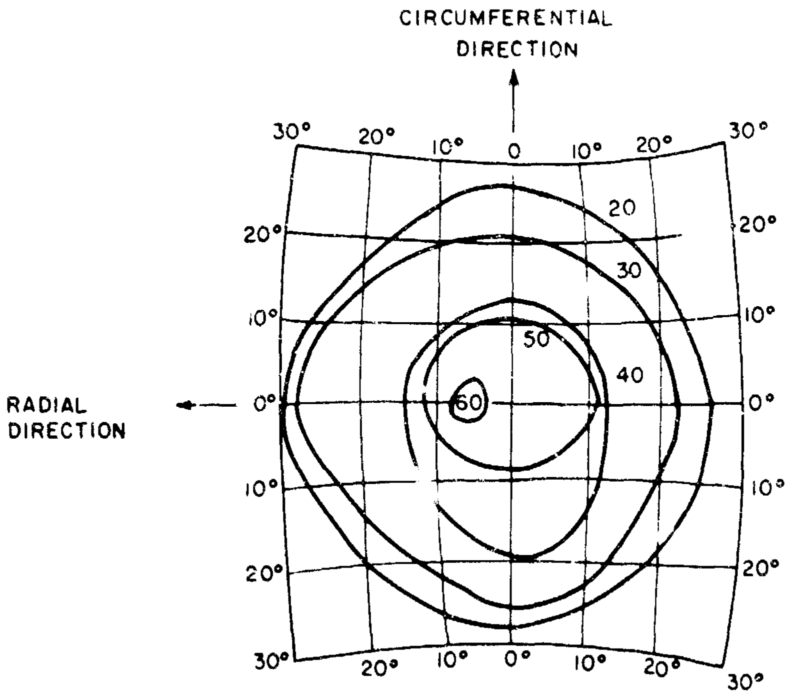

$Al_2O_3 + 1/4$ PERCENT MgO
63 PERCENT HEIGHT REDUCTION AT 1850°C
$\epsilon = -1.05$
$\dot{\epsilon} = 0.07 / \mathrm{min}$

Figure 3.18 POLE FIGURE FOR A BASAL REFLECTION FOR SAMPLE FA-126 to use ratios of basal [illegible]) to prism [illegible] reflections on surfaces parallel to and normal [illegible] the press-forging [illegible] Table 3.5 shows such measurements for [illegible] billets, all [illegible] h were thought to contain a deformation [illegible] which were [illegible] mechanical property tests (Section 3.10) [illegible] meaningful [illegible] can be made between reflections from the planes (110) and [illegible], of the form {1120} and {1010}) and basal [illegible] (00 [illegible] and (00 [illegible] of the form (0001) }.

In addition [illegible] from the plane (1.0.10) (i.e., 1.0.1̄.10) was [illegible] (0 [illegible] 1) ([illegible] 9°) and had favorable Bragg condit[illegible] [illegible] These studies revealed that preferred orientation [illegible] in all [illegible] forged to a height reduction greater t[illegible]

A plot of t[illegible] the (110), (030), and (1.0.10) reflection [illegible] height [illegible], 1850°, and 1900° is given in [illegible] It can be [illegible] the degree of orientation achieved at [illegible] given reduction i[illegible] independent of the forging temperature. The amount of texture determined in this way for the most extensively deformed specimen investi[illegible] height reduction at 1850°C) agrees well with the pole figure shown above.

Metallographic investigation of these samples also indicated a microstructural texture. Grain elongation was just apparent at 18% height reduction and became more marked at higher deformations. The extensive microstructural texture in pure alumina specimens was shown in Figure 3.13 while Figure 3.14 showed elongation in a specimen of Al_2O_3 + 1/4% MgO. The finer grain size of the latter specimen attests to the ability of the MgO addition to retard grain growth.

Microstructural texture could also be detected during chemical etching, even when no grain elongation occurred. Specimens cut and polished normal to the press forging direction, exposing basal planes for specimens with a pronounced basal texture, etched much more readily than specimens polished parallel to this direction (thereby exposing prism planes).

Recrystallization textures in equiaxed specimens were most commonly observed in specimens forged from powders, and Table 3.6 lists the X-ray evidence for this texture. It is not known why some specimens exhibited anisotropy mainly for basal reflections (FA-106) or mainly for prismatic reflections (FA-103, and FA-109) while others showed anisotropy for both sets of reflections. The degree of orientation indicated by these data approached that in the most extensively deformed specimens.

These optical properties of these recrystallized specimens are particularly interesting, as the crystallographic texture and high density leads to highly transparent polycrystalline specimens. This is possible because the texture allows specimens to be oriented so that light scattering due to birefringence becomes negligible. The effect can be seen in Figure 3.20; the birefringence in the randomly-oriented sintered sample (Lucalox) leads to scattering and to the loss of the image when the sample is raised off the paper,

TABLE 3.5

NORMALIZED INTENSITIES FOR VARIOUS CRYSTALLOGRAPHIC PLANES*
IN FORGED Al_2O_3 + 1/4% MgC

Specimen Number	Forging Temp. °C	Reduction (%)	Crystallographic Plane															
			01.2	104	11.0	006	113	024	116	122	124	030	1.0.10	0.2.10	0.0.12	134	226	1.2.10
Angle between (0001) and specified plane			57.6°	38.2°	90°	0°	61.2°	57.6°	42.3°	76.5°	64.4°	90°	17.5°	32.2°	0°	70.6	11.2°	39.8
Random Powder Pattern			75	90	40	1	100	45	80	5	30	50	15	7	3	7	13	11
FA-53B	1750	14.8	36 32	84 7	25 45	1 1	82 100	49 55	100 91	15 9	36 50	46 75	30 23	13 9	3 5	3 18	16 36	18 23
FA-93C	1750	16.8	31 37	79 67	20 35	2.4 1	72 100	35 52	100 82	12 11	31 44	38 78	23 17	11 9	4 1	10 15	15 26	15 19
FA-53D	1750	19.6	32 43	75 67	15 48	0 0	69 100	40 59	100 100	14 11	27 63	34 85	26 13	10 9	3 2	8 20	14 30	16 17
FA-93B	1750	22	31 40	84 52	17 48	3 1	71 100	37 58	100 92	15 12	26 52	29 88	34 14	13 8	5 1	6 12	15 32	18 16
FA-53C	1750	24.4	24 50	79 55	16 50	1 0	55 100	36 60	100 85	15 8	28 65	25 90	31 15	12 10	4 5	6 15	13 30	16 15
FA-93A	1750	28	28 34	80 45	17 55	2 3	59 100	30 59	100 62	13 7	24 52	23 93	34 12	11 7	4 4	5 20	13 34	17 16
FA-94B	1750	37	27 40	100 40	12 56	4 1	45 100	22 40	86 47	17 7	17 40	21 78	39 11	10 1	5 1	3 7	9 22	-- --

* See next page

TABLE 3.5 (concl'd)

NORMALIZED INTENSITIES FOR VARIOUS CRYSTALLOGRAPHIC PLANES*
IN FORGED Al_2O_3 + 1/4% MgO

Specimen Number	Forging Temp. °C	Reduction %	01.2	104	11.0	006	113	024	116	122	124	030	1.0.10	0.2.10	0.0.12	134	226	1.2.10
			Crystallographic Plane															
FA-81	1850	4.7	48 55	84 90	38 35	2 10	100 100	48 45	8 90	10 10	32 35	56 45	16 15	8 10	4 0	6 10	18 20	10 15
	1850	18	43 60	100 79	19 47	1 3	62 100	32 42	87 76	12 3	22 29	25 68	22 8	9 5	4 5	4 8	10 16	13 8
FA-86	1850	36 38	33 49	100 46	15 62	4 0	59 100	22 46	85 51	22 13	11 33	19 72	37 10	11 0	7 0	7 13	7 13	11 13
FA-87	1850	44 39	31 44	100 38	10 41	4 0	49 100	28 31	76 47	18 6	18 28	14 50	52 9	10 6	5 3	3 9	8 15	10 3
FA-52	1850	58	17 14	71 11	4 52	13 0	17 47	7 17	48 16	32 3	6 22	3 100	100 3	11 2	22 1	0 11	4 11	-- --
FA-90	1900	24	43 41	100 62	20 4[illegible]	4 0	64 100	34 47	90 86	12 10	20 48	28 79	24 12	12 7	4 2	4 12	10 24	-- --
FA-49	1900	44-48	40 37	92 51	15 43	3 0	57 100	36 46	100 89	14 6	26 43	18 100	33 11	9 9	5 3	5 14	10 31	16 14

* In each case, the upper lines give the normalized reflection from a section parallel to the press-forging direction, while the lower gives data from a section normal to this direction.

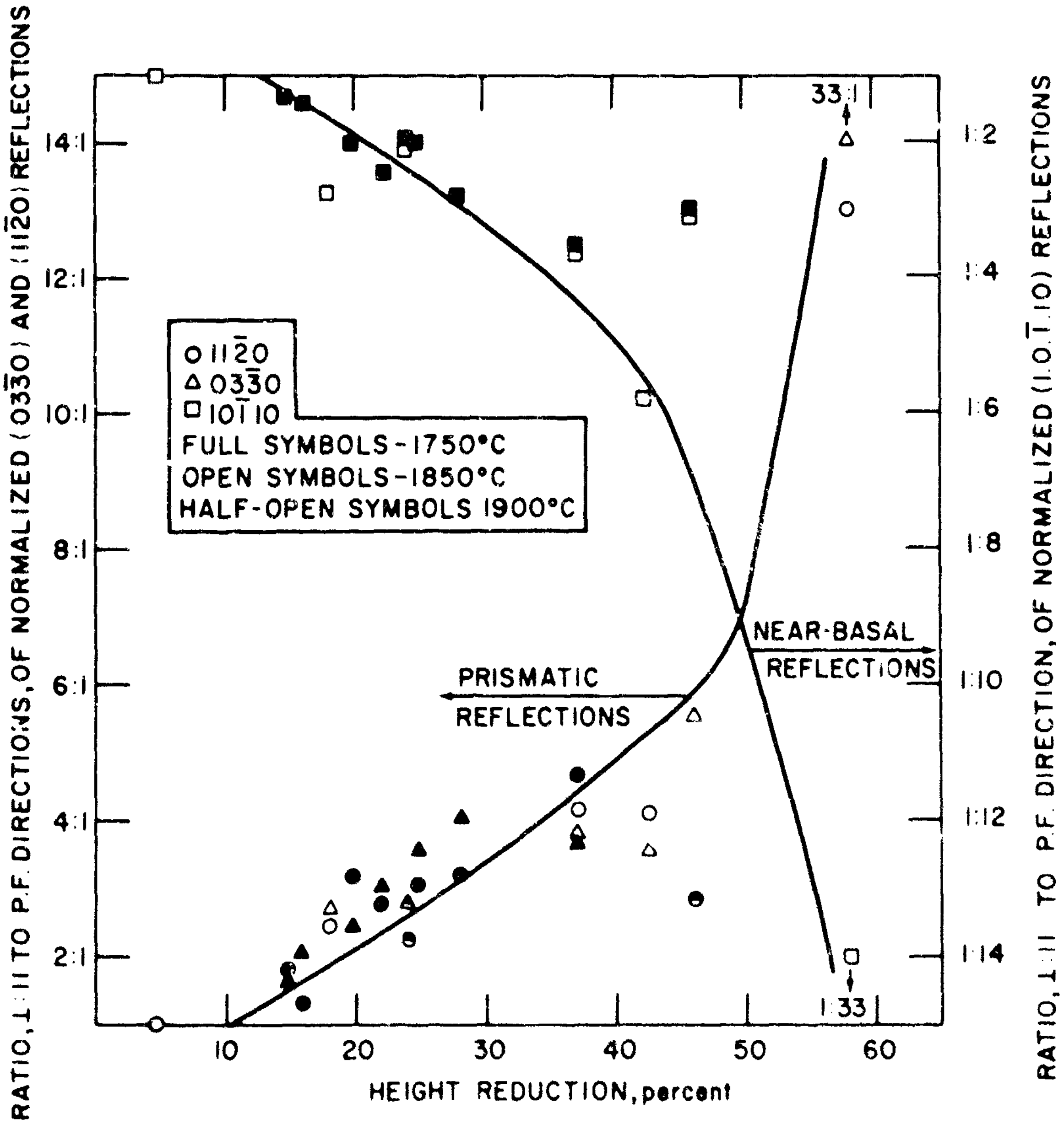

771122P

Figure 3.19. PLOT OF RATIO OF NORMALIZED INTENSITIES OF X-RAY REFLECTIONS FOR 2 PLANES, ONE PARALLEL AND THE OTHER PERPENDICULAR TO THE PRESS-FORGING DIRECTION

TABLE 3.6

X-RAY EVIDENCE FOR RECRYSTALLIZATION TEXTURES IN EQUIAXED SPECIMENS

		X-Ray Reflection				
Specimen		(030)	(110)	(006)	(00.72)	(10.10)
FA-45	parallel	19	15	0	17	66
	perpendicular	100	77	0	28	5
FA-47	parallel	1	12	8	18	100
	perpendicular	73	100	0	0	6
FA-103	parallel	0	0	0	0	11
	perpendicular	58	79	2	2	8
FA-106	parallel	16	47	36	15	63
	perpendicular	27	100	0	0	0
FA-107	parallel	18	12	14	14	77
	perpendiuclar	67	79	5	0	0
FA-109	parallel	8	6	7	2	9
	perpendicular	90	70	0	0	6
FA-110	parallel	3	4	5	9	24
	perpendicular	71	40	0	0	8
FA-136 (1/4% MgO)	parallel	8	14	5	5	37
	perpendicular	87	61	1	1	7

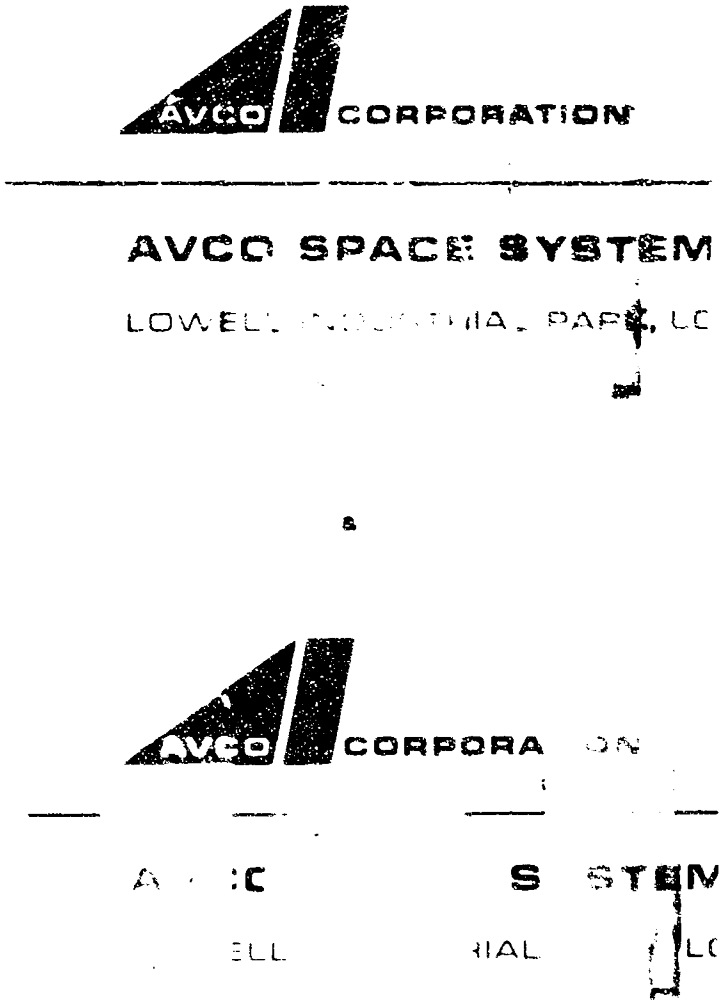

a

b

Figure 3.20 Comparison between optical transmission in forged alumina (left and right) and Lucalox (center). The samples are lying flat on the paper in (a) but raised 1" in (b).

even though the total transmission of this sample is quite good. This subject is under investigation under another program in our laboratory.*

Microstructural texture was also observed after forgings in the temperature range 1350-1500°C. (The experiments performed in this temperature range were listed in Table 3.2.) Of particular interest is specimen JC-8, which had been forged to a height reduction of 26% at 1350°C in 106 minutes at a load corresponding to 35,000 psi on the initial specimen diameter. The load was kept constant and the temperature increased to 1500°C, a total height reduction of 45% being achieved in 205 minutes. The texture observed can be seen in Figure 3.21 (it may be mentioned that the grain size increased by a factor of two during this experiment). Forging in this temperature range may be particularly interesting, particularly if it can be demonstrated that this range is below the "recrystallization temperature".

3.6 Deformation Mechanisms Occurring During Hot Working

It has been demonstrated that polycrystalline alumina is exceedingly ductile at the hot-working temperatures (see for example, Table 3.4) and it is pertinent at this point to discuss probable deformation mechanisms.

As in the case of most metals, slip and twinning have been well documented for single crystal alumina, and Table 3.7 lists the operative planes and direction, as well as the temperatures where each mode of plastic deformation has been found to be important.

The marked basal deformation texture is very good evidence that the primary deformation mode is basal slip; the texture arises from rotation of the basal planes, due to a superposed bending moment, so that they became perpendicular to the pressing direction. (The bending is due to constraints imposed by the punches, neighboring grains, etc.) Examination of thinned foils by electron microscopy of specimens possessing a deformation texture showed extensive evidence of slip, and similar evidence has been presented previously.(3) What was particularly interesting in the ease with which such dislocations were observed in these specimens, in contrast to the difficulty in detecting dislocations in hot pressed specimens or in specimens tested in bending in the temperature range 1300-1600°C. Figures 3.22 and 3.23 show evidence for dislocation networks and dipoles, respectively, and slip bands detected by chemical etching in a worked structure was shown previously.(3)

Although basal slip is undoubtedly the primary mode of deformation, it itself will now allow homogeneous deformation of a randomly oriented polycrystalline aggregate without void formation. Groves and Kelly(12) have analyzed the situation for alumina, and showed that even if both basal and prismatic plane slip were occurring, the Von Mises criterion would not be satisfied. Twinning may be occurring, although micrographic evidence of twinning was sparse at best. Alternatively, rhombohedral slip or a stress-enhanced Nabarro-Herring type of creep may provide the extra degree of freedom (the two experimentally observed slip systems will provide only four <u>independent</u> slip systems; the Von Mises criterion requires five). Although rhombohedral

---

* See footnote, page 25

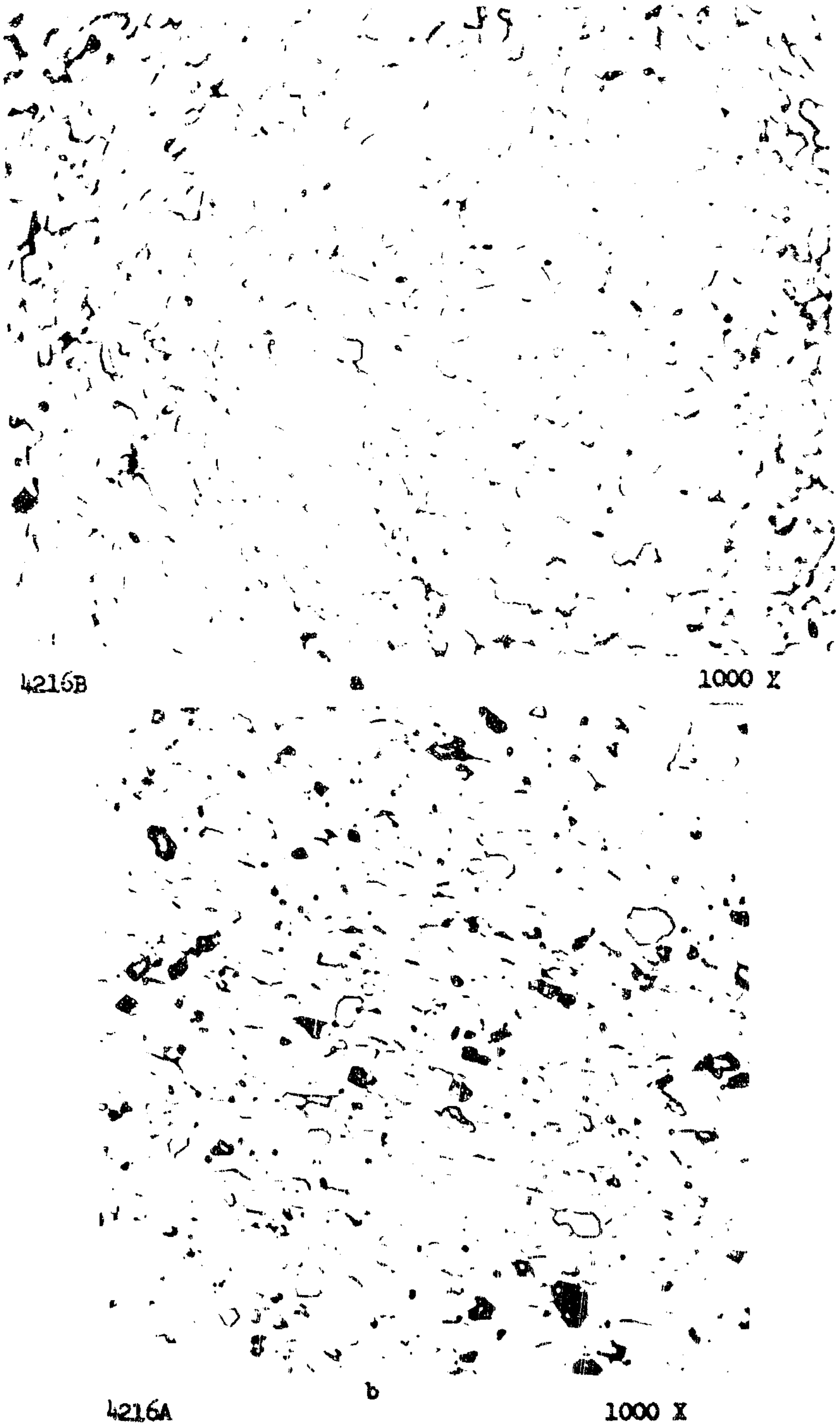

Figure 3.21 Microstructural texture in relatively low temperature press forged alumina. (a) Parallel and (b) Perpendicular to press forging direction.

TABLE 3.7

MODES OF PLASTIC DEFORMATION IN ALUMINA

System	Crystallographic plane* and direction	Temperature Regime where deformation mode has been observed
basal slip	(0001) $\langle 11\bar{2}0 \rangle$	900°C - 2000°C
prismatic plane slip	(1120) $\langle 10\bar{1}0 \rangle$	1600°C - 2000°C
rhombohedral slip	(?) $\langle 10\bar{1}1 \rangle$	?
basal twinning	K_1 (0001) n_1 $[\bar{1}010]$	23° - 1500°C
	K_2 $(\bar{2}021)$ n_2 $[10\bar{1}4]$	(hydrostatic pressure)
rhombohedral twinning	K_1 $(10\bar{1}1)$ n_1 $[\bar{1}012]$	-196° - 1500°C
	K_2 $(\bar{1}012)$ n_2 $[10\bar{1}1]$	
Nabarro-Herring creep	not applicable	1150 - 1950°C

* Based on morphological unit cell

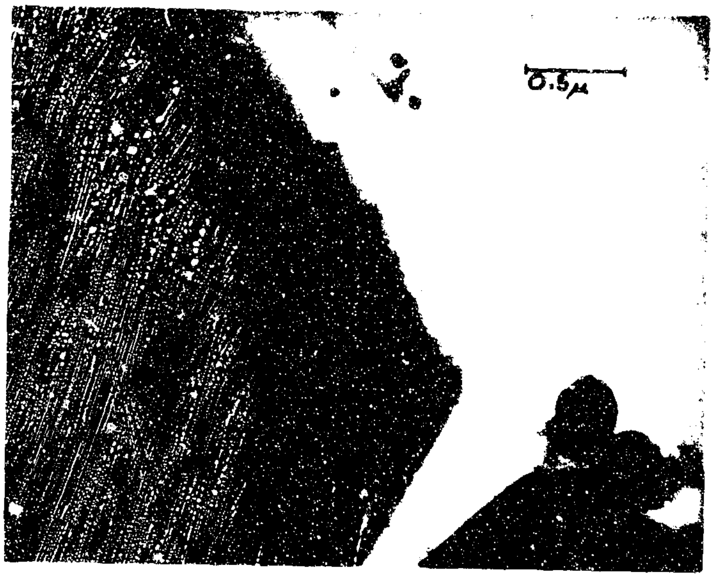

67327 30,000 X

Figure 3.22 Evidence for Dislocation Network in Thin Foil of Deformed Al_2O_3

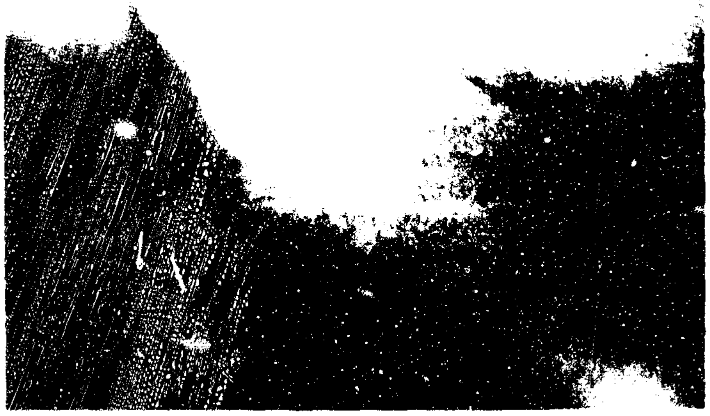

67328 40,000 X

Figure 3.23 Evidence for Dislocation Dipoles in Thin Foil of Deformed Al_2O_3

slip has not been experimentally confirmed in a tensile test in sapphire, Barber and Tighe(13) have found extensive evidence of dislocations with a rhombohedral Burgers vector. Also, Wachtman and Maxwell(14) observed creep in a sapphire specimen which was oriented so that no shear stresses could be resolved on either basal or prism planes; this probably deformed by rhombohedral slip. A similar situation occurs in zinc. Basal slip $(0002)\langle 11\bar{2}0\rangle$ is the major deformation mode, although $\{11\bar{2}2\}\langle\bar{1}\bar{1}23\rangle$ is a well-established secondary system, even though it is difficult to activate in tensile tests of single crystals at room temperature. In addition, slip on the systems $\{10\bar{1}1\}\langle\bar{1}\bar{1}23\rangle$, and $\{10\bar{1}1\}\langle 12\bar{1}0\rangle$ have been suggested, and at high temperatures, prismatic slip $\{10\bar{1}0\}\langle\bar{1}2\bar{1}0\rangle$. In all cases, constraints due to neighboring grains are the reason these secondary deformation modes become operative, even though the critical resolved shear stress is very much lower for basal slip. (In zinc, rhombohedral twinning is also very important.)

One electron micrograph of a hot-worked alumina specimen was obtained previously(3) which showed extensive dislocations, even though a strong basal reflection was operating. As this would be a condition for no contrast for either basal or prism plane dislocations ($g.b = 0$), this is further evidence for the probable occurrence of an additional (rhombohedral) slip system operating during hot working.

On the other hand, plastic deformation occurring via stress-enhanced vacancy diffusion, ie., Nabarro-Herring creep, has been found to be very prevalent in fine-grained alumina (Section 3.10), and it may be that some process such as this is providing the extra independent deformation system in hot working. Assuming a D of 10^{-9} at 1900 C (see Figure 3.41, Section 3.10) and a grain size of 5 u, a creep rate of .05/min is possible, and this is of the same order of magnitude as the observed strain rates (Table 3.3).

3.7 Effect of MgO on Primary Recrystallization

The inhibiting effect of MgO on grain boundary mobilities in alumina is well-known(15) and is the basis of the Lucalox process for sintering alumina to full density. The physical basis for this grain boundary inhibilitation apparently lies in the segregation of MgO (when added in concentrations of 1/4%) at grain boundaries. Much of the press forging work during the current research has been with the composition, Al_2O_3 + 1/4% MgO, which was intended to prevent excessive grain growth during the high temperature cycle needed for press-forging. This approach was successful, as 10 u was about the upper limit of grain size after forging. In addition, the inhibiting effect of the MgO additions on grain boundary mobility greatly retarded primary recrystallization. For example, no single crystals (arbitrarily defined as grains visible to the naked eye) have ever been observed after forging this composition. Under conditions which favor single crystal growth (powder compacts and long times at temperature), recrystallization only occurred in the most heavily deformed areas and resulted in equiaxed microstructures (Figure 3.24), which possessed a marked crystallographic texture. In all other cases, heavily deformed billets showed pronounced microstructural elongation deformation and a well defined texture.

Because of the lack of recrystallization, these latter specimens had appreciable dislocation densities within grains (see preceding section). Thus, the MgO aided in obtaining reproducibly a large group of unique alumina specimens-high in dislocations and possessing a marked microstructural and crystallographic texture - which were suitable for mechanical property evaluations and could be compared with hot-pressed or sintered alumina (Section 3.10).

One further possibility is that the differences in recrystallization between pure and magnesia-doped specimens originated in the distribution of strain energy in the deformed matrices. The magnesia containing samples will undergo less grain growth upon heating to the press forging temperature, and it may be that there is a more uniform distribution of slip in such a fine-grained matrix than in the coarser-grained pure alumina. (In particular, deformation bands due to single (basal) slip might be less prevalent in the finer-grained materials.) A somewhat similar case is known in TD-nickel,(16) where the optimum high temperature properties are achieved after successive strain and "recovery-anneal" cycles; the dislocation distribution is rearranged during each cycle so as to enhance resistance to recrystallization.

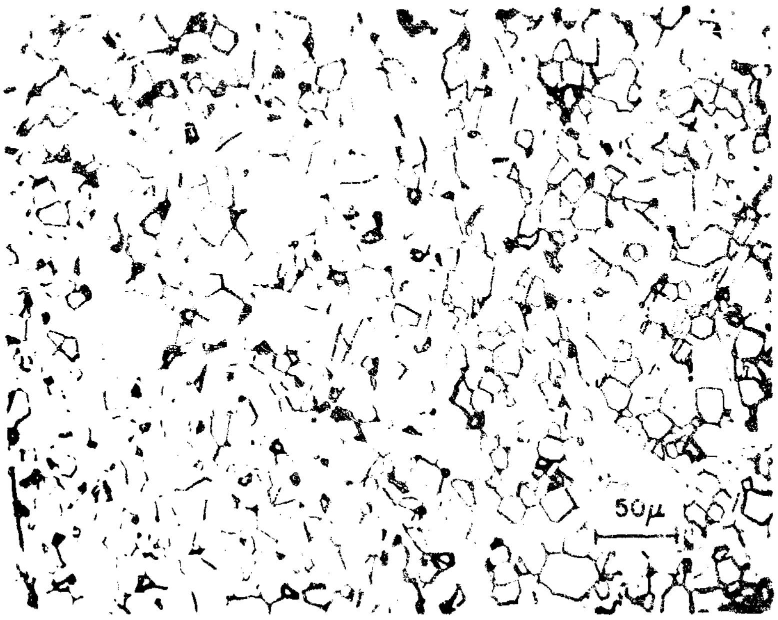

4384 250 X

Figure 3.24 Equiaxed Recrystallized Structure in Al_2O_3 + 1/4% MgO. This specimen had been forged from a powder.

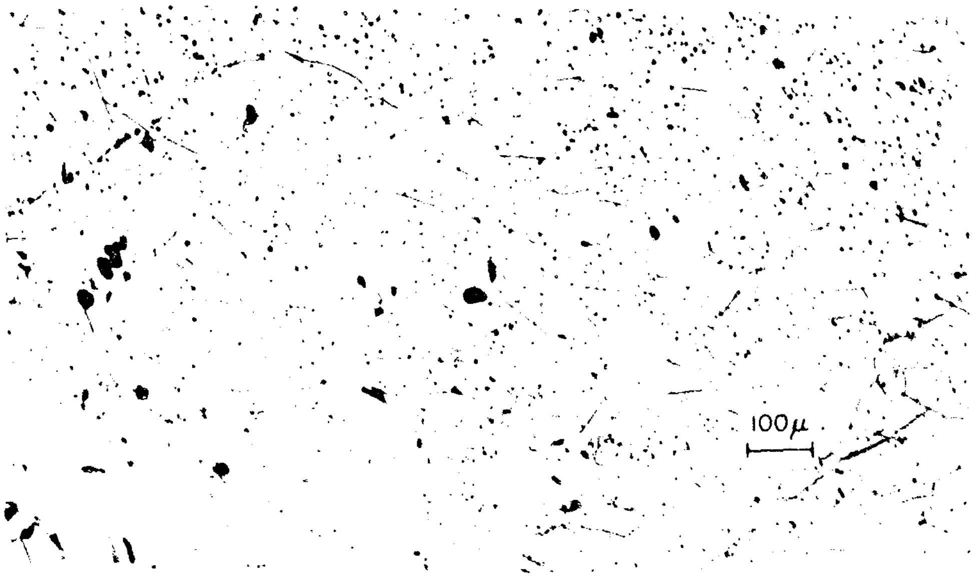

100X

Figure 3.25 Microstructure of FA-34 after Annealing for 2 Hours at 1900°C in Vacuum.

3.8 Annealing of Deformed and Recrystallized Materials

Selected high temperature (~ 1900°C) annealings have been conducted on both deformed and recrystallized structures, and these experiments helped clarify many details of the recrystallization process, particularly the distinction between deformed and recrystallized textures.

Figure 3.25 shows the microstructure of FA-34 after annealing at 1900°C for 2 hours (the unannealed microstructure is shown in Figure 3.13). Although some porosity was generated during this anneal, the main effect is an enormous increase in size, from 10 u to 80 u. This very rapid grain growth is about double that expected from an exaggerated grain growth mechanism*, and is thus attributed to the greater driving force resulting from recrystallization.

It was argued previously that elongated fine-grained structures occurred in samples with a deformation texture, while equiaxed fine grained structures occurred in conjunction with a recrystallization texture. The recrystallized structure shown in Figure 3.25 is relatively coarse and elongated, and it is pertinent to inquire about the origin of the microstructural anisotropy and whether it bears on the problem of the origin of the recrystallization texture.

It has already been mentioned that the deformation texture is unchanged upon recrystallization and alumina is in this way similar to some of the hexagonal metals - particularly zinc and its alloys$^{(17)}$. This may be evidence that the recrystallization texture originates in a preferred orientation in nucleation, rather than in enhanced grain growth rates of grains of a certain orientation. This is contrary to recrystallization in fcc metals, where the most recent evidence is that the texture arises from oriented growth.$^{(18)}$ However, it is difficult to see how the fine-grained equiaxed recrystallized structure shown in Figure 3.24 could have grown by oriented growth; anisotropy in a hexagonal material should also give rise to a microstructural texture, due to the uniaxial symmetry (c/a ratio = 2.73). However, there is unquestionably some anisotropy in grain growth rates in alumina, and this is manifested by platy or tabular grains in alumina hot-pressed or sintered at relatively high temperatures to produce large grains (see Figure 3.15). Thus, the correct interpretation for Figure 3.25 may be that the crystallographic texture arose from oriented nucleation, while the microstructural texture arose from oriented growth. This microstructural texture after recrystallization does not occur at small grain sizes because of the small amount of growth.

Recrystallization upon annealing was also observed in magnesia containing specimens, as shown in Figures 3.26 and 3.27. These specimens had been deformed to a height reduction of 18% and 50-58% respectively, and both showed

---

* I. Mistler, private communication, M.I.T.

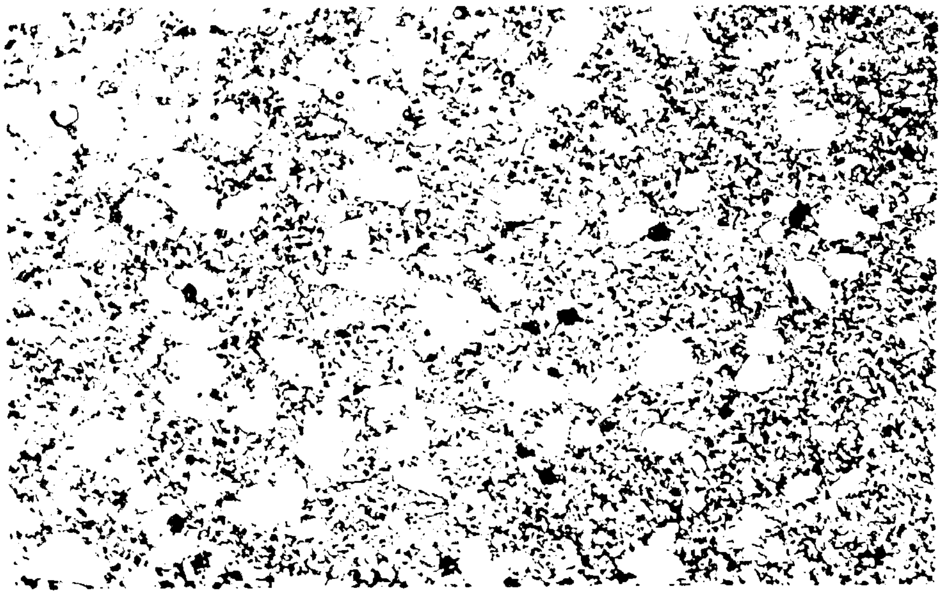

4414N-1 100X

Figure 3.26 Microstructure of FA 84 after Annealing for 5 Hours at 1860°C.

4414R-1 100X

Figure 3.27 Microstructure of FA-52 after Annealing for 5 Hours at 1860°C a microstructural deformation texture. (The microstructure of FA-52 before annealing is shown in Figure 3.14.) The annealed microstructural texture is more pronounced in FA-52, no doubt because the deformation texture was also stronger. It was surprising that the annealed grain size of FA-52 was not appreciably smaller than FA-84, as it has been more extensively worked (see Figure 3.1). This can probably be attributed to the sluggishness of recrystallization in these magnesia-doped specimens, which thus allowed considerable recovery (annealing out of strain energy by annihilation and diffusion of dislocations) before appreciable recrystallization commenced. This may also be the reason for the non-uniform grain growth in FA-84; areas of low strain underwent complete recovery during annealing.

To date, no successful annealing studies have been conducted on equiaxed recrystallized pure alumina specimens, but Figure 3.28 shows the microstructure of FA-136 (Al_2O_3 + 1/4% MgO, see Figure 3.24 for an unannealed microstructure) after an 80 hour anneal at 1800°C. Only normal grain growth occurred (the MgO suppressing all exaggerated growth), and this is very strong evidence that all dislocations had been removed during the recrystallization of the equiaxed structure.

Single crystal growth has also been observed during annealing, but only for specimens "quenched" at an early stage of the press-forging. Figures 3.29 and 3.30 are low magnification photo's of specimen FA-142, before and after annealing at 1900°C for 3 and 1/2 hours. This powder billet had been held at temperature and pressure for 1/2 hour during hot forging rather than the 1-5 hours usually used for such billets. These photos demonstrate the not unsurprising fact that single crystal growth is a critical function of time and deformation. Annealing a portion of a billet containing a well-developed single crystal either produced normal grain growth or exaggerated grain growth of the single crystal (Figure 3.31).

Finally, Figure 3.32 is a composite micrograph of a portion of FA-106 further removed from the composite area shown in Figure 3.8. (The fine grained matrix at the left of this micrograph is part of the same general area, but separated by ~7 mm, from the fine-grained matrix at the right of Figure 3.8.) The large grains may have grown by exaggerated grain growth after recrystallization. There are two possible gradients in this portion of the billet, a grain size gradient resulting from primary recrystallization, the grains becoming smaller further from the center of the billet due to the increasing shear deformation, and a thermal gradient, due to the heating arrangement (the die body being the susceptor); the smaller grains being at a higher temperature. Such gradients could give rise to the observed radial gradient in grains which had experienced exaggerated growth. However, this micrograph is similar to Figure 3.26, wherein the microstructure was though to result from recrystallization. It may therefore be due to a second primary recrystallization caused by continued deformation after the first primary recrystallization. The gradient in recrystallized grains would then follow the expected gradient in shear strain. However, such further deformation

4144T-1 100 X

Figure 3.28 Microstructure of Equiaxed Al_2O_3 + 1/4% MgO after 80 Hour Anneal at 1800°C. Note the lack of appreciable grain growth during this annealing.

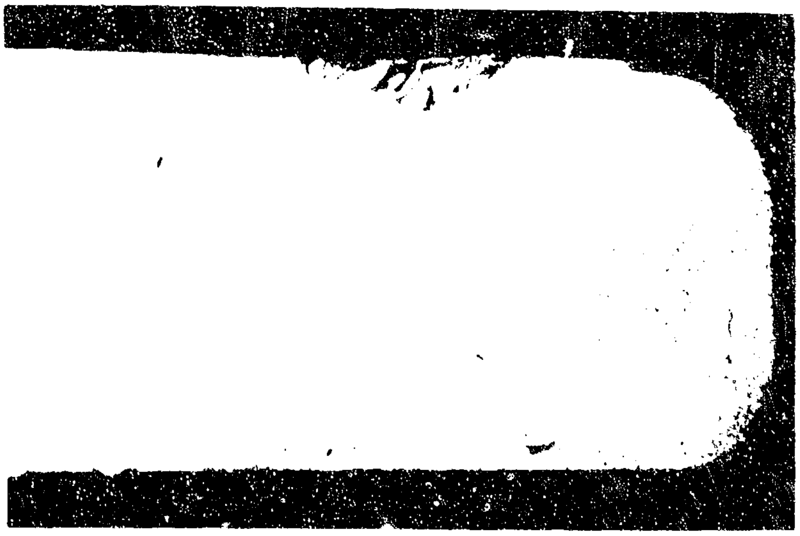

41442 10X

Figure 3.29 Macrophotograph of FA-142, "quenched" before Press Forging had been completed.

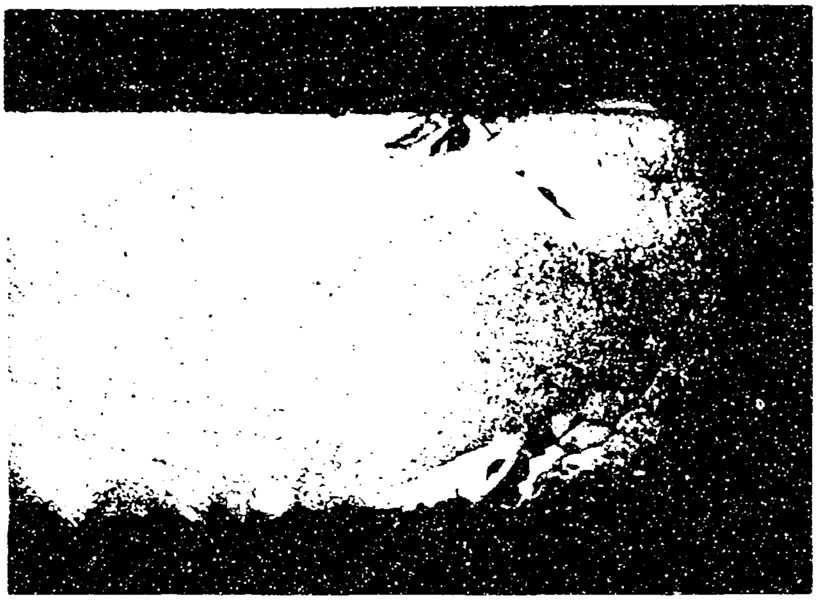

4414-AA-1 10 X

Figure 3.30 Microphotograph of FA-142 after 3 1/2 Hour Anneal at 1900°C in Vacuum.

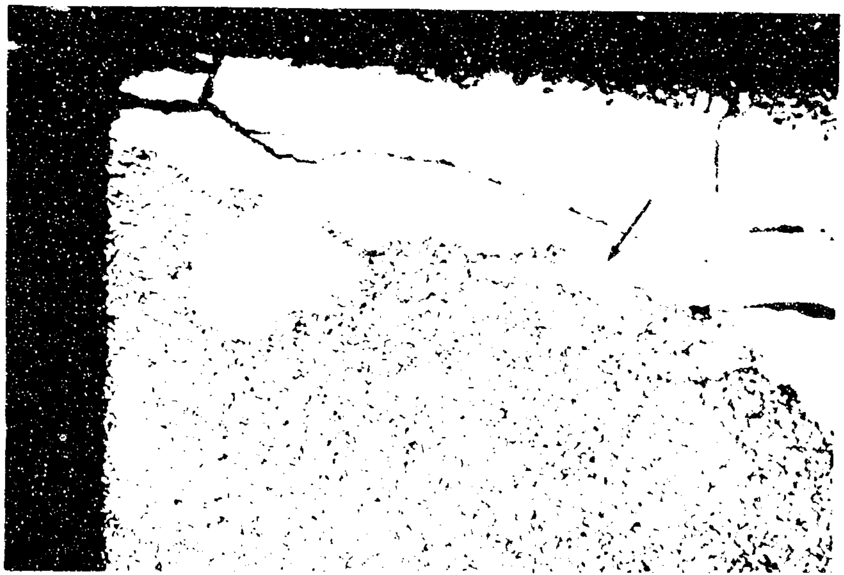

4414-Q-2 20 X

Figure 3.31 Exaggerated Grain Growth of Single Crystal in FA-110 During 3 Hour Anneal at 1900°C in Vacuum. The arrow denotes the position of the single crystal before annealing.

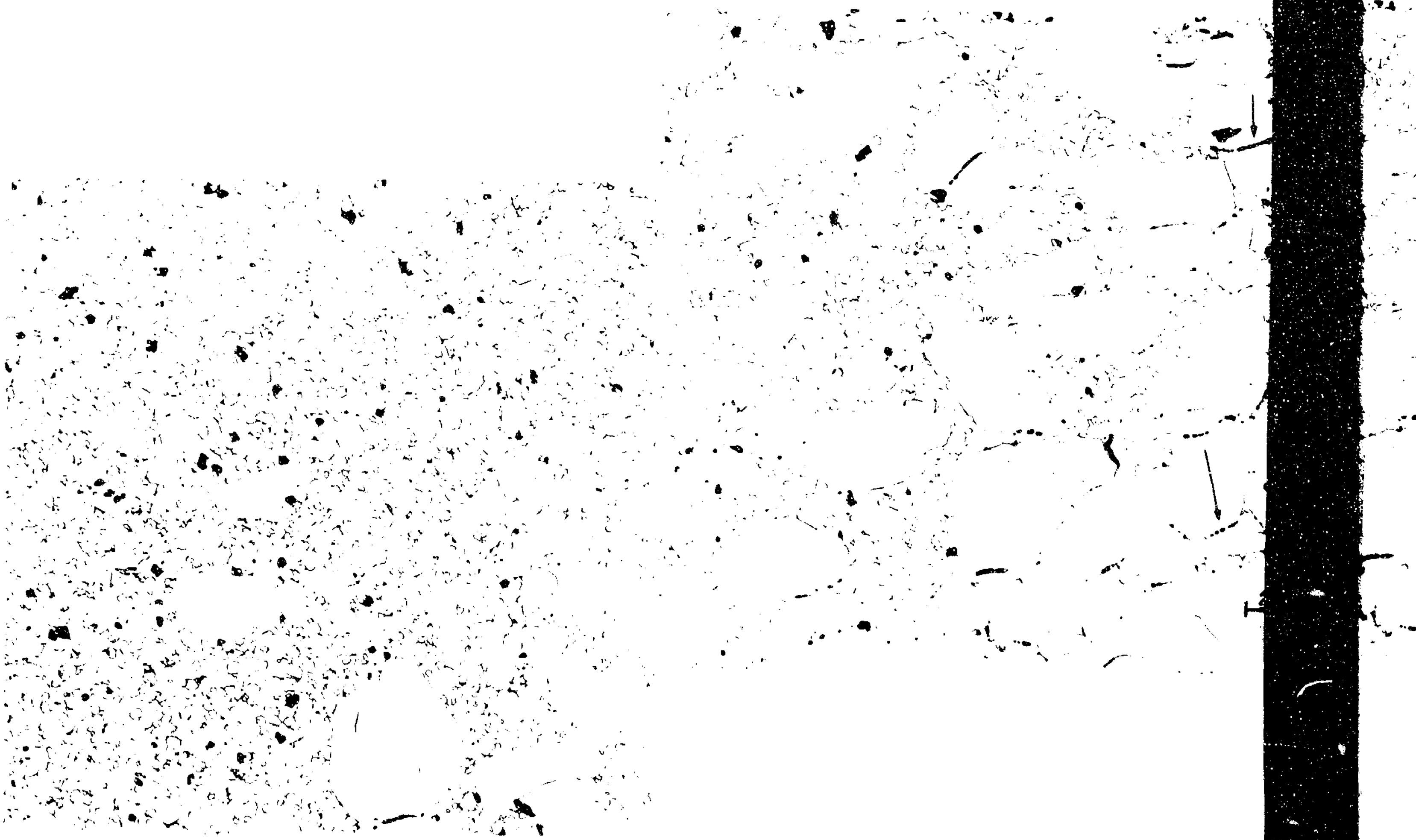

Figure 3.32 Composite photograph of popul
in FA-106. Note the radial g
of large grains. The arrowed
in a later section.

A

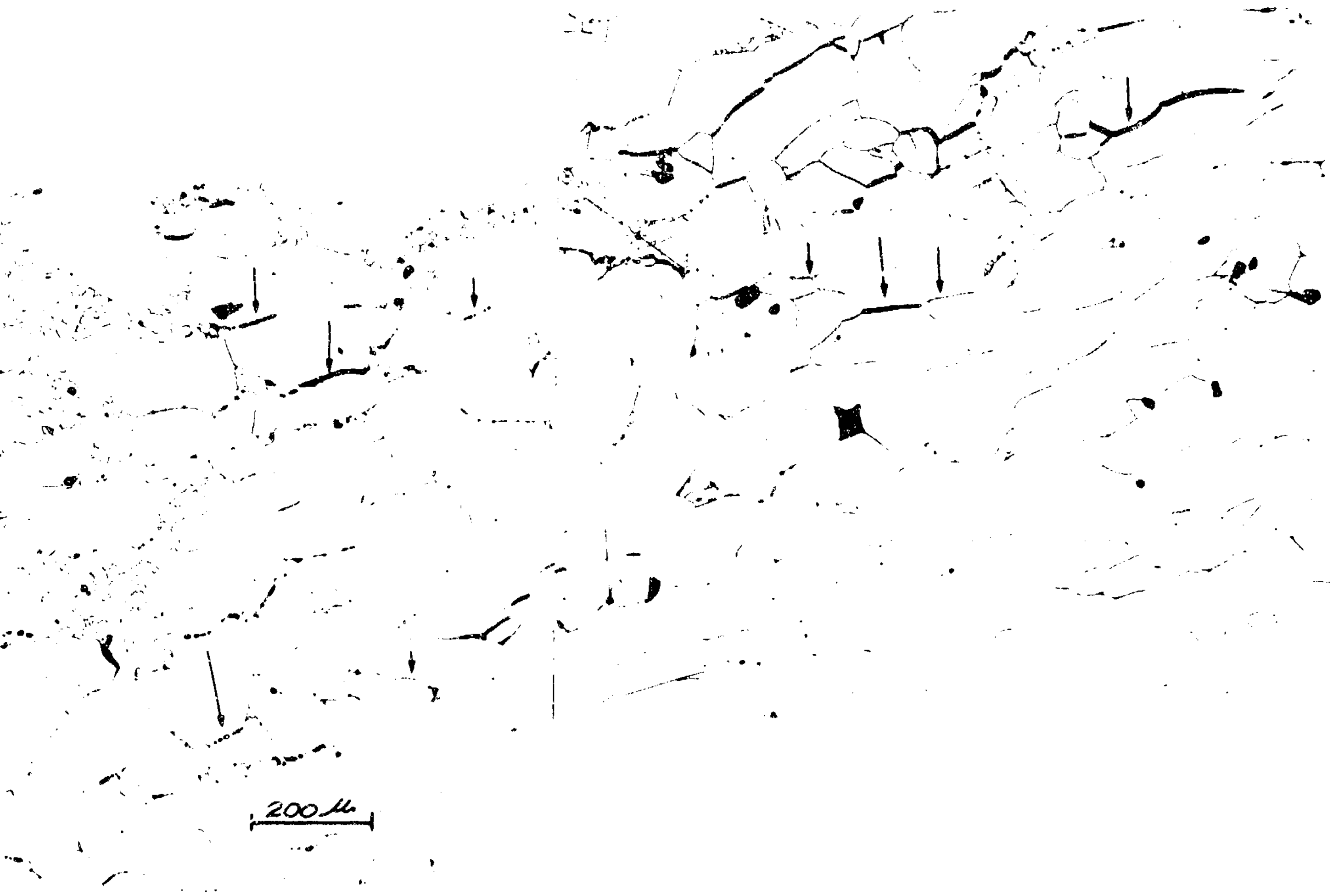

te photograph of populat on of larger grains
06. Note the radial gradient in the number
e grains. The arrowed features are discussed
ter section.

B

would require extensive nonbasal, non-prism plane slip, due to the pronounced recrystallization texture (there would be zero resolved shear stresses on both basal and prism planes). It will probably be necessary to experimentally separate deformation processes from recrystallization processes to resolve this point.

3.9 Removal of Porosity

The application of stress during ordinary pressure sintering greatly reduces the temperature necessary for the removal of the last porosity. It is now well established(19) that the densification mechanism in the final stages of this process is diffusional, the applied stress increasing the concentration gradient between the pores (source) and grain boundaries (sink). In normal (pressureless) sintering, the driving force for densification arises from the surface tension of the pores, and a certain concentration gradient of vacancies is established. The additional concentration gradient in pressure sintering can be described by the Kelvin equation:

$$\Delta C = \frac{Co\,\Omega}{kT} \left(\sigma_B - \sigma_P \right)$$

where Co is the equilibrium vacancy concentration, Ω the vacancy volume, σ_B and σ_P the stress on a grain boundary and on a pore, respectively, and k and T have their usual meaning. The following simple argument shows that σ_B must always be larger than σ_P. The normal compressive stress at a pore surface must be equal to the applied pressure σ if one assumes the solid compact distributes the pressure hydrostatically. Grain boundaries must also transmit this same force, but as a grain boundary will intersect a random number of pores, the solid area of the grain boundary must sustain, on average, a higher force. The success achieved in pressure sintering occurs because a larger flux of matter can travel along this increased vacancy gradient, and thus eliminate porosity, at temperatures low enough so that grain growth is limited. In other words, the two factors of importance are a high vacancy flux and a short source-sink distance.

The porous microstructure to the left of the single crystal in Figure 3.8, and the high temperature hot-pressed sample shown in Figure 3.15 are examples where the grain growth rates were high enough to isolate pores sufficiently far from grain boundaries so that they could not be removed by diffusion of vacancies. Thus, it appears that in the recrystallized area in Figure 3.8 (forged from powder), either the deformation or the subsequent recrystallization must have been effective in removing pores. The entrapped porosity in the left of the single crystal of this figure, as well as the porosity shown in the large etched single crystal in Section 3.3, suggested that the movement of a grain boundary during recrystallization may itself not be a particularly effective way of removing porosity, even if that grain boundary intersects a pore. This is not surprising, as a similar situation arises in pressureless sintering, whenever exaggerated grain growth occurs; porosity becomes entrapped because the mobilities of the grain boundaries of growing secondary grains are high enough to allow them to sweep past pores.

One possible explanation is that the deformation during hot working contributes to removal of porosity. The observation that the decreasing porosity gradient in Figure 3.8 seems to parallel the increasing strain gradient is evidence for this. The exact mechanism of porosity removal during deformation is not known with any certainty, but the following may be suggested:

1. "Pipe" diffusion along dislocations to grain boundaries;
2. Destruction of pore equilibration (shape, size, etc.) by deformation of the surrounding matrix;
3. Grain boundary shearing or sliding; and
4. Closing of pores by self welding. This last process requires that the gas entrapped in the pores have some solubility in the matrix.

It would appear that further theoretical work is needed to ascertain if any of these (or others) may be important in the present process. However, while rapidly moving boundaries of recrystallizing grains may not be able to remove porosity, the recrystallized structure may be much more suitable for subsequent densification than the original matrix. Such a situation is suggested by some of the work with powder billets. Quenching a forged powder billet as soon as the rate of punch travel has slowed down (~ 1/2 hour) lead to a porous partially recrystallized microstructure; this is shown in Figure 3.33. However, leaving such a billet under temperature and pressure for long times (4-6 hours) leads to the dense optically-transparent polycrystalline specimens shown in Section 3.5. The transparency is, of course, excellent evidence that <u>all</u> porosity was removed, as any remaining pores would scatter light.

One likely mechanism by which the recrystallized structure could effect pore removal is if all pores were situated on grain boundaries after recrystallization, while before recrystallization, they were far removed from the grain boundaries of the deformed matrix. This, of course, implies that the nucleation could take place at pores, as well as at grain boundaries, deformation bands, etc. Although such an effect has not been observed in the recrystallization of metals, there is abundant evidence(20) that coarse solid precipitates can enhance nucleation, and that there must be a critical degree of dispersion that is particularly effective in enhancing nucleation.(4)

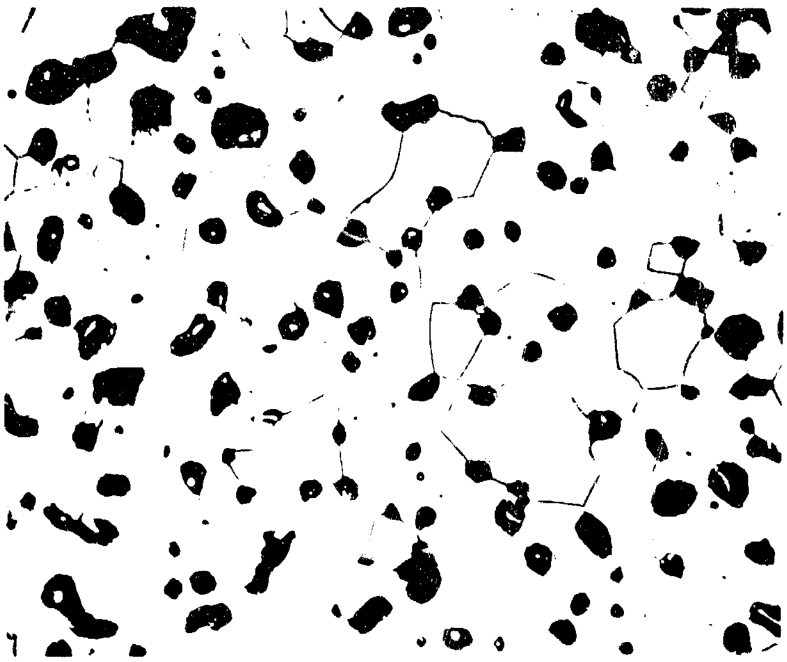

Figure 3.33 Porous Recrystallized Area in Powder Billet "Quenched" after Forging for 1/2 Hour.

The enhancement of nucleation is undoubtedly due to the local enhancement of the dislocation population, and large pores would have a similar effect.

A further effect leading to possible pore entrapment on recrystallized grain boundaries is that originally due to Zener(21). Pores (or inclusions) intersecting boundaries exert a drag on the boundary, lowering the boundary mobility and eventually leading to cessation of grain growth (at constant driving force) at a critical grain size. The critical grain diameter, where the drag balances the driving force, is proportional to r/f, where r is the radius of the pore or inclusion and f is its volume fraction. This relation, although never experimentally verified quantitatively, is generally accepted.

One can picture a situation such as shown in Figure 3.34, where the nucleation occurs at a pore and the boundary remains pinned at this pore. If we assume that a recrystallization nucleus formed at each pore, the fully recrystallized structure should be capable of undergoing extensive further densification and pore removal by normal vacancy flow (i.e., similar to the final stages of sintering). Figure 3.33 may be good evidence that such a mechanism can occur, as there is certainly a non-statistical distribution of pores on boundaries.

The micrographs shown in Figure 3.35 and 3.36, taken from a forged solid billet, (originally 95% of theoretical density) may be further evidence for such a mechanism. Here, the single crystal contained large amounts of porosity (which may appear exaggerated in this photo due to etching), while the area showing the duplex microstructure is dense. The fine-grained matrix is believed to be recrystallized from extensively forged material (cf., the polycrystalline matrix adjacent to the single crystal) and the larger grains in this region probably grew by exaggerated grain growth after the entrapped porosity had been removed from grain boundaries by a normal sintering process.

As porosity interacts with grain boundaries according to the Zener analysis, it is also possible for a grain boundary in the course of recrystallization to drags its complement of pores with it, if the driving force is powerful enough to overcome the drag due to the pore. Such a mechanism might explain the porosity at grain boundaries shown arrowed in Figure 3.32, and also the aggregation of pores in boundaries into voids. This has already been observed in the case of fission gas bubbles in UO_2(22).

However, another interpretation of Figure 3.32 may be suggested. It can be seen that most, if not all, of the pores are on "horizontal" rather than on "vertical" grain boundaries. The thermal gradient present in this billet was from left to right (the hot furnace being situated towards the right at the outside of the billet) and it may be that the pores are traveling along the thermal gradient. Such pore travel occurs because when pores move in this way, matter is removed from hotter to cooler regions, thus minimizing the gradient. This occurs regardless of the mechanism of pore travel (i.e., surface diffusion, evaporation-condensation, etc.) and such pore travel has also been observed in UO_2(23).

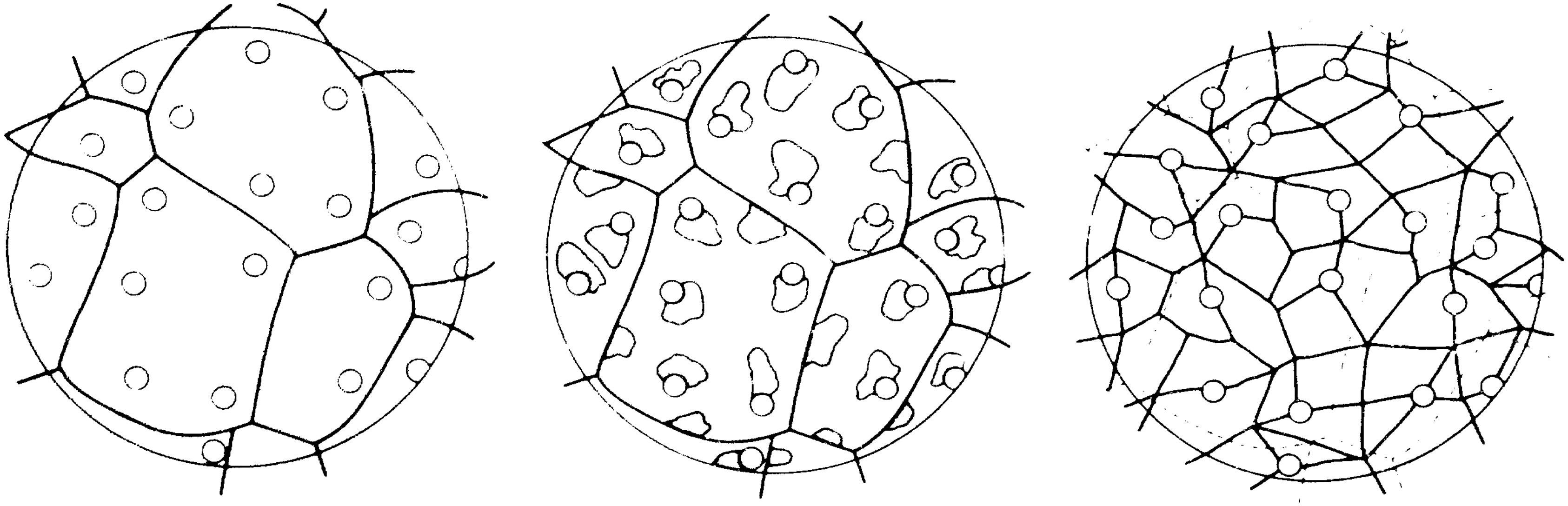

POROUS MATRIX BEFORE RECRYSTALLIZATION

EARLY STAGE OF RECRYSTALLIZATION

FULLY RECRYSTALLIZED STRUCTURE

Figure 3.34 SCHEMATIC REPRESENTATION OF NUCLEATION OF STRAIN-FREE RECRYSTALLIZED GRAINS AT PORES AND GRAIN BOUNDRIES IN A POROUS COMPACT

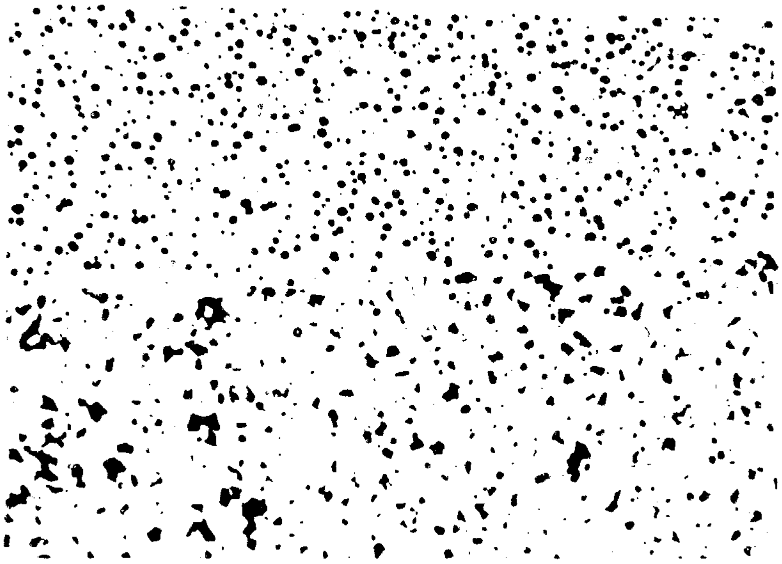

Figure 3.35 Porous Single Crystal in Forged Solid Billet FA-40 (originally 95% of theoretical density)

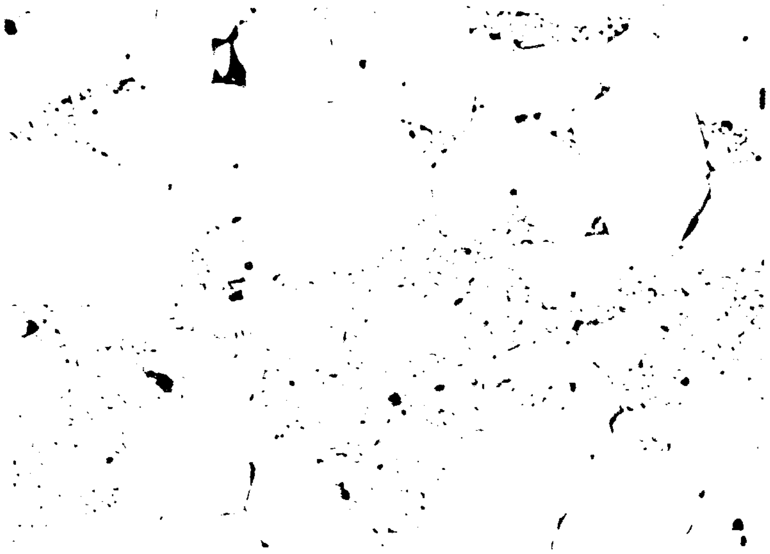

Figure 3.36 Dense area in billet FA-40 Showing Some Exaggerated Grain Growth

3.10 Mechanical Properties of Press-Forged Alumina

A preliminary investigation of mechanical properties of press-forged alumina, some of which was reported in last year's report,(3) suggested that these worked alumina specimens were stronger than hot-pressed and annealed specimens of equivalent density and grain size (data of Passmore, Spriggs, and Vasilos(24)). These data are included in Table 3.8, and it can also be seen that specimens containing 1/4% MgO were considerably stronger than the pure alumina specimens, no doubt due to the finer grain size. No adequate control samples were available however, to ascertain if the relatively high strengths of the forged specimens were due to an orientation effect due to the strong basal texture or whether some other explanation, such as changes in grain boundary "character" due to the working, were tenable.

Accordingly, a number of solid billets, each containing 1/4% MgO to prevent recrystallization and retard grain growth were forged to various height reductions (up to 50%) at temperatures of 1750-1925°C. Standard bend bars, 1.75" x .2" x .1" were cut from these forged billets and tested (with as-machined surfaces) at various temperatures from -196 to 1550°C.

All billets which had been deformed to a height reduction greater than 10-15% exhibited a crystallographic deformation texture (Section 3.5). Microstructural evidence of this texture was also observed in the difference of etching rates on sections cut parallel and perpendicular to the press-forging direction (for specimens deformed >15%) and by marked grain elongation (for specimens deformed >30%).

Strength results at -196 and 1200°C (below which any plastic deformation occurred) are listed in Table 3.9 and plotted in the form of histograms in Figure 3.37. The central conclusion that stands out is that no loss in structural integrity occurred due to the hot working. The histograms are arranged in order of increasing deformations at increasing working temperatures, and the strength values at -196°C, considering the associated scatter, was virtually the same for all groups of specimens. At 1200°C, the strengths of forged specimens were slightly below those of the as-hot pressed specimens. However, the forged specimens were stronger than the specimens hot-pressed and annealed (without load) at the forging temperature; the latter were the weakest specimens tested. Furthermore, strengths at 1200°C seemed to fall off as the forging temperature increased; the 1750°C specimens were the strongest. The strongest specimen at -196°C (86.4 kpsi - FA-94) was also from this group and it may be concluded that forging temperatures should be kept as low as possible for good mechanical properties. This temperature, of course, must be consistent with reasonable forging rates. This low forging temperature also has the advantage of maintaining finer grain sizes at a given degree of crystallographic orientation; it has been shown earlier (Section 3.5) that the degree of texture is dependent mainly on the amount of forging, but not on the temperature of forging.

TABLE 3.8

PRELIMINARY BEND STRENGTH RESULTS FOR PRESS FORGED Al_2C_3 and Al_2O_3 + 1/4% MgO

Billet	Comments	Temperature °C	Bend Strength* Kpsi	Bend Strength Reference Value Kpsi
FA-19	Pure Al_2O_3, duplex structure, average grain size of large grains 40 u, small grains 5 u, forged from powder	-196	29.3	
			28.8	
		23	26.3	9.7^{+5}_{-1}
			23.3	
			26.8	
			27.8	
		1200	20.6	6.1 ± 1.5
			20.6	
			20.6	
		1400	9.9	
			10.0	
FA-34	Pure Al_2O_3, microstructural texture, grain size 16 u x 38 u forged from powder	23	58.0	16.2 ± 5
			67.0	
			59.9	
			57.0	
			54.3	
			41.8	
		1300	24.0	8.4 ± 1.5
			28.1	(at 1200°C)
FA-52	Al_2O_3 + 1/4% MgO 5 u grain size, 52% HR at 1860°C	23	55.9	45.1 ± 15
			54.2	
		1200	41.5	23.3 ± 5
			48.6	
		1300	35.3	
			$\epsilon_T = 0.025\%$	

***** **See next page**

Note: HR = Height Reduction

TABLE 3.8 (concl'd)

PRELIMINARY BEND STRENGTH RESULTS FOR PRESS FORGED Al_2O_3 and Al_2O_3 + 1/4% MgO

Billet	Comments	Temperature °C	Bend Strength* Kpsi	Bend Strength Reference Value Kpsi
FA-52 (cont'd)		1350	29.0 ϵ_f = 0.05%	
		1400	27.5 ϵ_f = 0.10%	
		1500	20.1 ϵ_f = 0.52%	
FA-55	Al_2O_3 + 1/4% MgO 9 u grain size, 35% HR at 1820°C	23	48.7 31.5 33.5	31.2 ± 10
		1300	25.3 ϵ_f = 0.01% 26.3 ϵ_f = 0.013%	16.2 ± 5 (at 1200°C)
		1400	19.8 ϵ_f = 0.013% 22.7 ϵ_f = 0.026%	
		1450	18.7 ϵ_f = 0.049%	
		1500	23.0 ϵ_f = 0.04% 22.3 ϵ_f = 0.073%	

* When plastic deformation occurred, total strain at fracture is also given.

TABLE 3.9

TRANSVERSE BEND STRENGTHS (KPSI) AT -196°C AND 1200°C AND REFERENCE COMPARISON VALUES

Billet	Comments	-196°C	Reference Value at 25°C	1200°C	Reference Value at 1200°C
FA-61	as hot-pressed 2.1 u G.S. 99.8% T.D.	72.0* 66.5 56.7* 54.4* 54.0+ 66.8 51.7	89.6 ± 15.0	36.0* 33.0+ 42.4 39.3	46.0 ± 10.0
FA-85	hot pressed and annealed for 15 minutes at 1850°C, 3.4 u G.S. 97.6% T.D.	53.6* 51.6 41.8+ 5[illegible].8 57.5* 58.2*		30.4 18.6 21.4 22.9	
FA-53A	17.4% HR at 1750°C 3.5 u G.S. 98.6% T.D.	64.0	60.3 ± 15.0	34.8 33.8	31.0 ± 10.0
FA-93D	21.6% HR at 1750°C 3.5 u G.S. 98.1% T.D.	61.6 56.7*	58.2 ± 15.0	23.8 30.8 35.5*	30.2 ± 10.0
FA-94	34.4-38.0% HR at 1750°C 4.5 u G.S. 98.8% T.D.	54.9 64.2 64.2 86.4*	53.2 ± 15	37.0 32.6 31.2 26.5	27.5 ± 8.0
FA-81	3.6-5.4% HR at 1850°C 5.3 u G.S. 99.4% T.D.	41.4 57.3 73.2 51.7	50.4 ± 15.0	23.1 32.6+ 31.0	25.9 ± 8.0
FA-84	15.5-16.2% HR at 1850°C 5.5 u G.S. 99.4% T.D.	56.3 55.0 56.2* 53.8	49.4 ± 15.0	32.6 31.8	25.4 ± 8.0

*
\+ See next page

TABLE 3.9 (concl'd)

TRANSVERSE BEND STRENGTHS (KPSI) AT -196°C AND 1200°C

AND REFERENCE COMPARISON VALUES

Billet	Comments	-196°C	Reference Value at 25°C	1200°C	Reference Value at 1200°C
FA-87	39% HR at 1850°C	25.4*	33.1 ± 10	30.6	17.0 ± 5.0
	10.4 u G.S. 99.8% T.D.	50.3		27.9+	
	tensile surface parallel	62.5		29.0*	
	to pressing direction	56.0		26.7+	
	tensile surface perpendi-	56.3		26.2	
	cular to pressing	62.6		27.3*	
	direction	54.5		26.4	
		55.4*		27.5	
FA-80	41.5% HR at 1850°C	58.9	40.3 ± 15	33.2	20.7 ± 5.0
	8.3 u G.S. 99.7% T.D.			28.3	
				33.2	
FA-86	41.5% HR at 1350°C	67.6*	43.1 ± 15.0	26.0	22.0 ± 5.0
	7.3 u G.S. 99.9% T.D.	44.7		28.3	
				29.3	
				29.0	
FA-90	21.1-25.0% HR at 1900°C	60.6	36.8 ± 10.0	22.1	19.0 ± 5.0
	8.7 u G.S. 99.0% T.D.	59.7*		28.2	
		47.4		30.9*	
		50.3		29.4*	
FA-91	41% HR at 1900°C 7.2 u	43.3*	48.6 ± 15.0	25.0+	24.9 ± 6.0
	G.S. 99.8% T.D.	55.2*		25.2*	
FA-92	45% HR at 1900°C, 1925°C	54.9	45.4 ± 15.0	25.2	23.3 ± 5.0
	6.2 u G.S. 99.1% T.D.	70.4		25.7	

* Fracture under an inner knife edge

\+ Fracture outside gage length - note that higher stress was supported inside gage length.

HR Height reduction

G.S. Average linear grain intercept

T.D. Theoretical Density

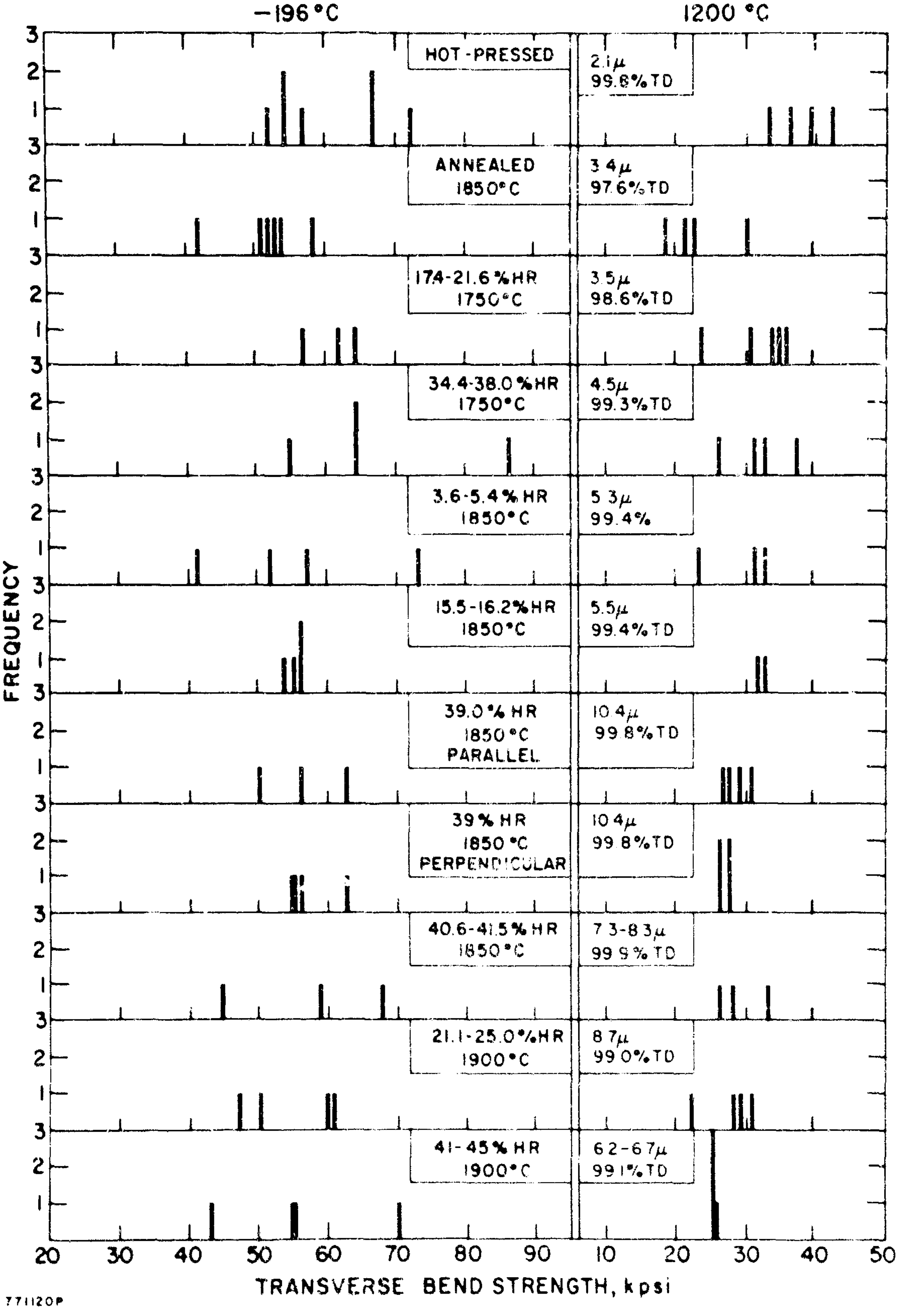

Figure 3.37. HISTOGRAMS ILLUSTRATING DATA PLOTTED ON TABLE 3.9

It was instructive to plot the -196°C and 1200°C strengths as a function of grain size, and this is shown in Figures 3.38 and 3.39. Contrary to almost all previous work in ceramics, there was virtually no strength dependence on grain size at -196°C and only a very small dependence at 1200°C. The best comparative data (Passmore, Spriggs, and Vasilos(24)) indicated that a strength decrease of ~50% occurred at both room temperature and 1200°C when the grain size was increased from 2 to 10 u. This predicted strength decrease for the larger grain size specimens can be ascertained from an examination of Table 3.9.

Thus, a comparison of the forged alumina with a pressure-sintered alumina specimen at a grain size near the upper limit of the range examined reveals that the forged specimens are stronger. There are two possible explanations for this behavior; one based on orientation effects and one on grain boundary "character". These will be discussed in turn:

<u>Orientation Effects</u> - it was argued in our previous work(3) that if <u>brittle</u> fracture in polycrystalline alumina involves any <u>plastic</u> deformation in the initiation or propagation stages, (which has been suggested recently, see References 25 and 26) then the strong basal deformation texture could profoundly incluence brittle fracture phenomena. Specifically, it is probable that if any micro-plastic deformation occurred, it would occur by basal slip, (0001) $\langle 11\bar{2}0 \rangle$, and this would be suppressed in the forged specimens - the basal texture would minimize resolved shear stresses on the active slip plane during transverse bending. Plastic deformation leading to fracture has been invoked by Carniglia(25) using the Petch relationship

$$\overline{\sigma_f} = \sigma_y + ky\,(D)^{-1/2}$$

where σ_f is the average fracture strength, σ_y a yield strength, and ky $(D)^{1/2}$ a back stress resulting from the restraint imposed on the surrounding grain configuration, to explain the strength dependence on grain size in relatively fine-grained (< 60 u) $MgO + Al_2O_3$). More recent data of Passmore, Spriggs, and Vasilos(24) was not considered by Carniglia, however, and these data obeyed the Knudsen relation, $\sigma_f = k_b\,(D)^{-1/2}$ down to the finest grain sizes examined (2 u). In the latter case, the flow controlling the fracture process is believed to extend by a true brittle or elastic process, rather than by the plastic yielding process implied by the Petch relationship. The strength constancy clearly does not support the Knudsen relation. If, however, the Petch relation (plastic flow) is normally operative, the grain size dependency may be normalized due to the retardation of basal slip. The slight grain size dependence of strength at 1200°C may be rationalized by noting that the orientation is not perfect and the critical resolved shear stress has without doubt fallen considerably from its value at -196°C.

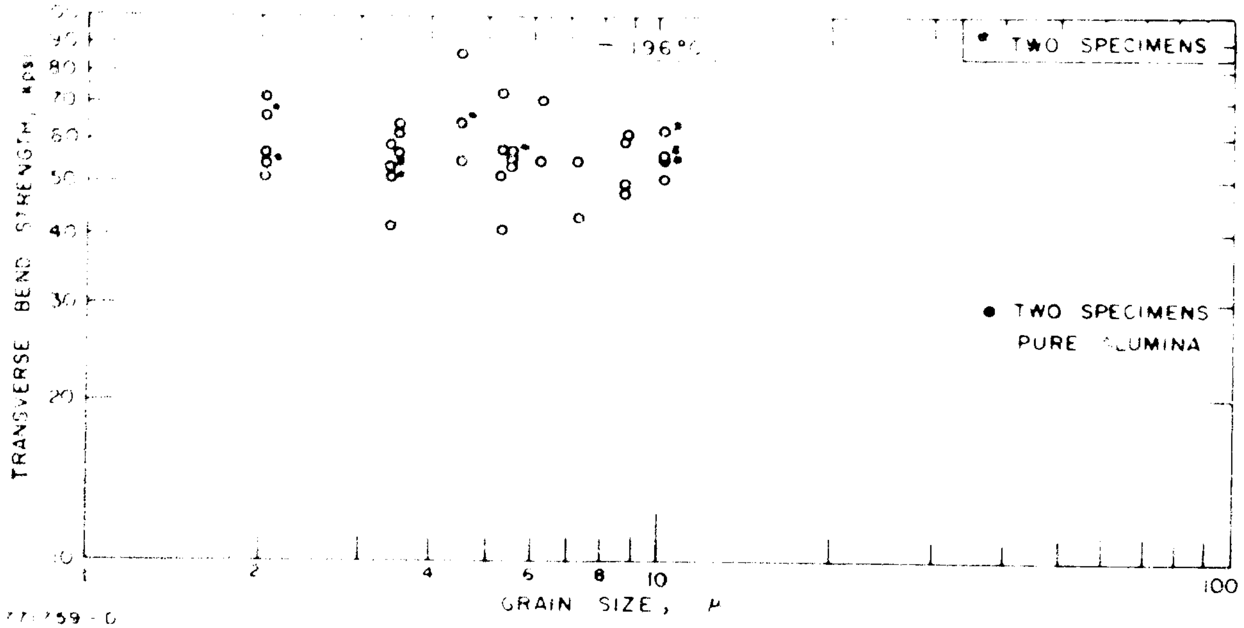

Figure 3.38 PLOT OF -196°C STRENGTH DATA (TABLE 3.9) AS A FUNCTION OF GRAIN SIZE

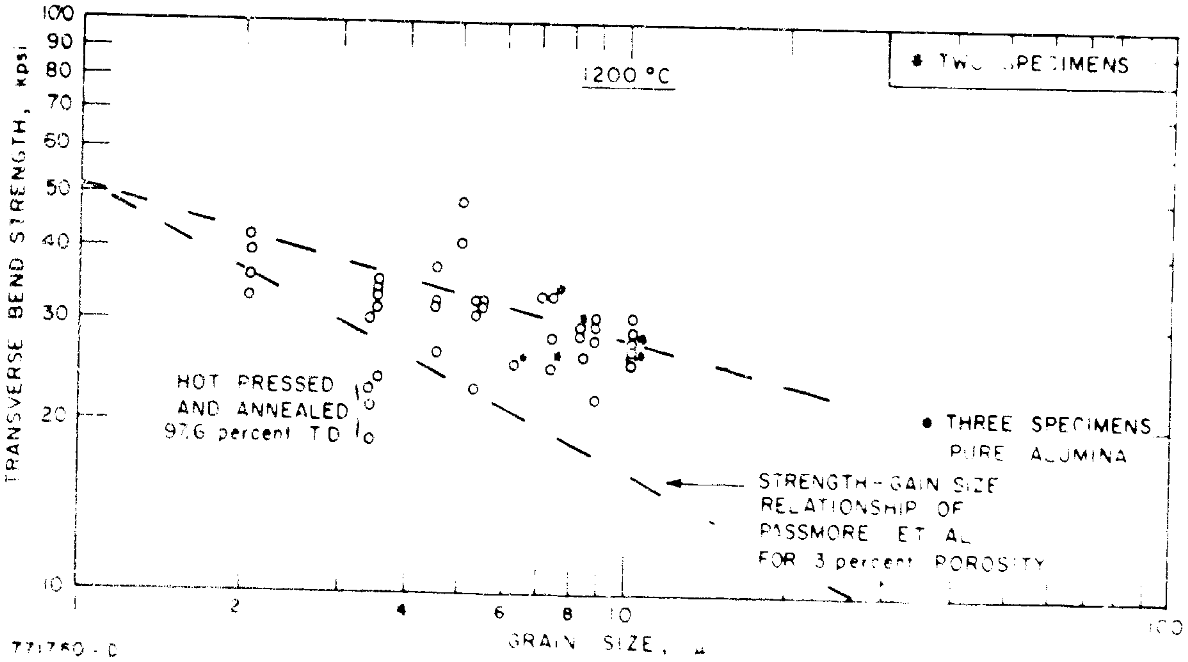

Figure 3.39. PLOT OF 1200°C STRENGTH DATA (TABLE 3.9) AS A FUNCTION OF GRAIN SIZE

It was mentioned above that the Griffith concept is maintained in all discussions of the brittle fracture of polycrystalline alumina, but there is some uncertainty over the mechanism of attaining the critical Griffith size. In the present case, the constancy of strength implies a constant Griffith flaw size, and some mechanism leading to this is necessary. It is possible that the "Griffith" flaw was introduced during machining of the test bars, rather than being associated with a grain boundary, and the size of the flaws so produced may have been limited to several microns by the high density of dislocations remaining after the hot working (see Section 3.0). The critical experiments needed to check the above hypotheses will be described in a subsequent paragraph.

There are several other possible orientation effects which could affect strength (in some cases at low as well as high temperatures) in a similar manner and arguments similar to the plastic deformation model are applicable. These are; unfavorable crystallographic orientation of a clevage plane to initiate fracture, unfavorable crystallographic orientation for the initiative of fracture by a twinning mechanism, and difficulty of grain boundary sliding in a specimen of high microstructural texture. It is thought that these possible orientation effects would be difficult to separate from the plastic flow model.

<u>Grain Boundary "Character"</u> - It is possible that changes in chemical bonding, atomic geometry, or orientation, morphology, etc., of the grain boundaries introduced by the hot-working could also have been responsible for the relative strengthening of the forged material. However, such an explanation requires first of all a very different concept that that given above of the factors affecting the strength and its variation with grain size of ordinary hot-pressed or sintered alumina. Rice(27) has shown convincingly that gases entrapped during hot pressing can have profound effects on mechanical properties, even when densities >99.5% of theoretical are achieved. Furthermore, many studies of strength-grain size relationships utilized hot pressed samples, where the larger grain sizes were achieved by annealing, and these anneals were often accompanied by an increase in pore volume, due to the above-mentioned entrapped gases. (Such an effect was found in the present study in the hot-pressed and annealed sample FA-85.) Thus, while the decreasing strength may have been accompanied by an increasing grain size, the actual weakening may have been caused by a change in the grain boundary "character" upon annealing, it being assumed that the "character" determines when a grain boundary can act as a Griffith flaw and propagate to fracture.

To argue in a similar vein, it cannot be assumed that strength is a single-valued function of grain size and porosity. Support for this also comes from comparisons of the strength of hot-pressed with sintered Al_2O_3 + 1/4% MgO. Up to the present, the upper limit of strength (4-point bending - 1 3/4 inch specimen) in polycrystalline alumina has been at about 100,000 psi, and this has been achieved in our laboratory on only the highest quality, densest, finest grained (< 1 u) vacuum hot-pressed samples, with most specimens falling in the range 60 - 100,000 psi. However, sintered Lucalox specimens, with grain sizes at least one order of magnitude larger, (12 u) and with a very slight porosity, can have strengths in this same range (Section 4) when tested under similar conditions of surface condition and sample size. Thus, it is clear that some other factor, probably grain boundary chemistry, is limiting strengths of hot-pressed samples, as strengths much in excess of the values for the sintered materials might be expected from the difference in grain size available by hot-pressing.

Therefore, the second explanation for the strength uniformity envisions that grain boundary "refinement" embodying changes in grain boundary "character", are occurring during the hot working, and may be responsible for the constancy of strength with grain size and for the relatively high strengths for the worked materials.

It is thus implied that gas removal, grain boundary bonding etc., are all aided by the applied load at the elevated forging temperature, and this is further enhanced by the massive material transport occurring during press forging. This effect would be different than previous work(3), which showed strength increases as a result of annealing, because it was envisaged that surface healing occurred during the annealing and may have been responsible for the strength response. It is worth emphasizing that the forged specimens were tested with "as-machined" surfaces. It is difficult to find convincing proof that changes in grain boundary chemistry may be occurring, primarily because of the dearth of detailed knowledge about grain boundaries in ceramics or of experimental techniques leading to such knowledge. The results of specimen FA-81, deformed 3.6-5.4% at 1850°C, lend support to this hypothesis, as the data are similar to data for more extensively forged specimens, although such light deformation does not give rise to any texture.

To summarize the discussion of low temperature strengths, two possible explanations were advanced to explain the relative constancy of strength with grain size; one due to the marked basal texture achieved during hot working, and the other due to a suggested grain boundary "refinement" which can be achieved during hot working. Both are speculative; the first assumes that plastic deformation (or one of several other orientation-controlled mechanisms) is important in the brittle fracture of alumina; the second that it is grain boundary "character", which cannot be properly defined, but which includes chemistry, bonding, morphology, orientation, etc., which is most important. However, it is possible to design several experiments which should be able to differentiate between these two and this will be attempted in the future. If a highly-oriented, relatively thick (after forging) billet could be produced, then bend bars could be cut oblique to the press forging direction such that basal planes are at some angle (30-45°) to the tensile stresses during mechanical testing. Resolved shear stresses would then be maximized onto basal planes and any strengthening effects due to suppression of basal slip would be negated. Strengths appreciably smaller than the present data would be excellent support for the orientation explanation; equivalent strengths would support the grain boundary refinement hypothesis.* The second experiment would test whether or not the Griffith crack length is dictated by the surface finish and dislocation substructure, which was also suggested to explain the constancy of strength with grain size. A series of specimens in the grain size range 2-10 μ and with surface finishes from 200 micro inches to 0.5 micro-inches would be fractured at -196°C. If the strength levels were constant for each surface finish over this grain size range, the Griffith relation would be tenable; this of course, would support the grain boundary refinement hypothesis.

Strengths were also determined at higher temperatures, up to 1550°C, and plastic deformation began to be appreciable at 1300°C These data are given in Table 3.10 and plotted as a function of temperature for each billet in Figure 3.40. In all cases, the strength levels began to drop off at some temperature which appeared to increase with increasing grain size. In addition, the stress-strain curves showed zero load-hardening, which is similar to the behavior of hot pressed or sintered alumina. The data suggested that the macroscopic deformation may have been due to Nabarro-Herring diffusional creep, the creep rate being enhanced sufficiently by the relatively fine grain sizes (this, in spite of the high dislocation content in these samples and the fact that dislocation slip was almost certainly important in the hot working (Section 3.6)). It was possible to calculate an apparent diffusion coefficient of the rate controlling species from the stress-strain curves at constant strain rate, utilizing the Nabarro-Herring equation

$$D = \epsilon \frac{kT\,(G.S.)^2}{13.3\,\Omega\,\sigma}$$

where D is the diffusion coefficient, ϵ the strain rate, G.S. 1.5 times the grain intercept (given above as grain size), Ω the vacancy volume, σ the stress, and k and T have their usual meaning, and these values are plotted as a function of temperature in Figure 3.41, along with similarly calculated values of unforged alumina from a study presently underway in our laboratory.(28)

---

* It may be mentioned that in one case, bars were cut from a single billet so that the tensile surfaces were parallel or perpendicular to the press forging direction (FA-87). (In either case, resolved shear stresses on basal planes would be near zero.) No strength differences were noted, and in the remaining billets, the orientation was chosen that would yield the greater number of test bars.

TABLE 3.10

STRENGTH PROPERTIES AT 1400-1550°C

Billet	Comments	Temp °C	Fracture (or Maximum) Stress (Kpsi)	Maximum Plastic Strain (%)
FA-61	As hot pressed - 2.1 u G.S.	1400	9.3 - N.F.	1.75
		1400	8.1 - N.F.	1.72
		1450	4.3 - N.F.	1.75
				1.56
FA-85	Hot-pressed and annealed-3.4 u G.S.	1400	26.0	0.096
		1400	25.4	0.37
		1450	18.5	1.10
		1450	14.4 - N.F.	1.64
FA-93C	16.8% HR at 1750 - 3.4 u G.S.	1400	25.3	
		1400	28.6	
FA-93B	22% HR at 1750°C 3.5 u G.S. 98.1% T.D.	1400	31.25*	0.365
		1400	28.0 *	0.16
FA-94	34.4 - 38.0% HR at 1750°C - 4.5 u G.S.	1400	14.6	0.24
		1400	23.7	0.35
		1450	11.8 - N.F.	1.53
		1450	15.0 - N.F.	1.79
FA-81	3.6 - 5.4% HR at 1850°C 5.3 u G.S.	1400	28.7	-
		1400	27.8	-
		1450	25.8	-
		1500	16.7	1.7
		1550	10.6	1.7
FA-84	15.5 - 16.2% HR at 1850°C - 5.5 u G.S.	1400	28.6*	-
		1400	25.8+	
		1550	6.9	1.7

* See next page
\+

TABLE 3.10 (concl'd)

STRENGTH PROPERTIES AT 1400-1550°C

Billet	Comments	Temp °C	Fracture (or Maximum) Stress (Kpsi)	Maximum Plastic Strain (%)
FA-80	40.7% HR at 1850°C 8.3 u G.S.	1400	11.3	-
		1400	11.6	-
		1450	23.1	-
		1450	11.9*	0.05
		1500	14.5+	0.09
		1500	22.1	-
		1550	18.7*	0.58
		1550	16.4+	0.32
FA-90	21.[illegible]-25.0% HR at 1900°C 8.7 u G.S.	1400	22.6	-
		1400	22.0	-
		1400	23.1*	-
		1500	18.2	0.1
		1500	15.7	0.1
		1550	10.8	1.7
FA-91	42% HR at 1900°C 7.2 u G.S.	1400	19.1*	-
		1400	23.2+	-
		1450	21.7+	-
		1450	18.1+	-
FA-92	40.3% HR at 1900-1925°C 6.2 u, G.S.	1500	11.3	0.15
		1500	15.4+	0.19
		1550	14.3+	1.49
		1550	11.3 - N.F.	1.91

* Fracture under an inner knife edge

\+ Fracture outside gage length - note that higher stress was supported inside gage length

HR = Height reduction; G.S. = Average linear grain intercept; N.F. not fractured.

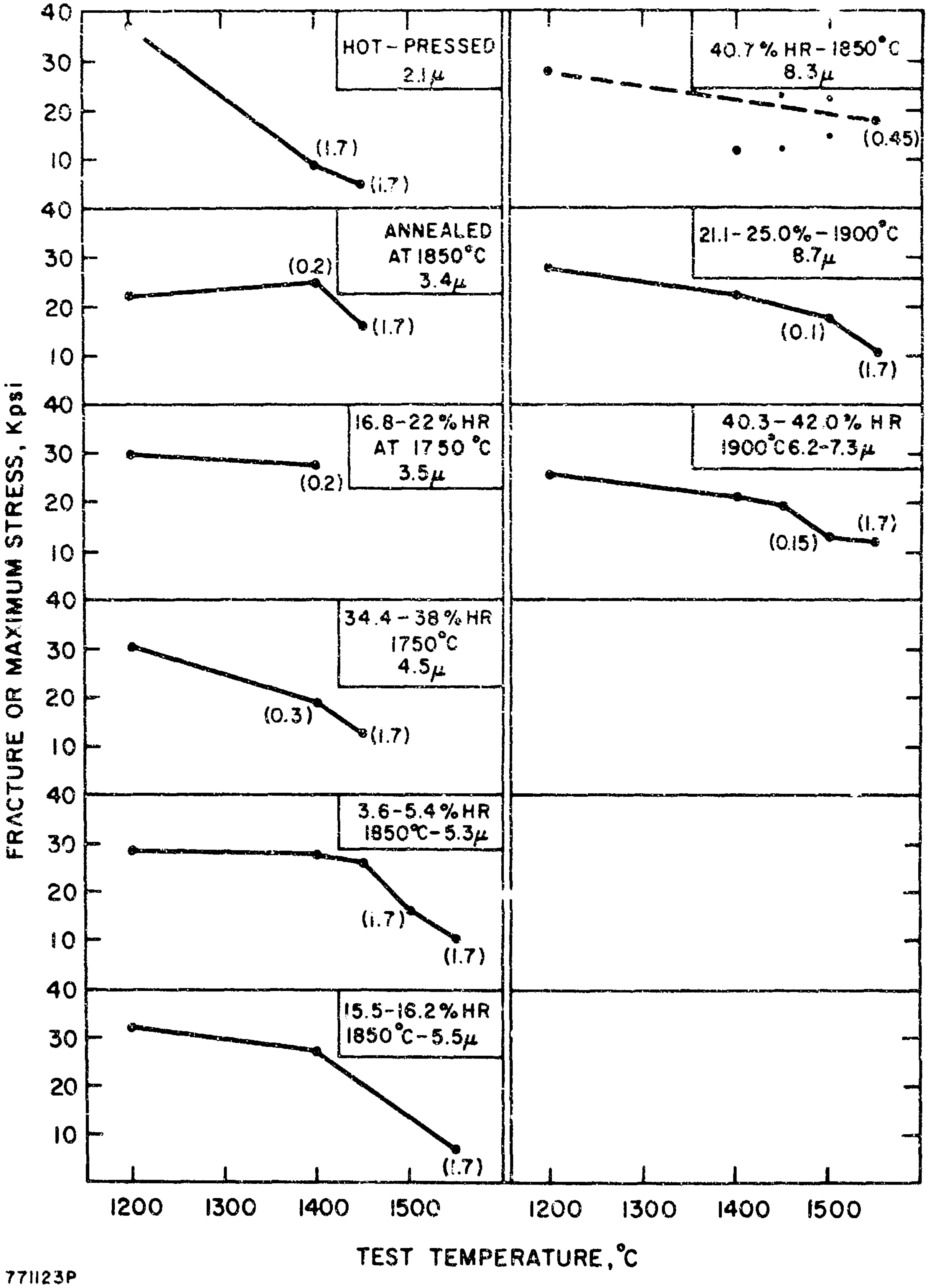

771123P

Figure 3.40. STRENGTH VERSUS TEMPERATURE PLOTS FOR A NUMBER OF PRESS-FORGED SAMPLES

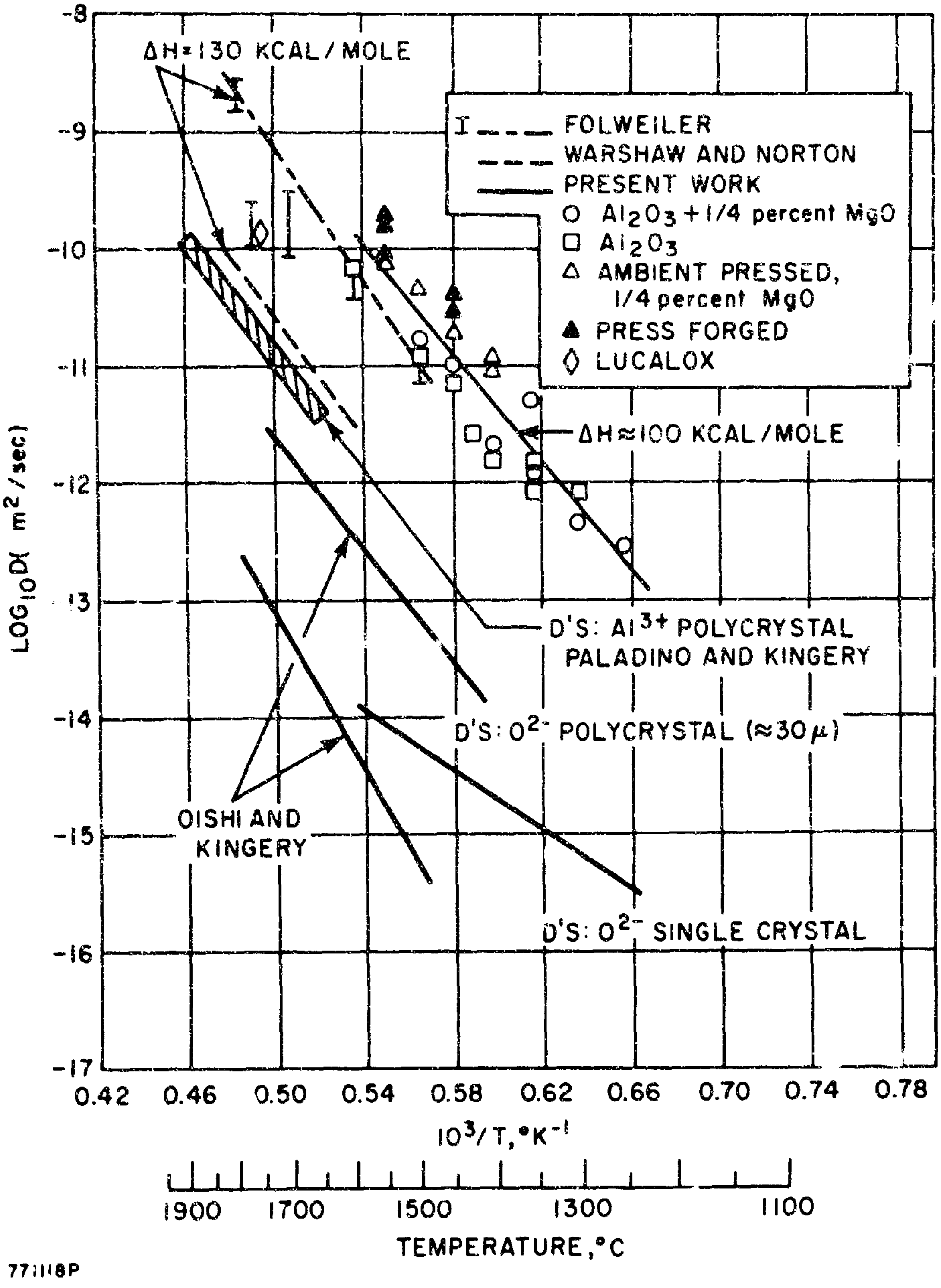

Figure 3.41. DIFFUSION COEFFICIENTS CALCULATED FROM PLASTIC BENDING EXPERIMENTS (ASSUMING NABARRO-HERRING CREEP)

It can be seen that these sets of data are similar, and they are plotted together with comparative data from previous creep work and self-diffusion data of Al and O. The calculated D's agree reasonably well with the work of Folweiler; however, the activation energy is slightly lower at about 100 kcal. It is difficult, however, to compare these D values and activation energies because it is known that at lease one other mechanism, probably grain boundary sliding, parting, or shearing is occurring and may be the explanation for the high D's. A detailed discussion of these data are given elsewhere(28); however, the similarity of the press forged data and unforged data is perhaps due to the orientation in the former, there being no resolved shear stresses on basal planes and hence, no means for slip to become more important than diffusional creep. However, to positively identify a Nabarro-Herring mechanism, it is necessary to show that $\sigma \alpha G.S.^2$ and $\sigma \alpha \dot{\epsilon}$. The small range of grain size and the inherent scatter makes it difficult to prove quantitatively the first proportionality; however, it is possible to vary the strain rate at constant temperature and thus determine if there is linearity between σ and $\dot{\epsilon}$. Tests for unforged alumina indicated a non-linearity which suggested that some strain could be attributed to a grain boundary phenomenon, as described above.

[illegible].1 Summary and General Discussion

Press forging techniques were used to hot work polycrystalline aluminum oxide. Both porous compacts, obtained by sintering of a loose powder, and dense, hot-pressed or sintered billets could be forged and generally gave similar results. The porous billets were easier to forge than the fully dense starting material, while fine-grained dense pieces were somewhat easier to forge than coarser-grained material. However, there was no real ductility problem with either starting material, and height reductions up to 7[illegible]% could be achieved above 1750°C.

The hot working induced recrystallization in some materials, and this resulted in either single crystals or equiaxed structures possessing a basal recrystallization texture (c-axis parallel to press forging direction). The microstructures obtained after working depended on the distribution of shear strain within the worked piece, which was complex because of the superposed hydrostatic stresses. It was suggested that the pores in the "powder" forgings were preferential sites for the formation of the strain-free recrystallization nuclei.

In other cases, recrystallization did not occur; rather materials with a marked deformation texture (which, however, was the same as the recrystallization texture) were produced. At sufficiently large deformations, materials with marked grain elongation normal to the pressing direction, i.e., a microstructural texutre, were also observed. The "strength" of the deformation texture depended only on the amount of deformation and was independent of the working temperature. 1/4% MgO additions proved to be very effective in suppressing recrystallization, and allowed samples with the marked deformation texture to be fabricated reproducibly.

Annealing such deformed samples also led to recrystallization. If the recrystallized grain size was large enough, a microstructural texture was also observed. Thus, as both fine-grained equiaxed and coarse-grained elongated structures could be obtained by recrystallization, it was suggested that the origin of the crystallographic recrystallization texture arose from oriented nucleation, while any microstructural texture which accompanied recrystallization arose from preferred growth.

Deformation mechanisms during hot working were briefly considered. The pronounced basal texture indicated that basal slip was the dominant mode. It was suggested that rhombohedral slip might also be occurring, which would satisfy the Von Mises criterion of 5 independent slip systems. Further, Nabarro-Herring diffusional creep was also suggested as important in providing adequate ductility.

A series of billets containing 1/4% MgO were forged at several temperatures up to height reductions of 50% and subsequently used for mechanical properties evaluation. These materials differed from ordinary hot pressed or sintered alumina in two important respects; they contained large numbers of dislocations and a pronounced basal texture. The mechanical properties of the worked materials were quite good, strengths in excess of 80,000 psi being achieved at -196°C. Moreover, the strengths were relatively insensitive to grain size, at least in the range 3.5-10.5 u, and this may perhaps be attributed to a different mechanism of fracture nucleation. Because of the marked basal texture, the easy slip plane was always parallel to tensile forces during mechanical testing, and thus only small resolved shear stresses were available. The dislocation structure seemed to have a minor (if any) effect on mechanical properties, even at elevated (1500°C) temperatures, and this was surprising.

The most important result of the mechanical properties tests was that no loss in structural integrity occurred during working. Thus, forging alumina to particular shapes can be expected to yield products whose mechanical properties are equivalent to presently available sintered or hot pressed articles.

3.12 Future Work

As was pointed out in several places in the discussion, there are certain areas where specific information is needed adequately to understand the processes occurring in hot working and primary recrystallization. These include:

1. Forging Parameters - A further understanding is needed of variables that determine the "ease" of forging and the homogeneity of shear strain within the billet. In particular, the aspect ratio and initial porosity of the billet, and stresses and strain rates imposed by the press are thought to be particularly important. In addition, factors involved in the removal of porosity during forgings of porous compacts need further elucidation.

2. Single Crystals - In addition to determining the means of obtaining large single crystals by strain-anneal reproducibly, it is necessary to determine the critical strain needed to induce recrystallization. It may be that traversing specimens deformed, but not recrystallized, through a sharp thermal gradient would be best for producing single crystals. Also, further etch pit and thin foil electron microscopy studies are needed to understand the defects which may be present in such strain-anneal crystals.

3. Deformation Texture in Pure Alumina - A means to produce deformed but not recrystallized specimens of pure alumina reproducibly is not now available. Relatively low temperature forgings should be investigated towards this end.

4. X-ray Studies - Further X-ray work to define the basal texture quantitatively and also to obtain a pole figure from prism plane reflections is needed.

5. Deformation and Nucleation Mechanisms - Further thin foil electron microscopy studies are needed to elucidate deformation mechanisms. In addition, this should be coupled with annealing studies so that a good model of the nucleation of strain-free regions can be advanced. Further, this may bear on the question of recrystallization texture - does it originate from oriented growth or from oriented nucleation.

6. Mechanical Properties of Forged Oxides - In particular, the experiments described in Section 3.10 to differentiate between the basal texture or grain-boundary refinement explanations for the constancy of strength with grain size at low temperatures should be performed. In addition, further studies at higher temperatures, where the orientation, dislocation substructure, and grain boundary "character" might all affect plastic properties would be useful.

7. Other Materials and Shapes - Finally, the merit of using the forging process for other oxides of structural interest and for producing unique shapes should be investigated.

IV. FLAME-POLISHING STUDIES

Previous work([illegible]) on flame polishing polycrystalline alumina revealed that appreciable differences in grain size after polishing sometimes occurred. Chemical analysis has now revealed that these were due to differences in the concentration of magnesia which was present as unintentional impurities. It was thus, of interest to attempt to flame-polish Lucalox, a high density polycrystalline alumina containing MgO as a deliberately-added grain growth inhibitor. Standard procedures for the flame polishing were used([illegible], 29). (A Lepel crystal growing apparatus allowed precise control of traverse rates and rotation speeds.) As previously described,(3) the polycrystalline specimens were much more difficult to "polish" than similar single crystals - a flame "ideal" for the latter was much too cool to achieve any surface melting or "polishing" of the polycrystalline specimens. This difference was believed to be associated with different heat transfer rates, probably due to scattering from pores and grain boundaries. In addition, there was no clear visual indication when a small molten pool had been established on the surface, which is believed to be the ideal condition for flame polishing. Thus, it was very easy to go from an "under-polished" to an "over-polished" condition. Nevertheless, ten specimens were polished using various traverse speeds, rotation rates, oxygen-gas compositions, and flame positions. The polycrystalline alumina specimens were prone to thermal shock using this apparatus, probably because the specimen holder constituted an efficient thermal sink and gave rise to large thermal stresses. This problem was finally overcome by traversing the specimens upwards rather than downwards through the flame. It was also observed that the yellow color characteristics of flame-polished polycrystalline alumina deepened to a dark brown on very "over-polished" (i.e., over-heated) specimens. Finally, the slight grooving visible on flame polished specimens, both single crystals and polycrystals,(29,30) could be eliminated at high rotation speeds; however, under these conditions, an entire traverse of the flame could not be made without the specimen departing from the shape of a right circular cylinder, i.e., appreciable bowing out occurred due to the centrifugal forces.

Four of the best flame polished specimens were tested along with an unpolished control sample at -196°C. The results, shown in Table 4.1, did not indicate any strength improvement due to flame polishing. Microscopic examination of polished cross sections of these five specimens confirmed that no surface melting of LFP-1 and -2 had occurred. Also, the magnesia addition in Lucalox was effective in preventing any marked grain growth, even when the surface had been successfully melted (Figures 4.1 and 4.2).

In addition to the cracks due to thermal stresses and thermal shock, Table 4.1 and Figure 4.2, a crazed appearance was occasionally observed. This was believed to result from surface tensile stresses set up during cooling, due to the temperature gradient between the interior and the previously molten surface. It is pertinent to ask whether a similar state of stress exists for single crystals. No crazing has heretofore been reported for single crystals, (3, 29, 30) although rhombohedral deformation

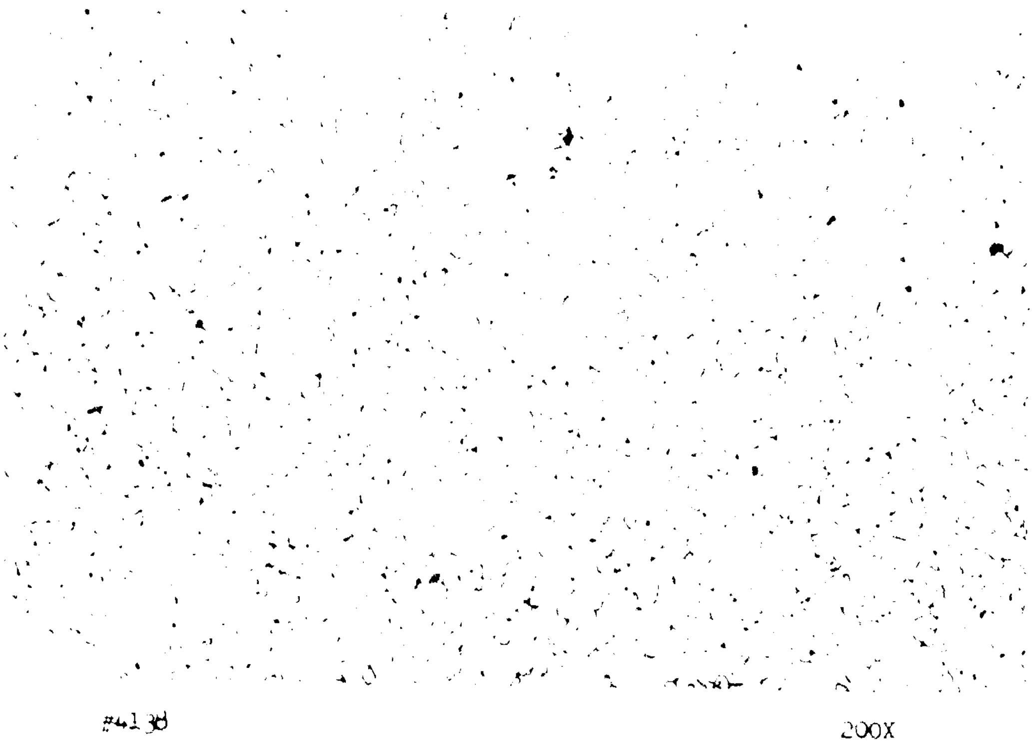

Figure 4.1 Lucalox Control Specimen (L-C-1)

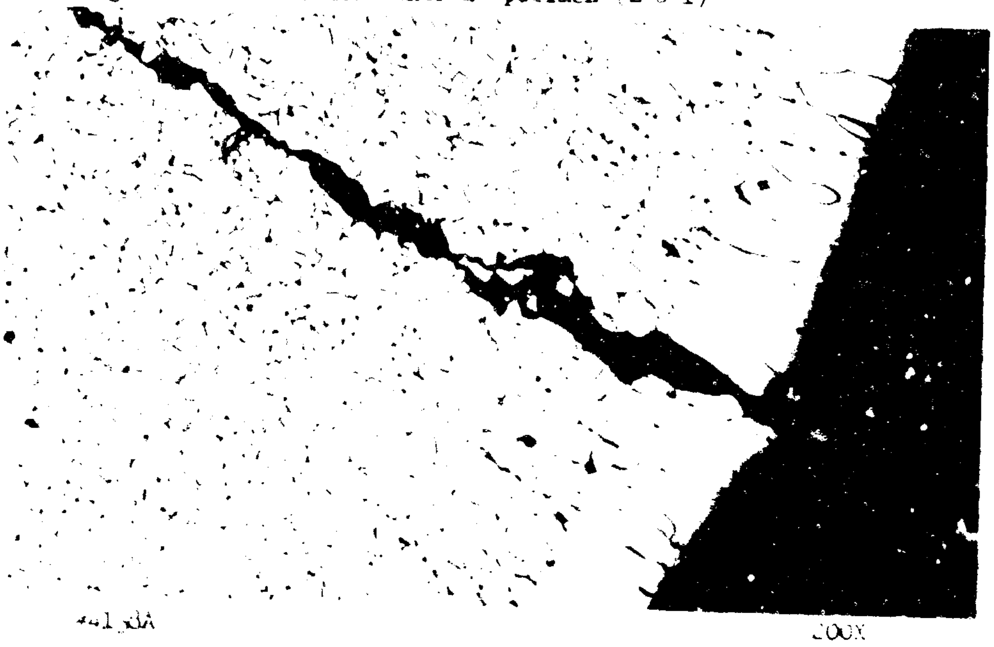

Figure 4.2 Flame Polished Lucalox (LFP-[illegible]) Showing Melted Exterior, Thermal Stress Induced Crack, and Little Grain Growth.

twins have been observed in single crystals just above the molten zone,(30) i.e., where thermal stresses are expected to be most severe. The project monitor, Mr. C. Bersch, has put forward the interesting suggestion that the surfaces of flame-polished single crystals may in fact be in compression, due to the more efficient cooling that might occur in the surface, and this could be a major factor in the high strengths realized for single crystals.

Because of the inability to strengthen polycrystalline alumina by flame-polishing, no future work was attempted in this area.

TABLE 4.1

STRENGTHS OF FLAME-POLISHED LUCALOX

Specimens	Test Temp. °C	Modulus of Rupture Kpsi	Comments
L-C-1	-196	88.8	Control specimen
LFP-1	-196	61.4	Light yellow color* - "Unglazed" appearance
LFP-2	-196	21.5	Similar to LFP-1 but looks better "polished" but still "Unglazed".
LFP-3	-196	17.6	Light brown color* - spiral thermal stress crack along length of specimen - well glazed appearance - "grooving" almost eliminated.
LFP-4	-196	18.6	Dark brown color* - spiral thermal stress cracks- well "glazed" appearance - very prominent grooving

* Color restricted to surface regions

V. GRAIN GROWTH IN ULTRA-HIGH PRESSURE-SINTERED MAGNESIUM OXIDE

Ultra-high pressure sintering has been employed(31) our laboratory to consolidate magnesium oxide to theoretical density while maintaining an extremely fine grain size of 500 - 700 A°. Optimum fabrication conditions for producing transparent pieces were found to be 250,000 psi at 900°C for 5-10 minutes. As this grain size is an order of magntiude smaller than is found in ceramics produced by ordinary pressure sintering, it was of interest to study grain growth kinetics.

Specimens for this study were obtained from a sample which had laminated into discs, ~ .050" in thickness, during cooling. They were introduced into heated furnaces for various times at temperatures of 1000° to 1500°C and then quenched. Replicas of both fractured and ground surfaces were examined in an electron microscope and grain sizes were determined using an uncorrected circular intercept method.(32) Results for the temperature range 1000-1200°C are shown in Figure 5.1.

These results were anomalous, in that the slopes of the isothermal linear curves of log grain size versus log time increased from a value of 0.13 at 1000°C to 0.20 at 1100°C to 0.31 at 1200°C, all of which were considerably less than the theoretical value of 0.50(33). Previous results in our laboratory(34) had shown that a conventionally hot pressed magnesia prepared from the same starting powder followed the theoretical t 1/2 law for normal isothermal grain growth at temperatures between 1300°C and 1500°C. On the other hand, a $t^{1/3}$ law is observed in most polycrystalline ceramics and has been ascribed to the influence of residual porosity;(35) during grain growth, the pores must migrate along with the grain boundaries.

An increase of slope with increased temperatures has been noted in some metals,(36) and seemed to be associated with primary recrystallization. This was not thought to be occurring during the present experiments.

Specimens became opaque upon heating, even after 10 minutes at 1000°C, and this suggested that submicroscopic impurities, both solid and gaseous, may have effectively pinned grain boundaries. Solution of impurities is known to occur in single crystal magnesia in this temperature range and to have profound effects on mechanical properties;(37) solution of impurities as temperature is increased could cause the observed increase of the slope of the isothermal grain growth curves. Further, Rice(27) has suggested that hydroxides and carbonates would not be decomposed during pressure sintering at such a low temperature, and the absorption bands below 5 u shown in the IR spectra of Figure 5.2 is evidence for this.

At higher temperatures, grain growth became very non-uniform and meaningful kinetics could not be obtained. This is also attributed to an impurity factor. At the highest temperatures employed (1500°C), glassy phases were found at grain boundaries. Similar exsolution of impurities have been found in MgO prepared by conventional pressure sintering(1) and reinforce the need for higher purity specimens (see Section 1).

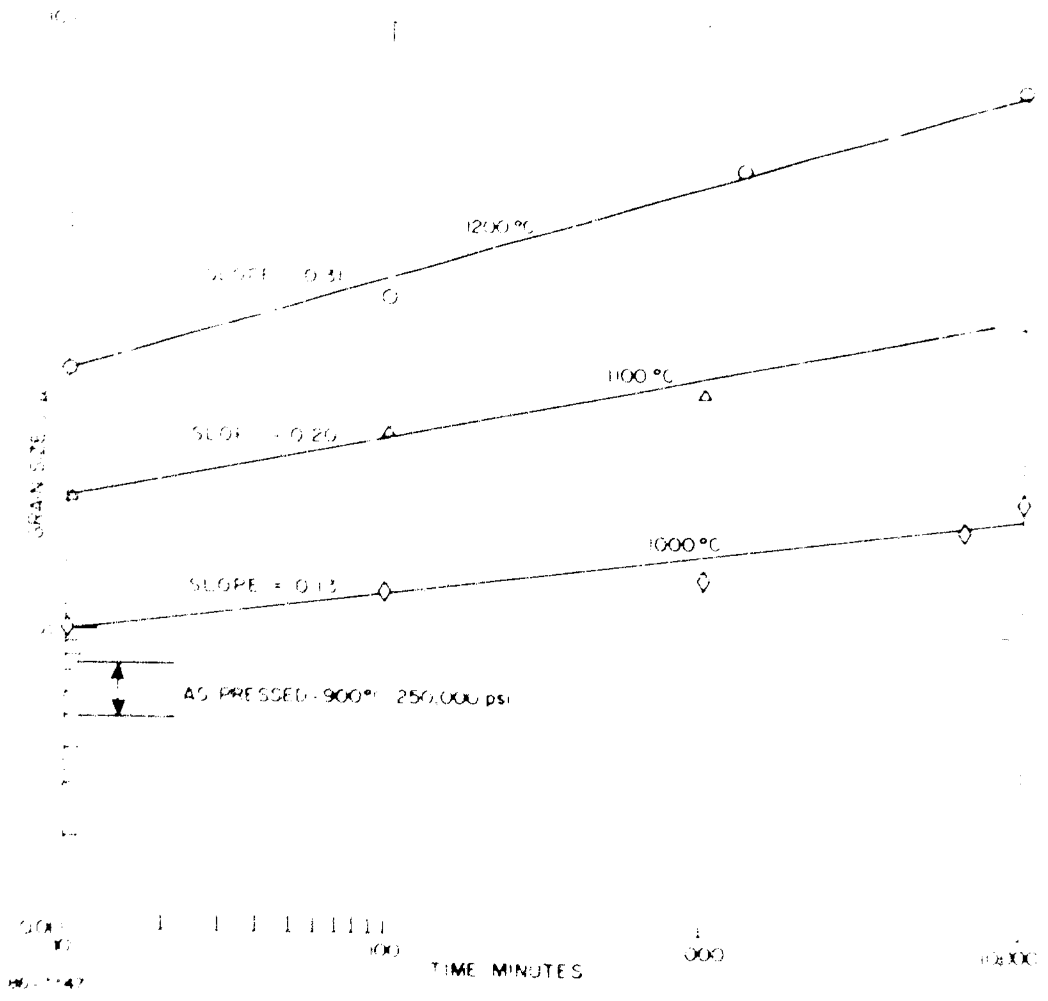

FIGURE 5.1. ISOTHERMAL GRAIN GROWTH CURVES FOR ULTRA HIGH PRESSURE SINTERED MgO

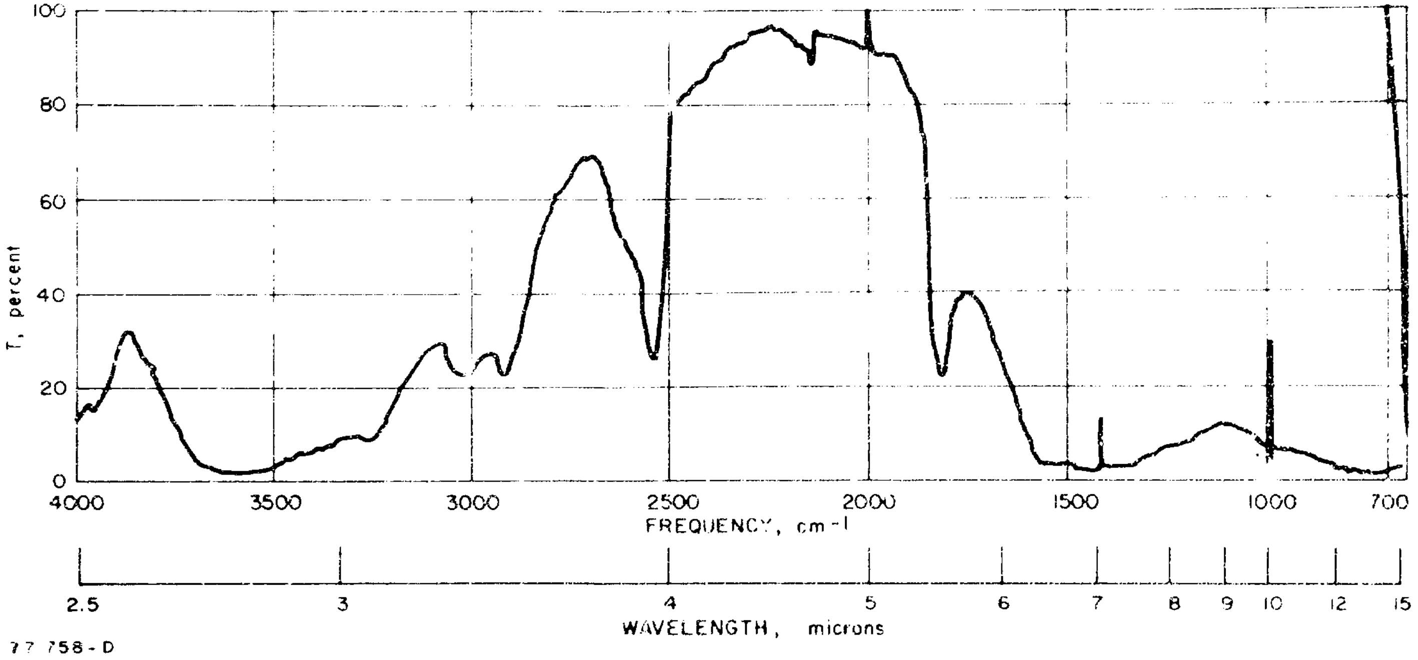

Figure 5.2. IR SPECTRA OF ULTRA-HIGH PRESSURE-SINTERED MgO

The low temperatures at which grain growth could be observed suggested that it might be possible to observe this growth directly in thin foils in the electron microscope, using the hot stage attachment. However, this could not be realized, due to the marked evaporation that occurred; high temperatures were achieved by the heating effect of the electron beam and the low thermal conductivity of magnesia. Although this has not been reported in previous electron microscopic investigations of magnesia,(38,39) the tendency for magnesia to evaporate in vacuo is well known;(40) in addition, this may have been enhanced by the fine grain size and/or impurities.

However, the most interesting aspect of the electron microscopy was the observation of whisker growth in situ. This occurred at low electron beam currents and at fairly high hot-stage temperatures (~ 1000°C). The growth was almost certainly due to thermal gradients in the stage and probably occurred after the matrix had "stabilized" due to grain growth. Figures 5.3 and 5.4 show the growth of one of these whiskers; the time difference is 2 minutes. The observation that growth was from the tip (the arrowed steps near the base attests to this) and the opaqueness of the tip suggest that the growth occurred by the VLS mechanism of Wagner and Ellis(41). This again relates to impurity effects; for example, a Ca-Si-Mg glass would satisfy many of the requirements of VLS growth.

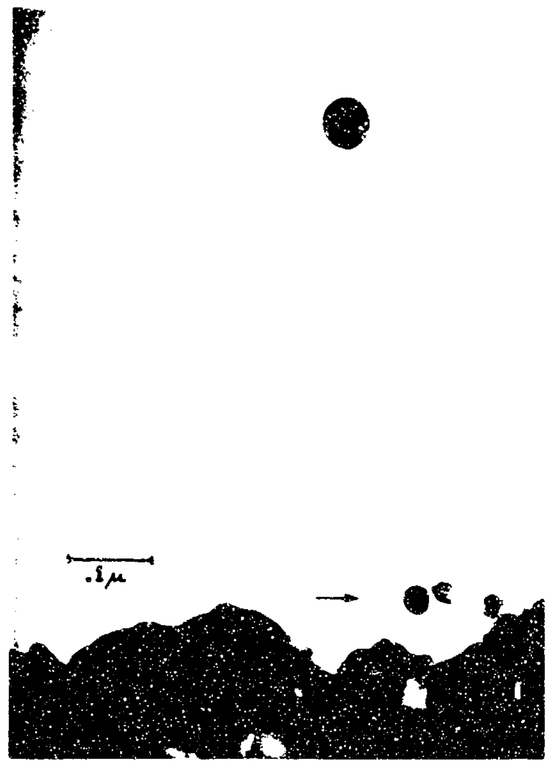

66C24 130,000 X

Figure 5.3 Magnesia Whisker Observed Growing in the Electron Microscope. See text for discussion of the arrow and the opaque sphere at the tip.

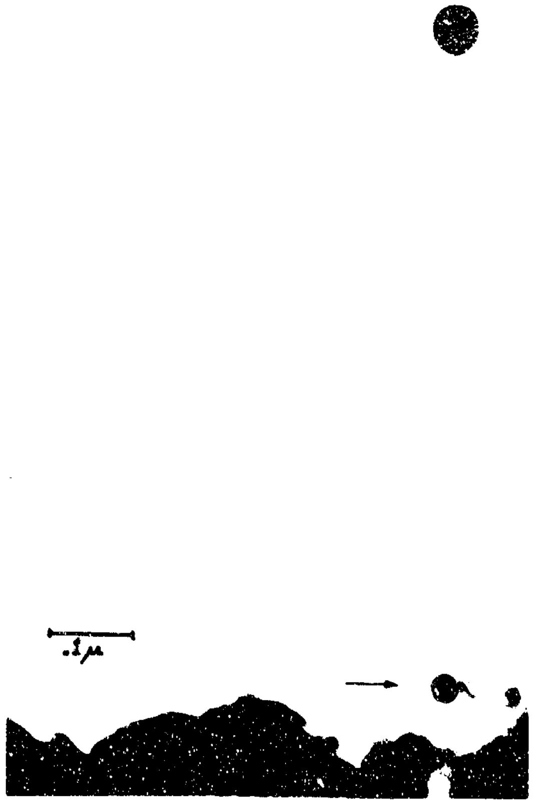

66C26 130,000 X

Figure 5.4 Whisker Growth after Additional 2 Minutes.

REFERENCES

1. M.H. Leipold, J. Amer. Ceram. Soc., 49, (9), p. 498, 1966.

2. R.S. Gordon and W.D. Kingery, J. Am. Ceram. Soc., 49, (12), p. 654, 1966; 50, (1), p. 8, 1967.

3. W.H. Rhodes, D.J. Sellers, T. Vasilos, A.H. Heuer, R. Duff, P. Burnett, "Microstructure Studies of Polycrystalline Refractory Oxides;" D.J. Sellers, W.H. Rhodes, and T. Vasilos, " Single Crystal Alumina Grown by Strain Anneal," Summary Reports, Contract NOw-65-0316f, March 24, 1966.

4. R.W. Cahn, "Recovery and Recrystallization in Physical Metallurgy," edited by R.W. Cahn, North Holland Publishing Co., 1965.

5. R.W. Cahn, "Recrystallization Mechanisms" in "Recrystallization, Grain Growth and Textures," American Society for Metals, 1966.

6. R.B. Day and R.J. Stokes, J. Amer. Ceram. Soc., 47, (10), p. 493, 1964; J. Amer. Ceram. Soc., 49, (2), p. 72, 1966.

7. R.W. Rice and J.G. Hunt, "Hot Extrusion of MgO," presented at 66th Annual Meeting, American Ceramic Society, Chicago, Illinois, April 1964.

8. K.T. Aust, "Large Crystals Grown by Recrystallization" in "The Art and Science of Growing Crystals," edited by J.J. Gilman, John Wiley & Sons, 1963.

9. A. Kimura, R. Maddin, and H. Kimura, Acta Met., 12, p. 1167, 1964.

10. W.J. Alford and D.L. Stephens, J. Amer. Ceram. Soc., 46, (4), p. 193, 1963.

11. W.G. Burgers, "Principle of Recrystallization" in "The Art and Science of Growing Crystals," edited by J.J. Gilman, John Wiley & Sons, 1963.

12. G.W. Groves, and A. Kelly, Phil. Mag., 8, p. 877, 1963.

13. D.J. Barber and N.J. Tighe, Phil. Mag., 14, (129), p. 53, 1966.

14. J. B. Wachtman, Jr., and L.H. Maxwell, J. Amer. Ceram. Soc., 40, (11), p. 377, 1957.

15. P.J. Jorgenson, J. Amer. Ceram. Soc., 48, (4), p. 207, 1965.

16. J.E. White and R.D. Carnahan, Trans. AIME, 230, p. 1298, 1964.

17. C.S. Barrett, "Structure of Metals," McGraw-Hill Book Co., 1952.

18. P.A. Beck and H. Hu, "The Origin of Recrystallization Textures" in Recrystallization, Grain Growth and Texture," American Society for Metals, 1966.

REFERENCES (concl'd)

19. T. Vasilos and R.M. Spriggs, Prog. Ceram. Sci., 4, p. 95, 1966.

20. P.R. Mould and P. Cotterill, cited by Cahn, reference 5.

21. C. Zener, cited by C.S. Smith, Trans. AIME, 175, p. 151, 1948.

22. A.D. Wahpham, Nucl. Appl. 2, (4), p. 123, 1966.

23. G.K. Williamson and R.M. Cornell, J. Nucl. Materials, 13, p. 278, 1964.

24. E.M. Passmore, R.M. Spriggs, and T. Vasilos, J. Amer. Ceram. Soc., 48, (1), p. 1, 1965.

25. S.C. Carniglia, J. Amer. Ceram. Soc., 48, (11), p. 580, 1965.

26. J. Congleton and N.J. Petch, Acta. Met., 14, p. 1179, 1966.

27. R. Rice, Bull. Amer. Ceram. Soc., 46, (4), p. 359, 1967.

28. A.H. Heuer, and R. Cannon, to be published.

29. F.A. Mallinder and F.A. Proctor, Phil. Mag., 13, No. 121, January 1966.

30. A.H. Heuer, Ph.D. Thesis, University of Leeds, 1966.

31. A.J. DeLai, R.M. Haag, and J.K. Hill, paper presented before the Fall Meeting, Basic Science Division, American Ceramic Society, December 1965.

32. J.E. Hilliard, Metal Progress, p. 102, May 1964.

33. D. Turnbull, Trans. AIME, 191, p. 661, 1951.

34. R.M. Spriggs, L.A. Brissette, and T. Vasilos, J. Amer. Ceram. Soc., 47, p. 417, 1964.

35. W.D. Kingery and B. Francois, J. Amer. Ceram. Soc., 48, p. 546, 1965.

36. P.A. Beck, J.C. Kremer, L.J. Demed and M.L. Holgworth, Trans. AIME, 175, p. 372, 1948.

37. J.E. May and M.L. Kronberg, J. Amer. Ceram. Soc., 43, (10), p. 53, 1960.

38. G.W. Groves, J. Washburn, A.Kelly, and G.K. Williamson, Phil. Mag., 5, p. 991, 1960.

39. E.M. Passmore, R.Duff, and T. Vasilos, J. Amer. Ceram. Soc., 49, (11), p. 1594, 1966.

40. R.L. Altman, J. Phys. Chem., 67, 366, 1963.

41. R.S. Wagner and W.C. Ellis, Trans. Met. Soc. AIME, 233, p. 1053, 1965.

Unclassified

Security Classification

DOCUMENT CONTROL DATA - R&D

(Security classification of title, body of abstract and indexing annotation must be entered when the overall report is classified)

1 ORIGINATING ACTIVITY (Corporate author)

Avco Corporation
Space Systems Division
Lowell, Massachusetts

2a REPORT SECURITY CLASSIFICATION

Unclassified

2b GROUP

3 REPORT TITLE

Microstructure Studies of Polycrystalline Refractory Oxides

4 DESCRIPTIVE NOTES (Type of report and inclusive dates)

Summary Report - 25 March 1966 - 24 April 1967

5 AUTHOR(S) (Last name, first name, initial)

Heuer, Arthur H. Sellers, David J.
Rhodes, William H. Vasilos, Thomas

6 REPORT DATE

April 24, 1967

7a TOTAL NO OF PAGES

115

7b NO OF REFS

41

8a CONTRACT OR GRANT NO

NOw-66-0506-(d)

b PROJECT NO

c

d

9a ORIGINATOR'S REPORT NUMBER(S)

Final Technical Report

9b OTHER REPORT NO(S) (Any other numbers that may be assigned this report)

10 AVAILABILITY/LIMITATION NOTICES

Distribution of this document is unlimited.

11 SUPPLEMENTARY NOTES

12 SPONSORING MILITARY ACTIVITY

U.S. Naval Air Systems Command
Washington, D.C. 20360

13 ABSTRACT

A program to fabricate dense, polycrystalline high-purity alumina and magnesia has begun. Fine-particle size powders of suitable purity have been obtained and characterized. Techniques for analysis and handling of these high-purity powders were established and initial fabrication experiments had a limited success.

Hot working polycrystalline alumina, utilizing a press forging technique, was extensively investigated. Primary recrystallization followed the working and resulted in either single crystals (strain-anneal technique) or relatively fine-grained structures. The basal texture present after recrystallization was identical to the deformation texture; this and the equiaxed recrystallized structures suggested that oriented nucleation was important. At larger grain sizes, an elongated grain structure was observed and was attributed to oriented growth. The marked basal texture suggested that basal slip was the predominant deformation mode; the probability of other deformation mechanisms was also discussed.

Addition of 1/4% MgO retarded recrystallization and a number of such samples, possessing a pronounced basal deformation texture, were used for mechanical properties determination. The working led to no loss of structural integrity, and the strength was surprisingly constant with grain size, at least in the range 3.5-10.5 microns. The larger-grained worked samples were stronger than hot-pressed samples o equivalent porosity and grain size.

The high ductility, up to 75% height reduction being achieved without much difficulty, suggested that hot working could be used to produce shaped bodies.

DD FORM 1 JAN 64 1473

Unclassified

Security Classification

14.

KEY WORDS	LINK A ROLE	LINK A WT	LINK B ROLE	LINK B WT	LINK C ROLE	LINK C WT
Alumina						
Magnesia						
Hot Working						
Press Forging						
Texture						
Primary Recrystallization						
Mechanical Properties						
Grain Growth						

INSTRUCTIONS

1. ORIGINATING ACTIVITY: Enter the name and address of the contractor, subcontractor, grantee, Department of Defense activity or other organization (*corporate author*) issuing the report.

2a. REPORT SECURITY CLASSIFICATION: Enter the overall security classification of the report. Indicate whether "Restricted Data" is included. Marking is to be in accordance with appropriate security regulations.

2b. GROUP: Automatic downgrading is specified in DoD Directive 5200.10 and Armed Forces Industrial Manual. Enter the group number. Also, when applicable, show that optional markings have been used for Group 3 and Group 4 as authorized.

3. REPORT TITLE: Enter the complete report title in all capital letters. Titles in all cases should be unclassified. If a meaningful title cannot be selected without classification, show title classification in all capitals in parenthesis immediately following the title.

4. DESCRIPTIVE NOTES: If appropriate, enter the type of report, e.g., interim, progress, summary, annual, or final. Give the inclusive dates when a specific reporting period is covered.

5. AUTHOR(S): Enter the name(s) of author(s) as shown on or in the report. Enter last name, first name, middle initial. If military, show rank and branch of service. The name of the principal author is an absolute minimum requirement.

6. REPORT DATE: Enter the date of the report as day, month, year; or month, year. If more than one date appears on the report, use date of publication.

7a. TOTAL NUMBER OF PAGES: The total page count should follow normal pagination procedures, i.e., enter the number of pages containing information.

7b. NUMBER OF REFERENCES: Enter the total number of references cited in the report.

8a. CONTRACT OR GRANT NUMBER: If appropriate, enter the applicable number of the contract or grant under which the report was written.

8b, 8c, & 8d. PROJECT NUMBER: Enter the appropriate military department identification, such as project number, subproject number, system numbers, task number, etc.

9a. ORIGINATOR'S REPORT NUMBER(S): Enter the official report number by which the document will be identified and controlled by the originating activity. This number must be unique to this report.

9b. OTHER REPORT NUMBER(S): If the report has been assigned any other report numbers (*either by the originator or by the sponsor*), also enter this number(s).

10. AVAILABILITY LIMITATION NOTICES: Enter any limitations on further dissemination of the report, other than those imposed by security classification, using standard statements such as:

(1) "Qualified requesters may obtain copies of this report from DDC."

(2) "Foreign announcement and dissemination of this report by DDC is not authorized."

(3) "U. S. Government agencies may obtain copies of this report directly from DDC. Other qualified DDC users shall request through

________________________________."

(4) "U. S. military agencies may obtain copies of this report directly from DDC. Other qualified users shall request through

________________________________."

(5) "All distribution of this report is controlled. Qualified DDC users shall request through

________________________________."

If the report has been furnished to the Office of Technical Services, Department of Commerce, for sale to the public, indicate this fact and enter the price, if known.

11. SUPPLEMENTARY NOTES: Use for additional explanatory notes.

12. SPONSORING MILITARY ACTIVITY: Enter the name of the departmental project office or laboratory sponsoring (*paying for*) the research and development. Include address.

13. ABSTRACT: Enter an abstract giving a brief and factual summary of the document indicative of the report, even though it may also appear elsewhere in the body of the technical report. If additional space is required, a continuation sheet shall be attached.

It is highly desirable that the abstract of classified reports be unclassified. Each paragraph of the abstract shall end with an indication of the military security classification of the information in the paragraph, represented as (*TS*), (*S*), (*C*), or (*U*).

There is no limitation on the length of the abstract. However, the suggested length is from 150 to 225 words.

14. KEY WORDS: Key words are technically meaningful terms or short phrases that characterize a report and may be used as index entries for cataloging the report. Key words must be selected so that no security classification is required. Identifiers, such as equipment model designation, trade name, military project code name, geographic location, may be used as key words but will be followed by an indication of technical context. The assignment of links, rules, and weights is optional.